CONTROLS ON THE GENERATION OF SECONDARY POROSITY IN EOGENETIC KARST: EXAMPLES FROM SAN SALVADOR ISLAND, BAHAMAS AND NORTH-CENTRAL FLORIDA, USA

By

PAUL J. MOORE

A DISSERTATION PRESENTED TO THE GRADUATE SCHOOL
OF THE UNIVERSITY OF FLORIDA IN PARTIAL FULFILLMENT
OF THE REQUIREMENTS FOR THE DEGREE OF
DOCTOR OF PHILOSOPHY

UNIVERSITY OF FLORIDA

2009

The world didn't turn color until sometime in the 1930s,
and it was pretty grainy color for a while, too.

Bill Watterson

To my Janie

ACKNOWLEDGMENTS

Completing a doctoral dissertation is not possible without the support of coworkers, friends, and family. First, I would like to acknowledge the support of my dad, Joe Moore, who instilled in me a work ethic and integrity that defines the person I am today. Never one to remain idle, he constantly challenged me to push harder, become better, and refuse to settle for anything less than that warranted through hard work and perseverance. His ability to overcome any obstacle gives me the strength to press forward each day.

While many teachers during my childhood and adolescence helped shape my intellect, none was more influential than my high school science teacher, Bob Pursley. His knowledge of mathematics, physics, and chemistry was unparalleled and often presented in a humorous manner. Each class offered an opportunity to understand important phenomena of the physical world, including calculating the trajectory of arrows piercing classmates – usually girls – on hilltops, making soap from beef tallow, or characterizing Brownian motion with hip gyrations rivaled only by Chubby Checker. He exposed me to critical thinking, which I never appreciated during those immature years but now embrace. Needless to say, he had a profound influence on my desire to evaluate and understand the world around me.

I would like to acknowledge Dr. John Mylroie, who not only became my de facto advisor during my formative years as an undergraduate at Mississippi State University, but also a dear friend. Whether jumping in and out of caves, hopping from island to island, or just enjoying some rum or bourbon, his infectious personality and passion for science redirected my journey through life. I am forever grateful for the moments we shared, and look forward to future discussions about time, eustasy, and the absence of rock – ESADMF.

I thank my primary advisor, Dr. Jon Martin, for agreeing to mentor (and fund) me during my six-year tenure at the University of Florida. Jon was not only instrumental in my

development as a scientist, but also as a person. He showed me the importance of a work-life balance, where one can be equally dedicated to both career and family. Although our paths now diverge, I will never forget those trips to South America and Antarctica, watching Gollum collect samples in Majors Cave, and those exciting adventures to O'Leno State Park – I never thought I would miss those, but amazingly I do.

In addition to these individuals, a host of others provided much needed support through the years. I thank my committee members, Drs. Liz Screaton, Phil Neuhoff, Dave Hodell, and Joe Delfino, for agreeing to oversee my project. Specifically, I thank Liz for always keeping me on my toes, and Phil for stressing the importance of chemical potential. I thank Kelly Deuerling for providing invaluable assistance in the lab, and Mou Roy for always sharing a good laugh or some of her amazing cooking. I thank Jason Gulley for the lively conversations, usually over scotch, about cave genesis and anything else that came up, which was often. Thanks go out to Jonathan Hoffman, Derrick Newkirk, and Laura Ruhl, for being great roommates and not shooting me in the middle of the night during my visits to the kitchen for milk and cookies. I would also like to acknowledge the office staff, Nita Fahm, Susan Birungi, and Pam Haines, for always accommodating my requests and pleads. You guys kept me sane through the final months.

Lastly, I would like to thank my family, whose love and support are my foundation. My siblings, Hope Mosley and Kameren Gibson, have always been there to take my mind off school and because of them I am uncle PJ to Addison, Jasmine, and Steven. My grandparents, Rita Hildick and Doris Moore, are my angels on Earth. I thank my aunt, Margaret Hildick-Pytte, for her encouragement, words of wisdom, and sharing of good wine. Finally, I wish to thank the love of my life, Jane Gustavson. She remained by my side during times of my own self doubt and

irritable mood swings, always ready to provide reassurance with a warm hug. She is my friend, my closest companion, and the reason this document reached completion.

TABLE OF CONTENTS

LIST OF TABLES

LIST OF FIGURES

Abstract of Dissertation Presented to the Graduate School
of the University of Florida in Partial Fulfillment of the
Requirements for the Degree of Doctor of Philosophy

CONTROLS ON THE GENERATION OF SECONDARY POROSITY IN EOGENETIC KARST: EXAMPLES FROM SAN SALVADOR ISLAND, BAHAMAS AND NORTH-CENTRAL FLORIDA, USA.

By

Paul J. Moore

May 2009

Chair: Jonathan B. Martin
Major: Geology

Carbonate rocks host large amounts of the world's water, petroleum, and natural gas reserves. Wise use and management of these resources require predictive models that characterize magnitudes and distributions of porosity and permeability. Predictive models are complicated by the formation of secondary porosity and coupled increases in permeability, which self-organize during dissolution and precipitation and facilitate the circulation of fluids. Most models describing porosity and permeability evolution have focused on telogenetic karst aquifers of dense, recrystallized limestone, where dissolution mainly results in conduits embedded in rocks with low matrix permeability. This study provides new insights into the generation of secondary porosity in eogenetic karst aquifers of San Salvador Island, Bahamas and north-central Florida, USA, where dissolution results in both conduits and isolated voids within rocks possessing high matrix permeability. Small carbonate islands, such as San Salvador, lack conduits, but develop secondary porosity as isolated voids in freshwater lenses. The location and size of these voids are functions of coupling dissolution and transport of reactions products, with small voids developed within the island's interior and large voids developed near the shoreline. Dissolution results primarily from CO_2 generating carbonic acid at or near the water

table rather than mixing of fresh and saline water as previously thought. Large carbonate platforms, such as Florida, contain conduits resulting from dissolution driven by carbonic acid, however, the high matrix permeability provides a significant component of flow that affects rates, magnitudes, and locations of dissolution. Dissolution along the conduit flow path is limited as water with elevated Ca^{2+} concentrations flows from the matrix into the conduit and restricts dissolution at the conduit wall. In contrast, flow of water undersaturated with respect to calcite from conduits to matrix porosity creates a dissolution halo surrounding conduits, unlike telogenetic karst aquifers where dissolution is concentrated along the walls of fractures and conduits. These new concepts highlight stark contrasts in the evolution of porosity and permeability in eogenetic karst aquifers compared to their telogenetic counterparts. This information provides a better understanding to accurately predict how secondary porosity and permeability develop in carbonate rocks prior to burial diagenesis.

CHAPTER 1
INTRODUCTION

Carbonate rocks supply an estimated 25% of drinking water to the world's population (Ford and Williams 2007) and host more than 60% and 40% of the world's petroleum and natural gas reserves, respectively (Schlumberger Market Analysis 2007). Wise use of these natural resources requires knowledge about the various types of porosity, both primary and secondary, that tend to be heterogeneously distributed in carbonate rocks. These various types of porosity include intergranular porosity within the matrix rock, fractures, faults, bedding plane partings, and conduits enlarged through dissolution. This porosity and its distribution influence nearly all aspects of aquifer-reservoir characteristics, including storage and distribution of permeability (e.g., Moore 2001; Ford and Williams 2007). The range of porosity and permeability determines flow paths and allows highly variable flow rates, which can be both laminar and turbulent (Worthington 1994; Quinlan et al. 1996; White 1999; Halihan et al. 2000). While most flow in carbonate rocks occurs through conduits and fractures, storage is primarily in the matrix porosity (e.g., Worthington et al. 2000).

The magnitude and distribution of porosity and permeability in carbonate rocks largely results from diagenetic and karst processes (e.g., Choquette and Pray 1970; Lucia 1995; White 1999; Worthington et al. 2000). While diagenesis refers to the sum of all chemical, physical, and biological processes affecting sediment following deposition (Morse and Mackenzie 1990), karst processes reflect the development of well-organized secondary porosity from dissolution, which facilitates the circulation of fluids (Huntoon 1995). Early work described the evolution of carbonate rocks based on time-porosity stages that reflect the rock cycle, with the terms "eogenetic" and "telogenetic" referring to before and after the reduction of primary depositional porosity by burial diagenesis (Choquette and Pray 1970). Recent work applied these terms to

karst to designate carbonate rocks of varying age, diagenesis, and karstification (Vacher and Mylroie 2002). Eogenetic karst refers to young limestone that has only undergone meteoric diagenesis near its area of deposition, and maintains high matrix porosity as localized mineral dissolution and precipitation redistributes porosity from interparticle to moldic pores (Vacher and Mylroie 2002). Examples of eogenetic karst include the Cenozoic rocks of Yucatan, Mexico, the Bahamas, and Florida, USA (Back and Hanshaw 1970; Carew and Mylroie 1997). In contrast, telogenetic karst has undergone burial diagenesis and uplift, resulting in a dense recrystallized limestone that develops conduits embedded in a network of fractures of otherwise low matrix porosity and permeability (Vacher and Mylroie 2002). Examples of telogenetic karst include the Paleozoic rocks of Appalachia in the eastern United States and the Alps of Europe (White 1988; Ford and Williams 2007). The hallmark property that distinguishes eogenetic karst from telogenetic karst is the role of the matrix permeability in hydrogeology (e.g., Budd and Vacher 2004; Florea and Vacher 2007).

Most conceptual and numerical models of the generation of secondary porosity in carbonate rocks have focused on conduit evolution in telogenetic karst aquifers (White 1988; Palmer et al. 1999; Ford and Williams 2007). Two critical processes affecting the evolution from fractures to conduits include the transition from laminar to turbulent flow and a kinetic shift in calcite dissolution rates (White 1977; Dreybrodt 1990; Palmer 1991). During early stages of conduit evolution, calcite dissolution rates drop from linear to fourth-order kinetics at about 90% saturation, thereby allowing slow widening of fractures under laminar flow. Low matrix permeability focuses flow and dissolution within the fractures, progressively enlarging competing flow paths until a preferential pathway captures most of the flow to become a proto-conduit. Once water in the proto-conduit drops below 90% of calcite saturation, linear

dissolution kinetics dominates resulting in rapid enlargement of the conduits (e.g., Palmer 1991). Under typical groundwater gradients, the kinetic shift moves from slow, high-order kinetics to fast, low-order kinetics approximately at the transition from laminar to turbulent flow during flow through an enlarging conduit (White 1977). These concepts have been used in deterministic and stochastic models to provide valuable insight on evaluating the early evolution of conduits (e.g., Groves and Howard 1994; Kaufmann and Braun 1999; Gabrovšek and Dreybrodt 2001; Romanov et al. 2003a; Gabrovšek et al. 2004), predicting the morphology of cave patterns (e.g., Palmer 1991; Howard and Groves 1995; Palmer 2001), modeling leakage rates beneath dam sites (Romanov et al. 2003b), and estimating the role of conduit growth on landscape evolution in a karst basin (Groves and Meiman 2005).

Less understood, however, are processes controlling the generation of secondary porosity in eogenetic karst, which produce both conduits as well as isolated meter-scale dissolution chambers (Mylroie and Vacher 1999; Florea et al. 2007). In Florida, conduits have been shown to occur primarily where streams flowing off siliciclastic sediments sink into underlying limestone and later reemerge downgradient (Katz et al. 1998; Screaton et al. 2004), and at springs where the convergence of groundwater flow lines concentrate diffuse flow (Beck 1986; White 2002). Although conduits develop in similar settings in telogenetic karst (e.g., Shuster and White 1971; Palmer 2001), flow in eogenetic karst may not remain focused within fractures or proto-conduits because large fractions of the flow occur in the high matrix permeability. The relationship between flow in conduits and the surrounding aquifer has been observed as mixing between conduit and matrix water depending on hydraulic head gradients between the conduit and surrounding aquifer (Katz et al. 1998; Screaton et al. 2004; Loper et al. 2005; Martin et al. 2006). Mixing of these chemically-distinct waters should reduce the magnitude and distribution

of dissolution, thereby diminishing enlargement of the proto-conduit (cf. Gabrovšek et al. 2004). These observations suggest that new concepts may be necessary to describe conduit development in eogenetic karst.

In addition, not all caves found in eogenetic karst reflect the evolution of conduit permeability (Mylroie and Carew 1990; Florea 2006). For example, many Florida caves are similar to caves found on small carbonate islands such as the Bahamas, which are characterized by laterally-extensive and vertically-restricted chambers with blind pockets and dead-end passages (Mylroie and Carew 1990; Florea 2006). In both locations, geomorphic and glacio-eustatic evidence suggests these isolated voids are phreatic in origin and develop along water-table horizons both within the interior and along shorelines. Cave morphology and the high matrix porosity and permeability of the surrounding aquifer suggests they likely formed under diffuse-flow conditions, and thus formed as dissolution chambers and not conduits that form from focused flow such as in telogenetic karst. Furthermore, they are believed to form with limited connection to the land surface, whereby diffuse recharge to the water table occurs through the epikarst and vertical preferential flow paths, such as narrow fracture trends (Florea 2006) or along well-developed karstic fissures (Whitaker and Smart 1997a). Cave entrances form when the voids are breached by surface denudation, hillside erosion, or land alteration such as road construction and quarrying.

One primary mechanism believed to drive cave development in these locations is the mixing of chemically-distinct water. In the Bahamas, voids known as banana holes form within the interior, reaching hundreds of m^3 in volume and are believed to have developed by mixing of vadose and phreatic water (Harris et al. 1995). Conversely, larger voids, called flank margin caves, can reach thousands of m^3 in volume and are believed to have developed at the edge of

freshwater lenses primarily from the convergence of two areas of mixing dissolution: mixing of vadose and phreatic water at the water table and mixing of fresh and saline water at the halocline (Plummer 1975; Mylroie and Carew 1990). The primary difference between banana holes and flank margin caves is size, which is largely attributed to more chemically-aggressive water along the lens edge (Mylroie and Carew 1990). However, in Florida, many large air-filled caves occur at water-table elevations consistent with present-day sea level or align with marine terraces of past sea-level highstands (Florea et al. 2007). These caves reach volumes in excess of thousands of m^3 and likely formed in the absence of mixing of fresh and saline water, since the thickness of fresh groundwater where these caves are located can exceed several hundred meters (Miller 1986). These observations suggest that processes in addition to dissolution mechanisms may influence the magnitude and distribution of cave development in eogenetic karst aquifers.

Statement of Purpose

The objective of this investigation is to develop an understanding of controls on porosity development in eogenetic karst aquifers. This study couples hydrogeological concepts with chemical compositions of water from San Salvador Island, Bahamas and north-central Florida, USA with the known distributions of dissolution voids including flank margin caves and conduits. Results contribute to the current understanding of secondary porosity generation in eogenetic karst in several ways, specifically, how chemical and physical factors control porosity density and distribution to provide new concepts to characterizing aquifers and reservoirs, and on fluid flow and recharge and their influence on water budgets and spring characterization.

To meet this objective, this study addresses several general questions pertaining to dissolution and porosity evolution in eogenetic karst aquifers:

1. Are flank margin caves caused primarily by the mixing of fresh and saline water? Does cave development depend on additional process to drive dissolution including the

generation of carbonic acid? What role does freshwater lens hydrodynamics play in their enlargement?

2. Can matrix permeability affect spring discharge and chemistry even in systems dominated by allogenic recharge and conduit flow? Does groundwater monitoring provide insight on sources of water to springs?

3. Does the presence of high matrix porosity and permeability affect the magnitude and distribution of conduit development in eogenetic karst aquifers? Are new concepts necessary for modeling conduit enlargement in eogenetic karst aquifers?

Dissertation Organization

This dissertation is presented in publishable paper format. Chapter 2 is titled "Rapid generation of macroporosity on carbonate islands: the flank margin cave hypothesis revisited" and is in review at the *Journal of Sedimentary Research*. This chapter contributes to the understanding of chemical and hydrologic processes most likely responsible for generating dissolution chambers within freshwater lens of small carbonate islands. The study was based on coupling bulk chemistry and geochemical modeling of water collected from San Salvador Island, Bahamas to the hydrodynamics of freshwater lenses. The major result of this chapter is a single unifying quantitative model that describes how meter-scale porosity can develop within diffuse flow fields. This chapter provides insight on predicting the location and magnitude of meter-scale secondary porosity across carbonate platforms that have experienced meteoric diagenesis.

Chapter 3 is titled "Geochemical and statistical evidence for recharge, mixing, and controls on spring discharge in an eogenetic karst aquifer" and is in review at the *Journal of Hydrology*. This chapter contributes to the understanding of matrix flow in eogenetic settings. The study was based on principal component analysis (PCA) of the bulk chemistry of surface and groundwater from a portion of the Upper Floridan aquifer in north-central Florida. The major result of this chapter suggests that matrix flow provides a significant component of flow even in eogenetic aquifers dominated by conduits that are sourced by continuous allogenic recharge. The

contributions of this chapter provide insight on how high matrix permeability affects aquifer recharge and spring discharge, and suggests that characterizing eogenetic karst aquifers requires attention to groundwater chemistry and additional flow paths rather than on the conduit water as is commonly the case for telogenetic settings .

Chapter 4 is titled “Conduit enlargement in eogenetic karst aquifers” and will be submitted to the *Journal of Hydrology*. This chapter contributes to the understanding of the physical and chemical factors responsible for dissolution and formation of conduits in eogenetic karst setting and the differences between these factors in eogenetic and telogenetic karst. The study was based on the geochemical equilibria of water chemistry from Chapter 3 and a mass-balance model that evaluates the mixing of water and mass transfer of mineral and gas phases within the conduit. This work found that dissolution of conduit walls is restricted by flow of Ca-rich water from the matrix and that dissolution is focused in matrix porosity surrounding the conduits as well as at the conduit walls during high-flow events. This chapter provides insight on how the evolution of eogenetic and telogenetic karst aquifers differ. Chapter 5 summarizes the principle findings of Chapters 2 through 4.

CHAPTER 2
RAPID GENERATION OF MACROPOROSITY ON CARBONATE ISLANDS:
THE FLANK MARGIN CAVE HYPOTHESIS REVISITED

Introduction

On Holocene- and Pleistocene-aged carbonate islands, freshwater lenses are sites of extensive meteoric diagenesis including dissolution of carbonate minerals and development of secondary porosity. Carbonate mineral dissolution commonly results from formation of carbonic acid by the hydration of CO_2 (Kern 1960), acids produced from oxidation-reduction reactions (Smart et al. 1988), and mixing of waters with dissimilar chemical compositions, such as seawater and freshwater (Runnells 1969; Plummer 1975). Although dissolution is common in freshwater lenses, bulk values of porosity do not change greatly throughout most of the lens because the porosity is largely redistributed from interparticle to moldic pores through localized dissolution and reprecipitation (e.g., Vacher and Mylroie 2002). In selected locations of freshwater lenses, however, the generation of secondary porosity can result in meter-scale macropores which have a significant impact on the accumulation and exploitation of freshwater and hydrocarbon resources (e.g., Craig 1988; Jaeggi 2006; Baceta et al. 2008; Labourdette and Mylroie 2008). Any development of macropores would require an environment that promotes dissolution while preventing reprecipitation of the dissolution reaction products (e.g., Palmer 1991).

In the Bahamas, geomorphic and glacio-eustatic evidence suggests macropores develop along the water table and at the distal edge of freshwater lenses in short time spans of thousands of years (Mylroie and Carew 1995). At the water table, macropores known as banana holes reach hundreds of m^3 in volume and are believed to have developed from mixing between vadose and phreatic water (Harris et al. 1995). Conversely, the largest macropores, called flank margin caves, can reach thousands of m^3 in volume and are believed to have developed at the edge of

freshwater lenses primarily from the convergence of two areas of mixing dissolution: mixing of vadose and phreatic water at the water table and mixing of fresh and saline water at the halocline (Mylroie and Carew 1990; Mylroie and Carew 1995).

Although significant effort has gone into developing conceptual models of how and where macropores form, a single unifying quantitative model for their formation has never been developed, regardless of macropore importance for subsurface storage of freshwater and hydrocarbons (e.g., Romanov and Dreybrodt 2006). Porosity generation could accelerate at the lens edge due to increases in specific discharge, which should contribute to dissolution by enhancing the mixing of different water masses (Raeisi and Mylroie 1995; Rezaei et al. 2005). However, on small carbonate islands, where most flank margin caves are found (Labourdette et al. 2007), mixing processes appear to have little influence on dissolution (e.g., Plummer et al. 1976; Budd 1988; Anthony et al. 1989; McClain et al. 1992; Matsuda et al. 1995; Ng and Jones 1995; Moore et al. 2006; Whitaker and Smart 2007a; Martin and Moore 2008). In addition to mixing, porosity generation may result from dissolution by acids generated by aerobic and anaerobic oxidation-reduction reactions within the mixing zone where density interfaces trap organic matter and bacteria (Smart et al. 1988; Bottrell et al. 1991, 1993; Schwabe et al. 2008). Although mixing and oxidation-reduction reactions may drive some dissolution, most dissolution on these islands may be linked primarily to increased concentrations of CO_2 generating carbonic acid. Nonetheless, average dissolution rates fail to explain the location and magnitude of porosity generation required to develop mapped flank margin caves. For example, most Bahamian flank margin caves formed during the Marine Isotope Substage (MIS) 5e highstand in about 12 ky or less (Carew and Mylroie 1995a); however, this amount of time would be insufficient to form the

caves given average estimates of dissolution rates for carbonate islands (e.g., Whitaker and Smart 2007a).

I suggest the generation of macropores, such as banana holes and flank margin caves, may occur in select locations of freshwater lenses from inputs of CO_2 coupled with the flow dynamics of freshwater lenses. Flow velocities in freshwater lenses are greatest at the water table and increase towards the lens edge, where the highest degree of specific discharge occurs (Vacher et al. 1990; Raeisi and Mylroie 1995). Consequently, the size of banana holes and flank margin caves may reflect the relative ability of the freshwater lens to transport reaction products away from the locus of porosity generation before they reprecipitate as cements. This hypothesis would predict flank margin caves are the largest macropores because they develop along shorelines at the edge of freshwater lenses where specific discharge is greatest and reaction products can be rapidly flushed to the ocean. Conversely, banana holes would be smaller than flank margin caves because they form along the water table within the island's interior, where flow velocities are less than at the lens edge. Their smaller size likely reflects these low flow velocities providing sufficient time for some reprecipitation of reaction products.

In this chapter, I evaluate the magnitude and rate of dissolution required for a flank margin cave on San Salvador Island, Bahamas to develop during the MIS 5e highstand, using chemical compositions of groundwater, freshwater-lens geometry, and the volume of a flank margin cave. The water-chemistry data suggests that most dissolution occurs in low-salinity water, is primarily governed by the influx of CO_2, and mixing has only a minor influence on dissolution. By coupling these estimates of dissolution with flow dynamics, I develop a mass balance model that estimates dissolution rates at the lens edge, and compare magnitudes of dissolution with the measured volume of a flank margin cave. The ability to predict the location of macropores in

carbonate islands will be important for understanding distributions of valuable natural resources such as freshwater and hydrocarbons.

Location and Geologic Setting

The Bahamian Archipelago is a NW-SE trending, 1400-km long series of carbonate islands and shallow banks located along the eastern margin of North America (Figure 2-1A). The archipelago is considered to be tectonically stable, but subsiding isostatically at a rate of 1-2 m per 100 ky (Mullins and Lynts 1977; Carew and Mylroie 1995a). Islands in the northwestern portion of the archipelago are isolated landmasses located on two large platforms, Little Bahama Bank and Great Bahama Bank. To the southeast, the archipelago consists of small, isolated platforms that are capped by islands that cover most of the platform area. The islands are composed of variably-cemented Holocene and mid-to-late Pleistocene carbonate sediments of subtidal, reef, beach, and dune facies that reach up to about 60 meters above present sea level (masl). Only dune facies exist above 8 masl, and all exposed marine facies in the Bahamas are believed to be deposited during the MIS 5e highstand (Carew and Mylroie 1997). Climate in the Bahamas includes a warm, rainy season from May to October and a cool, dry season from November to April (Whitaker and Smart 1997a). Rain delivers freshwater to the islands during the passage of cold fronts in the winter, convective thunderstorms during summer, and tropical storms.

San Salvador Island, located in the southeastern portion of the archipelago, is about 20 km long and about 8 km wide (Figure 2-1B). Annual rainfall ranges from 1000 to 1250 mm/yr, with potential evapotranspiration (PET) estimated between 1250 and 1375 mm/yr (Sealey 1994). The negative water budget limits groundwater recharge to rain events that exceed PET. Surface streams are absent due to the high porosity (≤30%) of the limestone (Vogel et al. 1990; Vacher and Mylroie 2002), but about one third of the island is covered by lakes ranging in salinity from

marine to hypersaline. Lakes with marine salinity have tidal fluctuations and bulk chemical compositions similar to seawater, suggesting a direct subsurface connection to the ocean (Davis and Johnson 1989; Martin and Moore 2008). Most of the land surface is covered by low-lying plains and eolian dunes that reach a maximum of 30 masl (Sealey 1994) and multiple freshwater lenses occur below the dunes (Figure 2-1B). These freshwater lenses drain into nearby interior lakes or along the coastline (Davis and Johnson 1989).

San Salvador Island has numerous flank margin caves that formed about 125 ka during the 12-ky MIS 5e highstand when sea level was 4 to 6 masl (Mylroie and Carew 1990; Chen et al. 1991; Carew and Mylroie 1995a). During this time, most of San Salvador's platform was flooded, and the bank was comprised of small, isolated strip-islands made up mostly of the eolian dunes observed today (Carew and Mylroie 1997). Flank margin caves are believed to have formed by freshwater and seawater mixing at the distal edge of freshwater lenses that developed within the strip-islands (i.e., hypogenic caves, Palmer 1991). The caves initially formed as small, isolated dissolution chambers and increased in size in the absence of turbulent flow as voids coalesce along strike at the edge of the freshwater lens (Labourdette et al. 2007). This mechanism has led to morphologies that are vertically-restricted, horizontally-extensive caves with volumes varying from 10 to 15,000 m^3 (Mylroie et al. 1995). Cave entrances form when the caves are breached by surface denudation and hillside erosion.

Altar Cave, a well-studied flank margin cave used in this study, is located in Grotto Beach Ridge on Sandy Point in the southwest portion of San Salvador Island (Figure 2-1C). The cave has an areal footprint of about 450 m^2 and a minimum volume of 1200 m^3 (Florea et al. 2004). Grotto Beach Ridge formed early in the MIS 5e transgression as a prograding sequence of subtidal, beach, back-beach, and eolian sediments (Carew and Mylroie 1995b). This material

would have been originally mostly aragonite (e.g., Budd 1988), but alteration has converted the rocks to about 60% calcite (Vogel et al. 1990; Carew and Mylroie 1995b). Fossil corals from the base of Grotto Beach Ridge located above modern sea level about 500 m north of Altar Cave yielded a U/Th age of approximately 125 ka (Hattin and Warren 1989). This timing indicates that Altar Cave formed concurrently with the deposition of its host rock (i.e., syndepositional karst; Labourdette and Mylroie 2008). While the MIS 5e highstand lasted for about 12 ky, Altar Cave must have formed in less time, perhaps at most 10 ky, to allow time for early development of both Grotto Beach Ridge and its freshwater lens following flooding of the bank during the transgression.

Water Chemistry

Methods

Sixty-three water samples, ranging from fresh to hypersaline, were collected from inland lakes, cave pools, blue holes, and wells on San Salvador Island between April 2005 and April 2007 during three different sampling trips (Moore and Martin 2008) (Table A-1). Most water bodies were sampled only once, including 12 wells from the Line Hole well field, which penetrate a single freshwater lens (Table A-1). The wells are evenly spaced approximately 30 m apart and are located about 200 to 500 m from the coast. Other water bodies, including cave pools and Ink Well Blue Hole, were sampled multiple times both spatially and temporally. The cave pools are at least several meters deep and were sampled in depth profiles to measure salinity gradients across the pycnocline (Moore et al. 2006). At Ink Well, two sets of samples were collected near the center of the 15-m diameter blue hole from the surface to the sediment-water interface during a single day. The first set was collected in the morning under cloud cover and the other under direct sunlight about one hour after the initial set was collected.

Water was collected from accessible locations by grab sampling, but wells, cave pools, and Ink Well Blue Hole were sampled using polyethylene tubing connected to a 12-V peristaltic pump (Moore et al. 2006). During sampling, I measured pH and temperature using an Orion #250A portable pH-temperature meter, and conductivity and salinity using an Orion model #130 portable conductivity meter. Samples for major ion and Sr^{2+} concentrations were collected in clean, dry HDPE bottles with no preservatives, and samples for dissolved inorganic carbon (DIC) were collected in glass bottles and poisoned with $CuSO_4$. No samples were collected for DIC during the April 2005 trip (Table A-1). Total alkalinity was measured using the Gran titration within 24 hours of collection (e.g., Drever 1997). Major ion, Sr^{2+}, and DIC concentrations were analyzed at the Department of Geological Sciences at the University of Florida. Major ions were measured with an automated Dionex 500DX ion chromatograph. Strontium concentrations were measured with a Thermo Finnigan Element 2 Inductively Coupled Plasma Mass Spectrometer (ICP-MS). Dissolved inorganic carbon was measured with a Coulometrics CO_2 coulometer using a 3% $AgNO_3$ scrubber solution, N_2 as the carrier gas, and 2N HCl to evolve the CO_2 from the water. Precision of the measurements (1 σ) was assessed by replicate measurements of internal standards, and was found to be about 1% for DIC concentration, 5% for the major ion concentrations, and about 8% for Sr^{2+} concentrations.

The geochemical code EQ3/6, Version 8 (Wolery 1992), was used to determine the partial pressure of CO_2, ion-activity products (Q), and carbonate mineral saturation indices [log (Q/K), where K is the equilibrium constant for a given mineral] for all water samples, as well as theoretical saturation states of mixtures of samples with compositions assumed to represent freshwater and seawater concentrations. All thermodynamic data were from the SUPCRT database (Johnson et al. 1992). Activity coefficients of aqueous species were calculated using the

extended Debye-Hückle equation of Helgeson (1969). Samples having a saturation index (SI) within ±0.1 are assumed to be in equilibrium with respect to calcite and dolomite based on analytical errors in measurements of pH, alkalinity, and concentrations of Ca^{2+} (e.g., Langmuir 1997). Charge balance errors for most samples are < 3%, but may be larger in freshwater samples with concentrations close to instrument detection limits.

I use Cl^- as a conservative tracer to determine the amount of ions in the water that originate from carbonate mineral dissolution by assuming that Cl^- is chemically conservative on San Salvador Island and that there are no other sources of reaction products to the water. These assumptions are reasonable since lithologies on San Salvador Island, other than minor quartzitic paleosols, are primarily calcite and aragonite with no other Ca- or Cl-bearing minerals such as halite, gypsum, or anhydrite (Martin and Moore 2008). Excess ion concentrations originating from water-rock reactions (X_{EXCESS}) were determined by

$$X_{EXCESS} = X_{SAMPLE} - (X/Cl)_{SEAWATER} \times (Cl_{SAMPLE}), \quad (2\text{-}1)$$

where X and Cl are molar concentrations of any dissolved ion and Cl^-, respectively.

Results

Bulk chemistry

Water on San Salvador Island consists of mixtures of two end members, rain water and seawater. Some of the water samples have been concentrated through evaporation as shown by their salinity, which ranges up to about 52 practical salinity unit (psu) or about 1.5 times seawater concentrations. Magnesium, Na^+, K^+, and SO_4^{2-} concentrations correlate linearly with Cl^- (Figures 2-2A, 2-2B, 2-2C, 2-2D) indicating their concentrations vary only through seawater dilution and evaporation. In contrast, concentrations of Ca^{2+}, Sr^{2+}, and total alkalinity are enriched compared to values expected from conservative mixing and evaporation, reflecting

carbonate mineral dissolution (Figures 2-2E, 2-2F, 2-2G). The measured total alkalinity correlates with DIC suggesting it is mostly carbonate alkalinity (Figure 2-3).

The greatest enrichments of Ca^{2+}, Sr^{2+} and alkalinity occur in samples with salinity less than 5 psu (e.g., Martin and Moore 2008). The concentration in excess of that expected from mixing of seawater and freshwater can be defined as the excess ion concentrations (i.e., Eq. 2-1). For example, excess Ca^{2+} in samples with salinity less than 5 psu average about 2.0 mM, while brackish samples (7 to 30 psu) and samples with marine salinity have excess Ca^{2+} concentrations averaging about 0.90 mM and 0.32 mM, respectively (Figure 2-2E). The greatest enrichment of 48 times occurs in Sample LH-A (0.4 psu), which has an excess Ca^{2+} concentration of about 3.5 mM. This sample also has an excess Sr^{2+} concentration of 0.098 mM and excess alkalinity concentration of 7.4 mM, which reflects a 155-times enrichment of Sr^{2+} and 430-times enrichment of alkalinity over seawater contributions.

CO_2 and saturation state

Speciation-solubility modeling shows the SI of most samples are within about 0.5 SI units of saturation with respect to aragonite, although a few samples extend to as much as 1 and -1.5 SI units away from saturation (Figure 2-4). This modeling also shows that log P_{CO2} values range over 2 orders of magnitude from -3.7 to -1.3 bars. The relationship between log P_{CO2} and saturation state follows two distinct trends: one is a linear correlation between log P_{CO2} and SI (Trend 1 in Figure 2-4), while the other shows variable P_{CO2} with little change in SI (Trend 2 in Figure 2-4). Samples forming Trend 2 were collected from groundwater wells with salinities less than about 5.0 psu, and from two flank margin caves (Majors Cave and Crescent Top Cave) which have salinities ranging from about 2 to 35 psu.

Trend 1 extends from water that is supersaturated with respect to aragonite and near equilibrium with atmospheric CO_2 to water undersaturated with respect to aragonite and calcite

and P_{CO2} above atmospheric values (Figure 2-4). Although samples from cave pools are near saturation with respect to aragonite and calcite, they also show a linear correlation between changes in SI and P_{CO2} (Figure 2-4). The four samples with P_{CO2} near equilibrium with atmosphere were collected from surface water sites (Watling's Blue Hole, Six Pack Pond, and Crescent Pond) where salinities range from about 24 to 52 psu. These samples are the most highly supersaturated with respect to carbonate minerals. All samples undersaturated with respect to calcite also come from a surface water site, Ink Well Blue Hole. In contrast with the other surface water sites, Ink Well Blue Hole exhibits a strong pycnocline with salinity ranging from 0.5 to 17.5 psu, but no thermocline with an average temperature of 24.2 ± 0.4 °C (1σ) (Figure 2-5A). Neither temperature nor salinity varies with time of collection, but P_{CO2} and the saturation state of the water with respect to calcite changed from the early to late morning (Figures 2-5B and C). The early morning samples have pH values of 6.74 to 7.32 with lower and more erratic P_{CO2} concentrations and they are more undersaturated than samples collected later in the day (Table A-1 and Figure 2-5C). Comparison of SO_4^{2-} versus Cl^- suggests sulfate reduction was not occurring at the time of sampling (Figure 2-5D).

Influence of mixing on saturation

Using the compositions of one freshwater sample and two samples with seawater salinity but with different P_{CO2} values, I estimate how mixing of these end-member waters may control the saturation state with respect to aragonite and calcite (Figure 2-6). The freshwater end member (GRC2-06), with a salinity of 0.6 psu, has a log P_{CO2} of -1.83 bars and is slightly undersaturated with respect to aragonite (SI_{ARG} = -0.03). The two saline samples (CP-05 and CT-05) have salinity and chemical compositions similar to seawater. Sample CP-05 was collected from Crescent Pond, an interior tidal lake, while CT-05 was collected from a pool in Crescent Top Cave about 15 m from the lake. The lake sample (CP-05) has a log P_{CO2} of -3.73 bars, near

equilibrium with atmospheric CO_2, while the cave sample (CP-05) has a log P_{CO2} of -2.69 bars, which is about an order of magnitude higher than equilibrium with atmospheric CO_2. The lake water is supersaturated with respect to both aragonite and calcite with SI of 0.72 and 0.86, respectively, but the cave pool is slightly undersaturated with respect to calcite (SI_{CAL} = -0.05) and aragonite (SI_{ARG} = -0.19). Estimates based on models of mixed compositions of these end-member waters show how saturation states with respect to aragonite and calcite should vary depending on the fractions of fresh and saline water, either with atmospheric P_{CO2} or elevated P_{CO2} in each sample (Figure 2-6). These modeled mixing lines represent the expected saturation states of water on San Salvador Island following mixing of freshwater and seawater. None of the samples have saturation states that fall along the modeled saturation state, regardless of their salinity.

Generation of Macroporosity

Mechanisms of Dissolution

Mixing dissolution

Comparison of the model of saturation states expected from mixing of fresh and saline water to sampled water indicates that mixing processes have little affect on dissolution (Figure 2-6). Dissolution by mixing processes depends on mechanical mixing of water with different compositions and P_{CO2}. Mixing of these distinct water types may be limited on small islands such as San Salvador from a combination of factors including magnitudes of recharge and the presence of well-defined transition zones. Transition zones form between the freshwater lens and underlying seawater from hydrodynamic dispersion and vertical mixing due to ocean tides, and their thickness depends on factors including transverse dispersivity and variations in vertical permeabilities (Bear and Todd 1960; Underwood et al. 1992; Griggs and Peterson 1993). On small carbonate islands, such factors are greatly influenced by rock deposition and diagenesis,

and thus transition zones can vary from a few meters (Cant and Weech 1986) up to tens of meters thick (Matsuda et al. 1995; Peterson 1997), and are typically thickest near the shoreline where tide fluctuations are greatest (e.g., Whitaker and Smart 1997b). Consequently, once a transition zone develops, its presence may inhibit mechanical mixing of fresh and saline water and thus diminish the magnitude of dissolution. Recent modeling suggests that flank margin caves could only form where heterogeneous hydraulic conductivities produce thin transition zones, and conversely, that thick transition zones near the shoreline are unlikely to produce flank margin caves (Romanov and Dreybrodt 2006). In addition to a thin transition zone, this model also required an annual recharge rate of 1.11 m to produce groundwater fluxes sufficient enough to drive mixing dissolution that would produce flank margin caves.

Most freshwater lenses on small islands, including San Salvador Island, occur under narrow, inland eolianite ridges and back-beach dunes with limited catchment size and recharge (e.g., Davis and Johnson 1989). These lenses receive recharge of about 0.3-0.4 m/yr based on the thickness of freshwater lenses (Budd and Vacher 1991). Although the amount of recharge is unknown for the Bahamas during the MIS 5e highstand when flank margin caves formed, it seems unlikely to be as high as 1.11 m/yr required for dissolution according to the Romanov and Dreybrodt (2006) model, considering the islands were forested during this time which would have increased evapotranspiration (Carew and Mylroie 1997). Furthermore, although recharge is nearly two times higher in the northern Bahamas than southern Bahamas (Cant and Weech 1986; Whitaker and Smart 1997a), flank margin caves are similar in size across the Bahamian archipelago (Labourdette et al. 2007), further suggesting flank margin caves may form where recharge is less than required by the Romanov and Dreybrodt (2006) model.

In contrast to small islands, large carbonate platforms, such as on the Yucatan Peninsula and South Andros Island, Bahamas, are characterized by mixed water that is undersaturated with respect to carbonate minerals, and could be responsible for the large caves found in these locations (e.g., Back et al. 1986; Stoessell et al. 1989; Whitaker and Smart 1997c). For example, dissolution has been observed on South Andros Island within a bank-margin fracture characterized by vertically-extensive blue holes where vertical mixing is enhanced by strong circulation within the fracture system (Whitaker and Smart 1997c). On the Yucatan Peninsula, mixing dissolution may lead to caves that extend about 12 km inland from the coast where an extensive catchment supplies large amounts of freshwater, resulting in sharp transition zones that range from about 0.4 to 4 m thick in the conduits (Beddows 2004; Smart et al. 2006). These hydrologic conditions, however, differ greatly from environments where most flank margin caves are found and the generated caves have different morphologies from flank margin caves.

Mixing of vadose and phreatic water has also been suggested as an important mechanism to dissolve carbonate minerals at the water table (Thrailkill 1968; Bögli 1980), and possibly in the development of flank margin caves (Mylroie and Carew 1990). Recent results from North Andros Island, Bahamas suggest mixing at the top of the freshwater lens does not drive significant amounts of dissolution on carbonate islands (Whitaker and Smart 2007b). A more likely cause of the dissolution is from elevated CO_2 concentrations at the top of the water table from microbial oxidation of organic matter in soil and vadose zones (Whitaker and Smart 2007b).

Role of CO_2 in dissolution and precipitation reactions

All samples from San Salvador Island either follow a linear correlation between P_{CO2} and SI (Trend 1 in Figure 2-4) or remain near saturation regardless of P_{CO2} (Trend 2 in Figure 2-4). The difference between these trends relate to the uptake and release of gaseous CO_2 from the

water to the atmosphere and from buffering by water-rock interactions. Of the samples following Trend 1, those from Ink Well Blue Hole exhibit the largest range in P_{CO2}, but all remain undersaturated with respect to calcite regardless of the concentration of P_{CO2}. These variations in P_{CO2} likely result from respiration and photosynthesis within the blue hole, which has fresh to brackish water and a large amount of sub-aquatic vegetation, following a reaction such as:

$$CO_2 + H_2O \leftrightarrow CH_2O + O_2, \quad (2\text{-}2)$$

where CH_2O represents solid organic matter. Respiration would elevate P_{CO2} values, thereby lowering pH and carbonate mineral saturation state as shown by the samples collected in the early morning while cloud cover limited sunlight. Photosynthesis would become increasingly important during mid-morning as sunlight increased, thereby consuming CO_2, increasing the pH and reducing undersaturation (Figures 2-5B and C). Water in the blue hole also probably remains undersaturated because limited contact between the water and the sides of the blue hole (about 7 m away) would reduce the buffering influence of the carbonate minerals.

In contrast to Ink Well Blue Hole, other locations open to the atmosphere, including Watling's Blue Hole, Six Pack Pond, and Crescent Pond, are supersaturated with respect to aragonite and calcite (Figure 2-4). All of these locations have near marine salinity and show diurnal tidal fluctuations with periodicities that are similar to, but out of phase with, ocean tides, suggesting they are connected to the oceans through preferential flow systems (Teeter 1995; Crump and Gamble 2006). Unlike the water chemistry at Ink Well Blue Hole, carbonate mineral saturation at these locations reflect influence of mixing with open ocean water, rather than uptake and release of CO_2 during photosynthesis and respiration.

Unlike surface-water samples, samples collected from groundwater wells and two flank margin caves have equilibrated with aragonite and calcite, regardless of the magnitude of the

flux of CO_2 to the water. Sources of CO_2 at these sites could include root respiration and oxidation of organic matter, and these processes are heterogeneously distributed in the vadose zone and along the water table (Atkinson 1977; Wood and Petraitis 1984; Whitaker and Smart 2007b). The range of P_{CO2} along Trend 2 reflects this heterogeneous distribution of CO_2, with the flank margin cave samples clustered around log P_{CO2} of -2.7 bars and groundwater samples ranging over an order of magnitude, from a value similar to those in the flank margin caves to a log P_{CO2} of -1.3 bars (Figure 2-4). The two samples collected from Crescent Top Cave have marine salinity, but those from Majors Cave were collected from a 5 m thick transition zone with salinities ranging from about 2 to 30 psu, similar to the transition zone in Ink Well Blue Hole (Table A-1). No photosynthesis occurs in this pool because of its location in a cave, and thus CO_2 concentrations do not have diurnal variations. Regardless of the lack of variations in CO_2 concentrations, their saturation state is not controlled simply by mixing of fresh and saline water (Figure 2-6).

If elevated CO_2 concentrations control carbonate mineral dissolution, then concentrations of excess Ca^{2+} should correlate to changes in P_{CO2}, reflecting the buffering capacity of carbonate mineral dissolution. This relationship occurs at the Line Hole well field where concentrations of excess Ca^{2+} (2 to 4 mM) correlate with log P_{CO2} (-2.3 to -1.3 bars) over a distance of about 300 m extending across the freshwater lens (Figure 2-7). Heterogeneity of the system is shown by the fact that the highest and lowest concentrations occur only 60 m apart. Regardless of the variation in P_{CO2} and excess Ca^{2+} concentration, all of the samples are within 0.2 SI units of saturation with respect to aragonite, reflecting fast equilibration between water and carbonate minerals as the CO_2 concentration of the water changes. Rapid variation in P_{CO2} could result from the local generation of CO_2 in the vadose zone (e.g., Whitaker and Smart 2007b). The high porosity of

eogenetic rocks allows sufficient contact between the air mass in the vadose zone and the water table. If the fugacity of CO_2 in the vadose zone exceeds the P_{CO2} in the water, CO_2 will diffuse into the water, resulting in temporary undersaturation with respect to carbonate minerals, which is then modified by mineral dissolution. Conversely, CO_2 degassing will occur once the P_{CO2} in the water exceeds CO_2 fugacity in the vadose zone, leading to carbonate mineral supersaturation and ultimately precipitation. Although these waters remain saturated with respect to carbonate minerals, the high range in excess Ca^{2+} suggests heterogeneous dissolution and precipitation can occur across the water table. Dissolution in these water-table settings has been suggested for the development of banana holes (Harris et al. 1995).

In summary, these results indicate dissolution is a result of variations in CO_2 concentrations in the water on San Salvador Island. Enrichment of Ca^{2+} in low salinity water indicates that most of the dissolution has occurred since the freshwater recharged the island, and is a near-surface phenomenon (e.g., Vacher et al. 1990; Martin and Moore 2008). The correlation between P_{CO2} and excess Ca^{2+} suggests that while groundwaters remain near saturation at the water table, increases in CO_2 in the vadose zone can lead to further dissolution. Although this mechanism may lead to a significant increase in dissolution at the water table, the following section explores if CO_2-driven dissolution is sufficiently fast to form macroporosity at the edge of the freshwater lens where short residence times may restrict reprecipitation.

Calculation of Dissolution Rates

Under steady-state conditions, all recharge to a freshwater lens is lost to the ocean annually along with any $CaCO_3$ dissolved in the water (Plummer et al. 1976; Anthony et al. 1989; Vacher et al. 1990). This dissolved $CaCO_3$ would represent the amount of secondary porosity formed, and when coupled with estimates of the volume of recharged water could provide information on the amount of secondary porosity forming in a particular region (e.g., Plummer et al. 1976; Budd

1988; Anthony et al. 1989; Vacher et al. 1990; McClain et al. 1992; Whitaker and Smart 2007a). I make these estimates for the Sandy Point region of San Salvador, where a well-studied flank margin cave has been mapped, depositional and diagenetic timing are known, and the freshwater lens can be constrained by topographic relief and glacio-eustatic sea-level variations.

Average recharge across San Salvador Island is estimated to be 25% of annual rainfall or around 300 mm/yr (Cant and Weech 1986; Budd and Vacher 1991). Effective porosity is estimated at 30% (Vogel et al. 1990). The size of the freshwater lens at Sandy Point is estimated to be about 1.5 km^2 for the MIS 5e highstand by assuming the 6 m contour interval represents the boundary of the lens (Carew and Mylroie 1997) (Figure 2-1C). Recharge over this area would provide around 4.5 x 10^8 liters of water available to discharge to the ocean each year. The average excess Ca^{2+} concentration of 2.0 mM in San Salvador freshwater (Figure 2-2E) represents an average amount of Ca^{2+} derived from dissolution of $CaCO_3$, similar to values estimated from other islands in the region (Budd 1988; Whitaker and Smart 2007a). These values of discharge and excess Ca^{2+} concentration suggest 2.1 x 10^{-4} kg/l of $CaCO_3$ would be flushed to the ocean each year. With a density of 2.93 g/cm^3 for aragonite, this magnitude of dissolution reflects 46 m^3 of $CaCO_3$ dissolved per year or 31 $m^3/km^2 \cdot yr$ when normalized to lens area (Table 2-1). Given a dissolution rate of 31 m^3/km^2 yr, approximately 138 m^3 of rock would have dissolved at the location of Altar Cave (areal footprint of 4.5 x 10^{-4} km^2) during the estimated amount of time, about 10 ky, available for the cave to form. A volume of 138 m^3 is only about 12% of the cave volume, which has been mapped to be a minimum of 1200 m^3 (Florea et al. 2004). This calculation indicates dissolution rate at the site of Altar Cave was greater than the average value across the island.

The amount of dissolution required to form Altar Cave can also be estimated from the volume of water flowing through the space occupied by the cave. Flank margin caves, observed on this cliff and elsewhere throughout the Bahamas, commonly have a semi-regular spacing parallel to the paleo-shoreline, suggesting all caves at any one location formed concurrently, rather than sequentially (Vogel et al. 1990; Labourdette et al. 2007). Although dissolution voids may alter the flow field, high porosity of island carbonates suggests flow would not have been diverted much beyond the boundary of the void (Lascu 2005). Consequently, I estimate the width of the catchment supplying water to form Altar Cave was 50 m, and if it extended about 200 m upslope to the groundwater divide to the east, the catchment area would be about 0.01 km^2 (Figure 2-1C). The width for the catchment area is probably a maximum given that the greatest width of the cave is about 15 m (Florea et al. 2004). Assuming 300 mm/yr recharge, the annual flushing rate for this catchment area would be about 3.0×10^6 l/yr, which would need to remove only 8.2×10^{-5} kg/l of dissolved $CaCO_3$ away from the locus of cave development to form Altar Cave in 10 ky (Table 2-2). This amount is about 40% of the average dissolved $CaCO_3$ concentration of 2.1×10^{-4} kg/l measured in freshwater samples of San Salvador Island and other islands in the region (Budd 1988; Whitaker and Smart 2007a). Although the magnitude of dissolution required to form Altar Cave is only 40% of that estimated across the entire island, the calculation suggests the dissolution rate was about 267 m^3/km^2 yr where Altar Cave formed, or about 9 times the average value of 31 m^3/km^2 yr (Table 2-2).

Conclusions

Diagenesis on carbonate islands usually dissolves and reprecipitates carbonate sediments with little loss or gain in bulk porosity. The presence of flank margin caves and banana holes, however, indicates that secondary macroporosity forms along the water table and at the edge of freshwater lenses in relatively short time spans of thousands of years. Although the distal edge of

freshwater lenses has been proposed to experience mixing dissolution, the models assume mechanical mixing between fresh and saline water end members. I suggest such mechanical mixing may be limited on small carbonate islands due to factors including limited recharge and thick transitions zones that inhibit mixing of the end members. Instead, most dissolution on San Salvador occurs in freshwater from elevated concentrations of CO_2. This dissolution is sufficient to produce flank margin caves but only when the hydrodynamics of the freshwater lens flush reaction products from the zone of dissolution. Within a freshwater lens, specific discharge is elevated at the water table and increases to a maximum at the seaward edge of the lens. Where local sources of CO_2 drive dissolution near the water table at the lens edge, flank margin caves may develop as reactions products are flushed to the ocean. Where local sources of CO_2 drive dissolution at the water table, banana holes may form. Banana holes are smaller than flank margin caves since lower flow velocities away from the lens edge may provide sufficient time for some reprecipitation. This hypothesis predicts that cementation may be greater around the boundaries of banana holes than in areas that lack these caves. Mass balance calculations indicate that with focused dissolution, only about 40% of the carbonate found to be dissolved annually on San Salvador Island is required to form the observed flank margin caves. Because all excess Ca^{2+} must be derived from carbonate dissolution, macroporosity through small ocean islands may be more widespread than is observed, possibly because not all caves have been breached or because some of the secondary porosity is not large enough for human exploration. Results of this study suggest that distribution of resources, such as water and hydrocarbons, in ancient carbonate platforms may be concentrated in areas where local sources concentrate CO_2 and flow is sufficient to remove reaction products from the region where dissolution occurs.

Table 2-1. Calculated dissolution in a freshwater lens at Sandy Point during the MIS 5e highstand.

Freshwater lens at Sandy Point	
Lens area (km^2)	1.5
Rainfall (mm/yr)	1200
Recharge (mm/yr)[a]	300
Flushing (l/yr)	4.5×10^8
Dissolved $CaCO_3$ (kg/l)[b]	2.1×10^{-4}
Dissolution (kg/yr)	9.5×10^4
Volume dissolved	
(m^3/yr)[c]	46
($m^3/km^2 \cdot yr$)	31

[a]Based on estimated recharge of 25% of average total rainfall. [b]Based on average excess Ca^{2+} in freshwaters from San Salvador Island. [c]Assuming aragonite density of 2.93 g/cm^3 and porosity of 30%.

Table 2-2. Calculation of dissolution at Altar Cave.

Lens section for cave development	
Catchment zone (km^2)	0.01
Rainfall (mm/yr)	1200
Recharge (mm/yr)	300
Flushing (l/yr)	3.0×10^6
Area of Alter Cave (km^2)[a]	4.5×10^{-4}
Required Dissolved $CaCO_3$ (kg/l)	8.2×10^{-5}
Dissolution (kg/yr)	246
Volume dissolved	
(m^3/yr)	0.12
($m^3/km^2 \cdot yr$)[b]	267

[a]Areal footprint. [b]Dissolution rate for the formation of Altar Cave in 10 ky

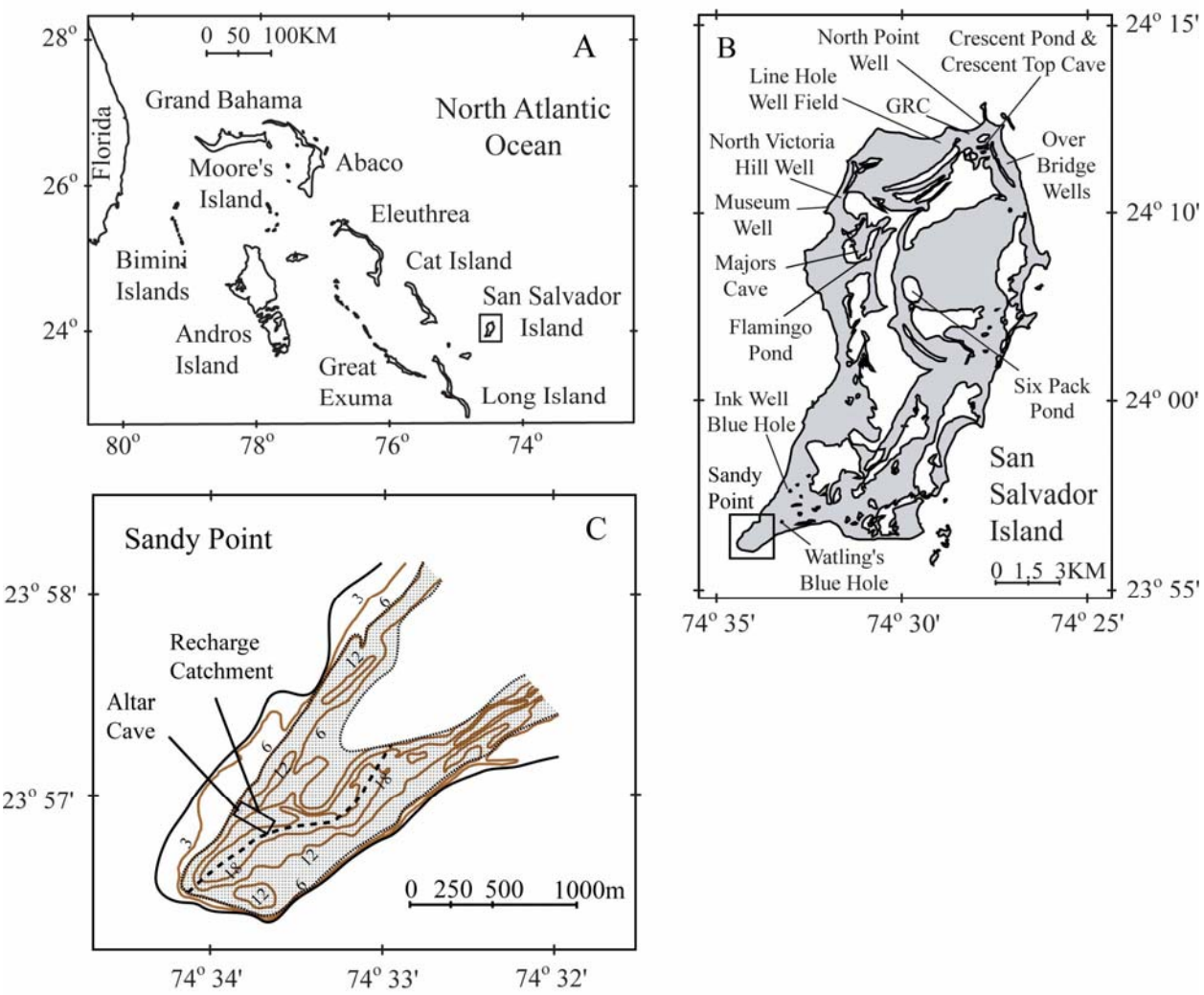

Figure 2-1. Maps of Bahamian archipelago and San Salvador Island. A) Map of Bahamian archipelago showing location of San Salvador Island. B) Map of San Salvador Island showing location of sample sites and location of Sandy Point. Gray area is land and white area is water. C) Map of Sandy Point in the southwest portion of San Salvador Island showing location of Altar Cave and recharge catchment for Altar Cave. Contour lines represent present-day land elevation in meters above sea level. Stippled area shows the area of the freshwater lens at Sandy Point during the MIS 5e highstand, and dashed line approximates the ground-water divide. Catchment area shows estimated maximum area (~0.01 km^2) of the freshwater lens that would contribute flow to Altar Cave location.

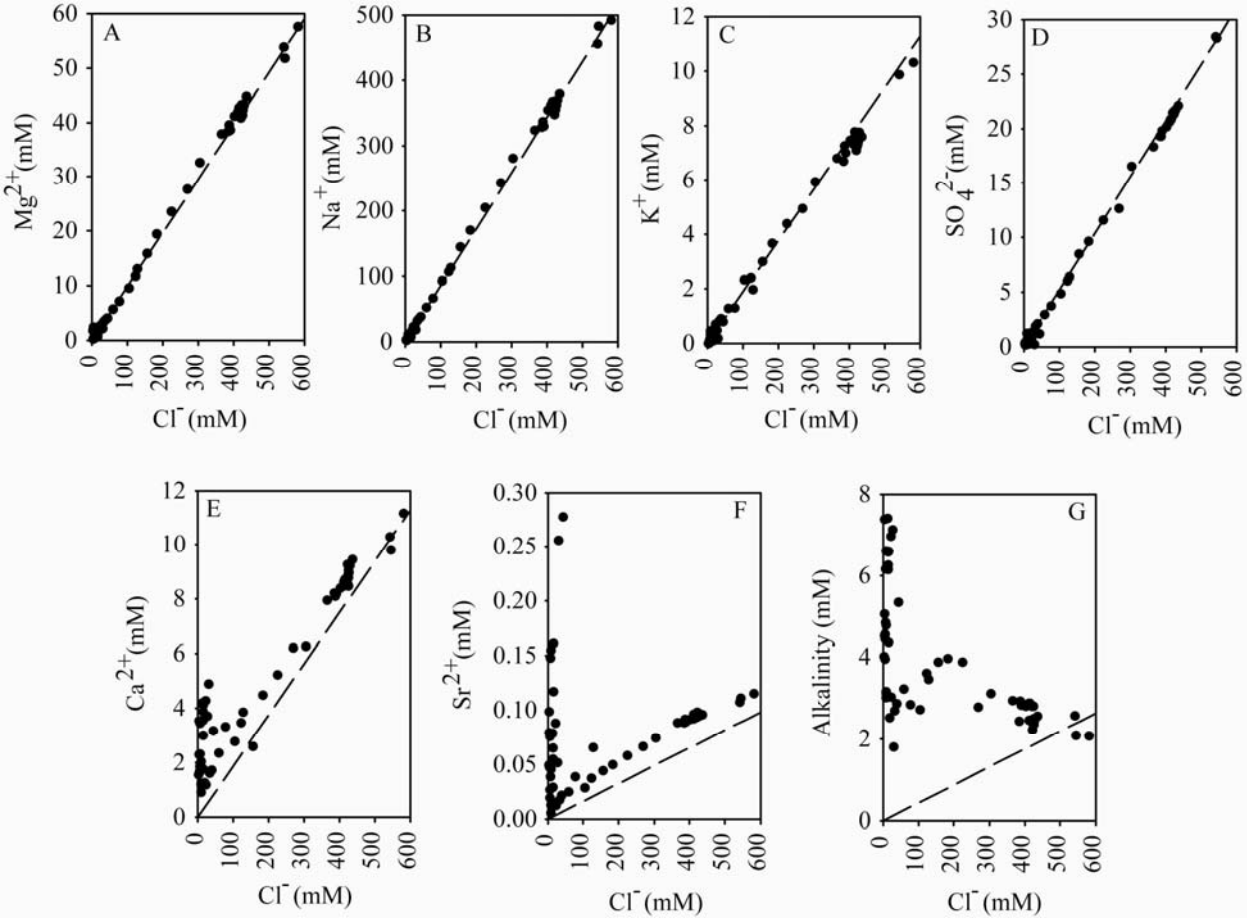

Figure 2-2. Plots of major ion versus chloride concentrations in all samples. A) Plot of Mg^{2+}. B) Plot of Na^{+}. C) Plot of K^{+}. D) Plot of SO_4^{2-}. E) Plot of Ca^{2+}. F) Plot of Sr^{2+}. G) Plot of Alkalinity. Dashed line in each plot represents conservative mixing between freshwater and seawater end members.

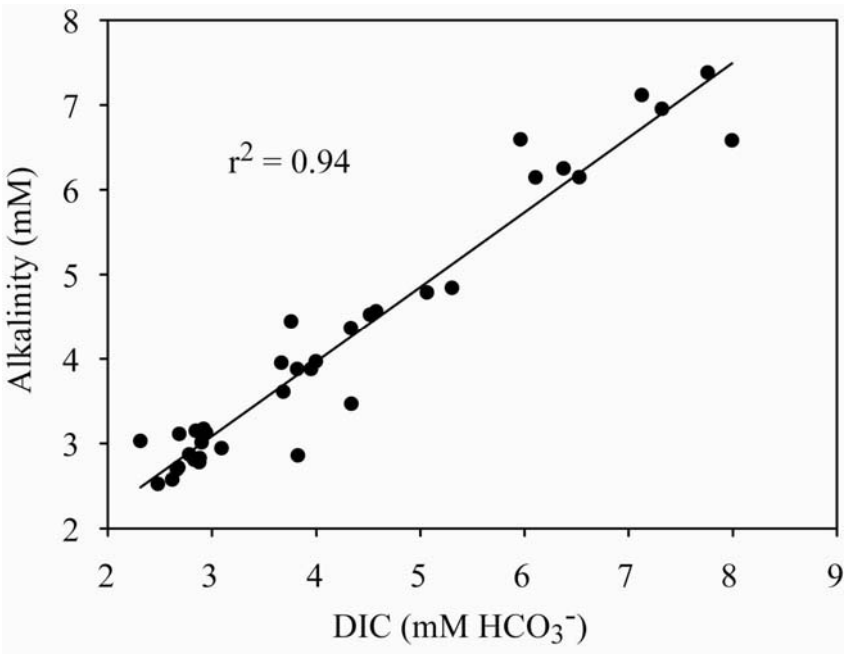

Figure 2-3. Comparison of DIC and total alkalinity in samples collected in June 2006 and April 2007. Solid line is a linear regression DIC and total alkalinity.

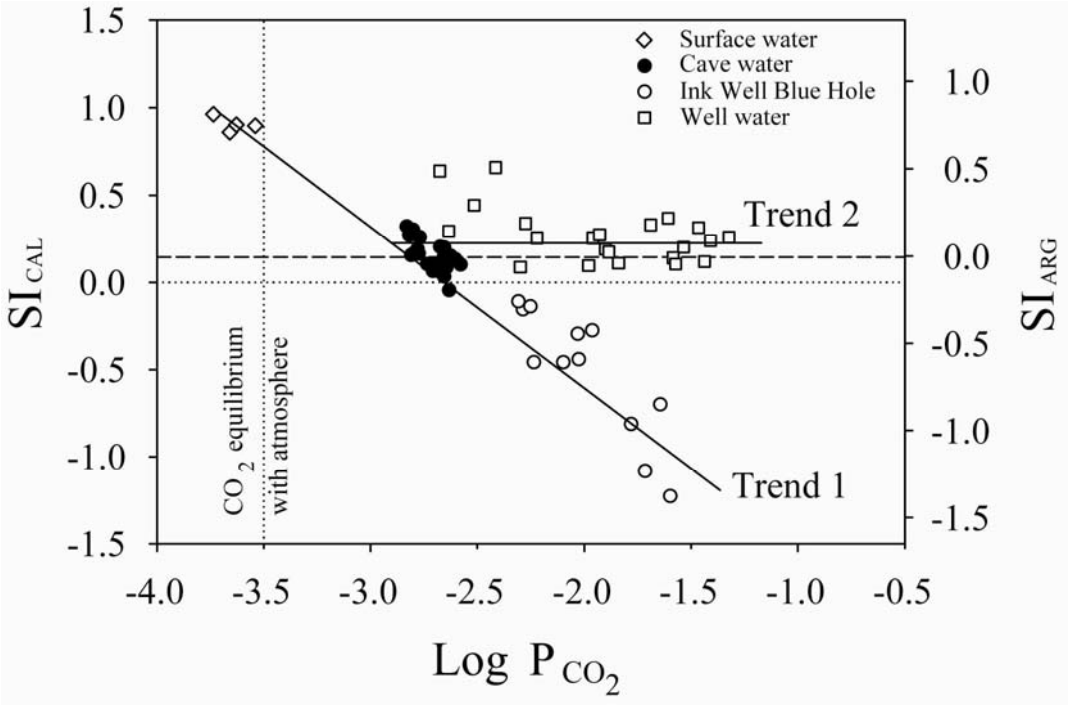

Figure 2-4. Relationship between P_{CO_2} and aragonite and calcite saturation in all water samples. Carbonate mineral saturation in samples following Trend 1 is controlled by P_{CO_2}. Conversely, samples following Trend 2 are in equilibrium with respect to aragonite regardless of P_{CO_2}.

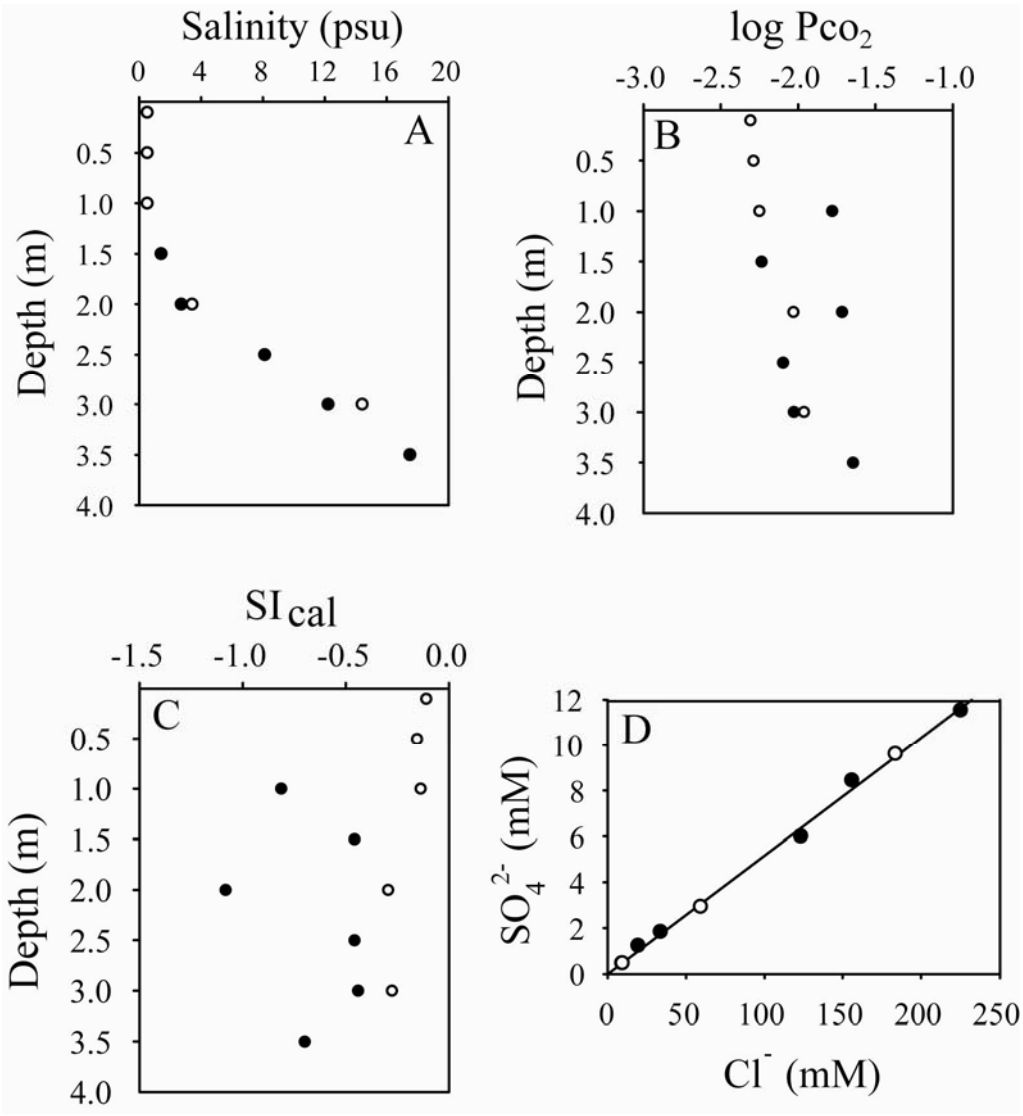

Figure 2-5. Water samples collected from Ink Well blue hole in April 2007. Black circles represent first series of samples collected in the morning during a one hour period with cloud cover, and white circles represent a second series of samples collected mid-morning with no cloud cover immediately following the first series of sample collection. A) Salinity versus depth. B) Comparison of P_{CO_2} versus depth. C) Comparison of calcite undersaturation versus depth. D) Plot of SO_4^{2-} versus Cl^-. Solid line represents expected SO_4^{2-} concentration due to conservative mixing. Three white circles have similar chemistry, and thus overlay each other near the graph's origin.

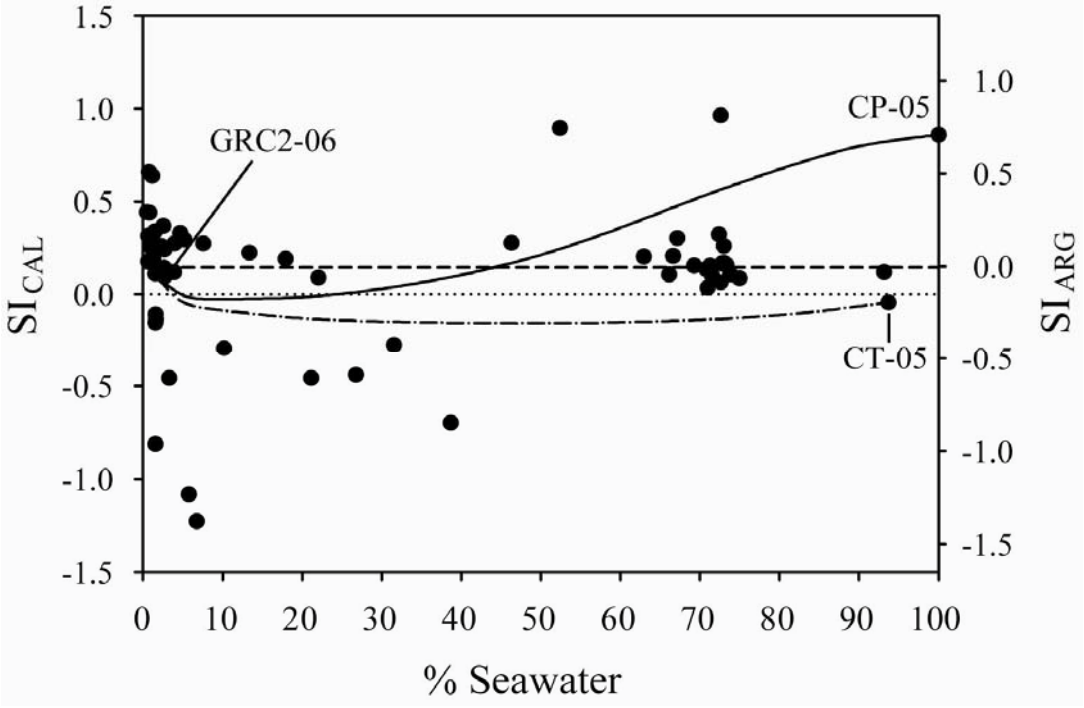

Figure 2-6. Saturation indices (SI) for all San Salvador waters relative to aragonite and calcite versus percent seawater. Curved lines show SI for mixing between freshwater sample GRC2-06 and seawater sample CP-05 (solid line) and saline water sample CT-05 (dashed line).

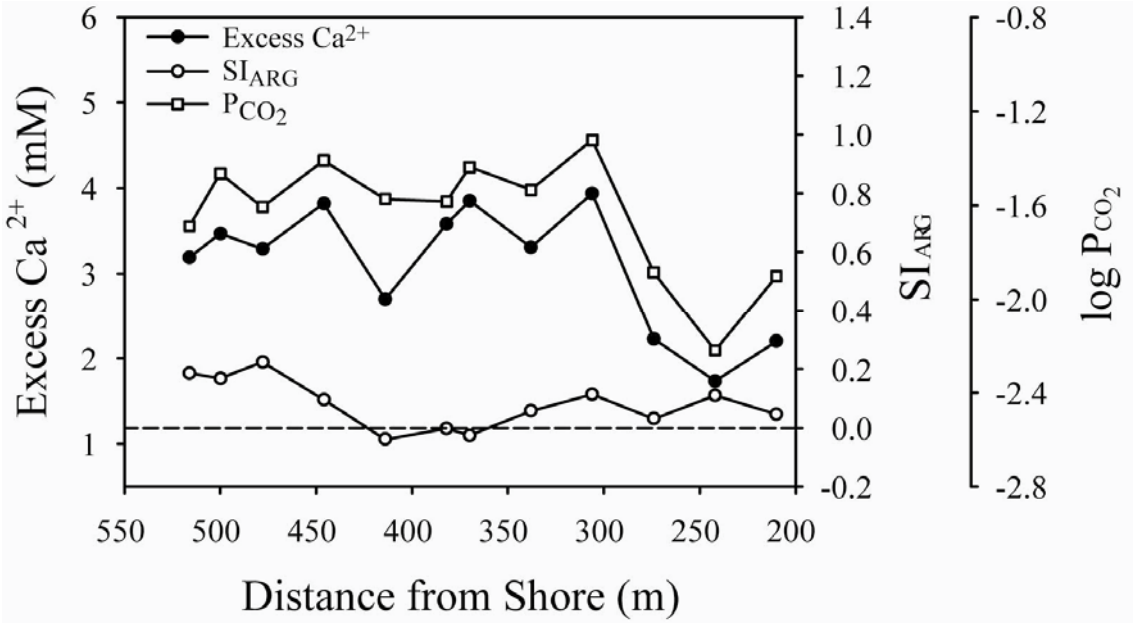

Figure 2-7. Plot of excess Ca^{2+}, saturation index of aragonite, and log P_{CO2} of water from the Line Hole well field, showing a strong correlation between P_{CO2} and excess Ca^{2+}. The wells penetrate the top of a single freshwater lens, and are aligned almost perpendicular from the shore from about 200 to 500 m.

CHAPTER 3
GEOCHEMICAL AND STATISTICAL EVIDENCE FOR RECHARGE, MIXING, AND CONTROLS ON SPRING DISCHARGE IN AN EOGENETIC KARST AQUIFER

Introduction

Karst aquifers are characterized by heterogeneous distributions of various types of porosity including intergranular porosity within the matrix rock, fractures along joints, faults and bedding planes, and conduits enlarged through dissolution. This porosity distribution influences nearly all aspects of aquifer characteristics, including aquifer storage and distribution of permeability. The range of porosity and permeability determines flow paths and allows extreme flow rates including both laminar and turbulent flow (Worthington 1994; Quinlan et al. 1996; White 1999; Halihan et al. 2000). While most flow in karst aquifers occurs through conduits, storage is primarily in the matrix porosity (e.g., Worthington et al. 2000). Matrix porosity and permeability also affect recharge to the aquifer, which can vary on seasonal and individual storm time scales. Karst aquifer recharge commonly occurs as point source (allogenic) recharge into swallets or as diffuse recharge through the vadose zone (e.g., White 1988; Ford and Williams 2007; Ritorto et al. in press). Upward flow of water from deep within an aquifer may also contribute to an aquifer's shallow water budget and chemistry, depending on the distribution of porosity, permeability, and hydraulic head (Kohout et al. 1977; Smith and Fuller 1977; Hughes et al. 2007).

Flow paths and sources of recharge to karst aquifers have long been assessed through physical and chemical variations in springs (e.g., Shuster and White 1971; Dreiss 1989). In most well-studied cases, springs are in regions with dense, recrystallized rocks (i.e., telogenetic karst, Vacher and Mylroie 2002), where low matrix permeability restricts most of the flow to conduits and fracture networks. Individual springs exhibiting large variations in discharge and chemical composition through time have been inferred to be dominated by allogenic recharge and conduit

flow. In contrast, springs with smaller amounts of chemical variability and discharge have been inferred to be dominated by diffuse recharge and diffuse flow through fracture networks (Shuster and White 1971; Ternan 1972; Smart and Hobbs 1986; Hess and White 1988; Dreiss 1989). These studies assume that spring variability results largely from variation in recharge and the flow paths of that recharge. Considering only these few parameters limits the understanding of the karst system that can be derived from variations in spring-water chemistry. For example, physical and chemical variations in springs issuing from the karstic Inner Bluegrass region of Kentucky fail to reflect the geometry of the aquifer's conduit system because differences in lengths of flow paths mask variations in conduit sizes that source the springs (Scanlon and Thrailkill 1987). Consequently, a question I explore in this paper is what additional insight can be gained from physical and chemical monitoring of spring flow and chemical composition.

Large springs also discharge from carbonate rocks that retain high matrix porosity and permeability (i.e., eogenetic karst, Vacher and Mylroie 2002). In these rocks, high matrix permeability allows access to aquifer storage and diffuse recharge, which constitute a substantial component of spring discharge (e.g., Florea and Vacher 2006; Ritorto et al. in press). Numerous springs that discharge from the eogenetic Upper Floridan aquifer (UFA) appear to be fed primarily from diffuse recharge transmitted through the rock matrix (e.g., Martin and Gordon 2000; Florea and Vacher 2006). Other springs discharging from the UFA are directly connected by conduits to allogenic inputs so that the source of water to these springs depend on the hydraulic head gradient between the conduit and surrounding aquifer matrix (Katz et al. 1998; Screaton et al. 2004; Loper et al. 2005; Martin et al. 2006). When allogenic inputs allow conduit hydraulic head to exceed head in the surrounding matrix, allogenic recharge accounts for most to all of the spring discharge, with an additional fraction of the recharge stored temporarily in the

matrix until the flood pulse recedes and hydraulic head gradients reverse (e.g., Screaton et al. 2004; Martin et al. 2006). Following head reversal, spring discharge is a mixture of water stored temporarily in the matrix, allogenic recharge, and water recharged diffusely to the matrix from the surface. This interaction between allogenic recharge and diffusely recharged water can lead to high variability in discharge and spring-water chemistry (e.g., Katz et al. 1998; Crandall et al. 1999; Katz et al. 2001; Martin and Dean 2001; Katz 2004; Katz et al. 2004; Screaton et al. 2004; Martin et al. 2006). Assessing origins of water, which is needed to understand susceptibility of karst areas to contamination, requires a clear understanding of processes causing variations in groundwater chemistry and connectivity between conduit and matrix porosity (e.g., McConnell and Hacke 1993; Plummer et al. 1998; Katz 2004).

In this chapter I use major element chemistry, physical conditions including river stage, precipitation, evapotranspiration (ET), temperature gradients of groundwater, and a multivariate statistical method (principal component analysis; PCA) to evaluate how multiple sources of water and variations in aquifer flow paths influence a first magnitude spring draining a portion of the eogenetic UFA. I suggest that knowledge of the spatial and temporal variation of groundwater chemistry is necessary to separate sources of water and components of flow, which cannot be resolved by only monitoring spring discharge, and that mixing of these water sources plays an important role in temporal variations of spring chemistry. Because of the importance of groundwater sources to spring-water chemistry, matrix porosity in eogenetic aquifers appears to be significant to spring discharge even where dominated by conduits.

Study Area

The Santa Fe River is a tributary of the Suwannee River, with a watershed covering about 3600 km^2 in north-central Florida (Hunn and Slack 1983). Land use in the watershed is mainly agricultural, primarily as improved pastures and row and field crops (Kautz et al. 2007). In the

watershed, Oligocene and Eocene carbonate rocks make up the UFA (Figure 3-1). The aquifer is confined by the Hawthorn Group to the northeast, comprised in part of Miocene and younger siliciclastic-dominated rocks (Scott, 1988; Groszos et al., 1992), and is unconfined in the southwest where the confining unit has been removed by erosion (Figure 3-2). The erosional edge of the Hawthorn Group is referred to as the Cody Scarp (Puri and Vernon 1964). To the northeast of the scarp, surface water is common on the confining unit, but is limited to the southwest where streams crossing the scarp either become losing streams, sink underground and reemerge, or disappear underground with no clear point of reemergence.

The Santa Fe River flows westward from Lake Santa Fe for about 40 km until it reaches the Cody Scarp, where it sinks into a 36-m deep sinkhole at the River Sink in O'Leno State Park (Figure 3-2). The river flows underground through a network of conduits until it reemerges about 6 km from the River Sink as a first magnitude spring, called the River Rise, marking the headwaters of the lower Santa Fe River (Martin and Dean 2001). The conduits rise to the surface intermittently between the River Sink and River Rise at several karst windows (Figure 3-2).

At the Santa Fe Sink-Rise system, the UFA is about 430 m thick, unconfined at the surface, and is covered by a thin veneer (about 4 m, depending on land-surface elevation) of unconsolidated sands and sediments (Miller 1986). In this area, Oligocene carbonate rocks are absent and no middle confining unit exists, resulting in the UFA extending from the Upper Eocene Ocala Limestone to the lower confining unit of the Lower Eocene Cedar Key Formation (Miller 1986) (Figure 3-1). Potable water extracted from the aquifer is estimated to come from the upper 100 m of the Ocala Limestone, with more mineralized water in deeper portions of the aquifer (Hunn and Slack 1983; Miller 1986). Porosity and matrix permeability of the Ocala Limestone average about 30% and 10^{-13} m^2, respectively (Budd and Vacher 2004; Florea 2006).

Exploration of the submerged conduits upstream of the River Rise has resulted in over 15 km of surveyed passage (Poucher 2007). Average dimensions of the conduits range from 18 to 24 m wide and 12 to 18 m high with an average depth of about 30 m below the ground surface (mbgs) (Screaton et al. 2004; Poucher 2007). The conduit system has not been completely mapped from the River Sink to River Rise, but high flow rates detected by natural and artificial tracers show the two locations are linked by conduits (Hisert 1994; Martin and Dean 1999; Moore and Martin 2005).

Previous work has shown that water discharging from the River Rise varies between sources from the River Sink and from groundwater, defined here as water stored in the aquifer surrounding the conduits (e.g., Martin and Dean 1999; Martin and Screaton 2001; Screaton et al. 2004; Martin et al. 2006). During high flow, discharge at the River Rise is mostly derived from water entering the conduit system at the River Sink. As river stage and input into the River Sink decreases, increasingly larger percentages of groundwater drain from the surrounding aquifer into the conduit system to discharge at the River Rise (Martin and Screaton 2001).

Methods

River Stage and Potential Recharge

Stage of the Santa Fe River was monitored about 200 m downstream of the River Rise with an automatic pressure transducer with an accuracy of ±0.03 m. A separate barometric data logger (±0.0045 m) was used for barometric compensation of the non-vented transducer. The water levels were recorded at 10-minute intervals, and the data were downloaded from the recorder at four- to five-week intervals. When the data were downloaded, the river stage was measured from a staff gauge, and the recorded water level was referenced to the gauge for each download period to correct for drift. The relationship between stage and discharge at the River Rise was calculated based on the rating curve developed by Screaton et al. (2004), using data

collected by the Suwannee River Water Management District (SRWMD). Potential recharge was estimated as precipitation minus evapotranspiration (P-ET) during the study period by Ritorto et al. (in press). Briefly, daily values of P-ET are estimated using daily precipitation data collected in O'Leno State Park using an automated rain gauge maintained by SRWMD (http://www.srwmd.state.fl.us/index.asp?NID=99), and the Penman-Monteith model for estimating daily ET, which estimates water loss to the atmosphere from a vegetative surface (Dingman 2002).

Field Sampling and Laboratory Analysis

Sixteen sampling trips were conducted from January 2003 to April 2007 to collect water from eight groundwater monitoring wells, one sinking stream (River Sink), one first magnitude spring (River Rise), and four intermediate karst windows (Figure 3-2). Monitoring wells were drilled to depths of about 30 mbgs, approximately at the depth of the conduits, and screened over 6-m (20 foot) depth intervals using 250 µm PVC screening material attached to 51 mm (2 inch) diameter PVC linear. Groundwater samples were collected from monitoring wells using a Grundfos II submersible pump. Surface-water samples were collected on shore with a peristaltic pump attached to tubing that was pushed close to spring boils when visible, or in the deepest part of the sinkhole if no boil was present. Field measurements of temperature (T), pH, and specific conductivity (SpC) were recorded with a YSI multiprobe model 556 prior to sampling. The probe was calibrated at the start of each sampling day, and calibration was checked several times while in the field. All samples were collected unfiltered in high density polyethylene (HDPE) bottles. Samples collected for cations were preserved with either sulfuric (Na^+ and K^+) or nitric acid (Ca^{2+} and Mg^{2+}) to a pH < 2.0, while samples for anions and alkalinity were collected with no preservatives. Samples were stored on wet ice until they were delivered to the laboratory for analysis.

Concentrations of major ions (Na^+, K^+, Ca^{2+}, Mg^{2+}, Cl^-, and SO_4^{2-}) and alkalinity were analyzed by a NELAC-certified laboratory, Advanced Environment Laboratories, Inc., in Gainesville, FL. Analyses were determined in accordance with Environment Protection Agency (EPA) protocols for each analyte (EPA 1983). Data from quality-assurance samples indicate no contamination resulted from sampling procedures and equipment, and that good analytical reproducibility occurred in the laboratory. Charge balance errors for most samples were ±5% except for samples whose concentrations were near instrument detection limits.

Principal Component Analysis

Principal component analysis (PCA) is a multivariate statistical technique used to reduce the complexity of and decipher patterns within large data sets by determining a small number of variables that account for the greatest variance in all of the original variables (Wold et al. 1987; Jolliffe 2002). For this study, PCA was applied to a normalized data matrix of 9 variables (river stage, pH, Cl^-, SO_4^{2-}, Ca^{2+}, Na^+, Mg^{2+}, K^+, and alkalinity concentrations) from 211 water samples using the *princomp* function in Matlab (Statistics toolbox 5.0, Mathworks, Waltham, MA). Because the data have large ranges and different units of measurement (e.g., stage and concentration), data were normalized by centering the data set about zero by subtracting the means of each variable set from the measured value for individual samples and dividing each value within the variable set by its standard deviation (Stetzenbach et al. 1999; Chen et al. 2007). Consequently, each variable was normalized to unit variance and thus contributes equally to the analysis.

Principal components (PC) are eigenvectors of the correlation matrix of the normalized data set, and represent correlation coefficients, called loadings, between each variable and each PC. Since the correlation matrix is symmetrical, the eigenvectors are orthogonal and thus each PC is projected as an uncorrelated axis in a new space that helps explain the relationship among

data points or variables along each PC. Positive loadings show a direct relationship, and those with the strongest absolute magnitude exert the greatest influence on the PC. The first PC accounts for the greatest fraction of variance of the correlation matrix, followed by subsequent components reflecting less variance. Principal component scores are transformed data points projected into PC space by axis rotation and correlating the weight of each loading variable to the original, normalized data. By plotting PC scores, similarities and disparities can be observed between the samples. For example, PC scores that cluster show their variance results from similar variable loadings, and thus suggest similar processes influence the samples. Furthermore, PC scores that vary along linear trends suggest variable loadings that affect these samples may exhibit some systematic variations such as, in this case, through time or with changing stage. In contrast, dissimilar PC scores show samples that are unrelated, likely suggesting these samples are influenced by independent processes.

Estimate of Vertical Flow Rate from Temperature Perturbations

Upwelling of deep water can be estimated assuming vertical flow within the UFA drives heat transfer following one-dimensional steady-state flow described by:

$$\frac{\partial^2 T_Z}{\partial z^2} - \left(\frac{c_w \rho_w v_Z}{k}\right)\left(\frac{\partial T_Z}{\partial z}\right) = 0 \qquad (3\text{-}1)$$

where T_z is temperature at depth z, ρ_w is density of water, c_w is heat capacity of water, v_z is vertical Darcy velocity of water (positive for downward flow and negative for upward flow), k is thermal conductivity of the porous material (Bredehoeft and Papadopulos 1965). With boundary conditions of T_O as the uppermost T at z = 0 and T_L as the lowermost T at z = L yields a solution to Equation 3-1 for T_Z of:

$$T_Z = T_O + (T_L - T_O)\left(\frac{\exp\left(\beta\left(\frac{z}{L}\right)\right)-1}{\exp(\beta)-1}\right) \quad (3\text{-}2)$$

(Bredehoeft and Papadopulos 1965), where L is the thickness of the vertical section and β is the dimensionless Peclet number for heat transfer:

$$\beta = \frac{\rho_w c_w v_Z L}{k}. \quad (3\text{-}3)$$

Rearranging Equation 3-3 for v_z yields an expression for the vertical flow rate of:

$$v_Z = \frac{k\beta}{\rho_w c_w L}. \quad (3\text{-}4)$$

Results

River Stage and PE-T

Average river stage during the entire study period was 10.2 masl with an average discharge of about 16 m^3/s (Figure 3-3). Samples collected during trips S-2, S-9, and S-11 occurred during high flow events when the river was above average stage. All other samples were collected during average or low flow.

Within the study area, changes in river stage appear to correlate positively over long time periods with P-ET, but this relationship seems to breakdown for individual events suggesting that antecedent conditions are important to river stage and discharge (Figure 3-3). Between January 2003 and April 2007, average annual P-ET was about 400 mm (Ritorto et al. in press). The maximum annual P-ET of about 990 mm occurred in 2004 due to an active hurricane season (see Florea and Vacher 2007), which resulted in the highest stage of 14.1 masl. This high stage occurred immediately after Hurricane Frances delivered a total of 400 mm of P-ET to O'Leno State Park over a 6-day period in September 2004 (Figure 3-3). The lowest stage of 9.6 masl

occurred in April 2007 following a year-long drought that resulted in the area receiving a total of 83 mm of P-ET.

In addition to long-term events affecting stage, short-duration storms that exceed ET also cause variable responses in river stage, but these events did not cause a systematic response in the river (Figure 3-3). Six rain events that produced a total of 232 mm of P-ET over a 39-day period in February and March 2003 caused a 3-m rise in river stage on March 13, 2003. In February 2004, about half of the P-ET in February and March 2003 (144 mm) produced only a tenth of the increase in river stage (0.33 m) seen the previous year. Conversely, only about 82 mm of P-ET over an 11-day period in March 2005 resulted in a 1.8-m rise in river stage on March 30, 2005.

Water Temperature and Chemistry

Temperature of the water at the surface water sites vary depending on the air temperature (e.g., Martin and Dean 1999), but temperature of the groundwater is more consistent, although variable among the wells. Temperatures at all wells, except Well 2, averaged around 21°C with small variations between sampling times (Table 3-1). These measured temperatures are similar to average air temperature in the region as well as the typical temperature of water discharging from the regional springs (Hunn and Slack 1983). In contrast, water temperatures are higher and more variable at Well 2 than all other wells, ranging from about 22 to 26°C, with the highest temperature measured following a one-year drought.

The chemical variations from two surface-water sites (River Sink and River Rise) and three groundwater wells (Wells 2, 4, and 7) are shown in a Piper diagram (Figure 3-4). A statistical summary of the major chemistry is shown in Table 3-1. These five sites show the greatest variation in water chemistry, and all of the other sites that were sampled during the study (data not reported here) have chemical compositions similar to one of these five sites. These five

sites are thus used to represent the continuum of water chemistry across the region (Figure 3-4). The variation in water chemistry reflects three end-member sources that develop two mixing trends. One trend extends from one end member characterized by a Ca-HCO_3 composition (① in Figure 3-4) to another with Ca^{2+} and Mg^{2+} as the primary cations, but with more SO_4^{2-} and less HCO_3^- as the charge-balancing anion (② in Figure 3-4). The composition of Well 4 reflects the Ca-HCO_3-type end member. Water from Well 2 has a chemical composition reflecting a strong influence from the Ca-Mg-SO_4-type end member, although the high CV of major element concentrations, SpC, and T suggests contributions of this end member are variable at this site (Table 3-1). For example, SpC and T at Well 2 range from 488 to 1315 μS/cm and 22 to 26 °C, respectively. Well 7 falls along the mixing trend between Well 4 and 2, suggesting it may be influenced by both sources of water (Figure 3-4).

The third end member is characterized by elevated concentrations of Na^+ and Cl^-, and occurs at the River Sink at high flow (③ in Figure 3-4). This end member develops a second mixing trend that is confined to water collected from the surface-water sites, but this trend reflects extensive mixing between all three end members. During certain sample trips (e.g., S-3, S-4, S-6, S-10, and S-12 through S-16), water from the River Sink and River Rise fall along the mixing line between Wells 4 and 2, reflecting little influence from the Na-Cl-type end member (Figure 3-4).

Principal Component Analysis

Principal component analysis identifies which of the measured components provide the greatest variation in the composition of the water (e.g., Stetzenbach et al. 1999, 2001; Chen et al. 2007; Fournier et al. 2007). The first three PCs (eigenvalues of 4.87, 2.13, and 1.16, respectively) explain a total of 91% of the variance, or 54%, 24%, and 13%, respectively (Table 3-2). When PC 1 and 2 are considered together, differences in the loadings are represented by

two clusters and one outlier (Figure 3-5A). One cluster shows a strong positive loading (loading > 0.3: *italics* font Table 3-2) of Na^+, Mg^{2+}, K^+, Cl^-, and SO_4^{2-} on PC 1. While these components carry similar weights on PC 1, only K^+ also has a strong positive loading on PC 2 followed by weaker positive loadings of Cl^- and Na^+. Although SO_4^{2-} and Mg^{2+} are heavily loaded on PC 1, they show no loading on PC 2. The other cluster of pH, alkalinity, and Ca^{2+} has a weak positive loading on PC 1 and a strong negative loading on PC 2. The single variable that plots as an outlier in Figure 3-5A is river stage, which has a weak negative loading on PC 1 and a strong positive loading on PC 2. When PC 2 and PC 3 are considered together, a strong inverse relationship exists between the pH and river stage, suggesting that these two components are responsible for most of the 13% variance on PC 3, since Ca^{2+} has similar loadings on both PC 2 and PC 3 and alkalinity remains negatively loaded on PC 3 although less on PC 2 (Table 3-2).

The PC scores for each sample are calculated as the sum of the PC loading times the normalized values for that sample, e.g.,

$$\begin{aligned}\text{PC 1 score} = {} & 0.08(\text{pH}) + 0.42(\text{Cl}) + 0.44(\text{SO}_4) + 0.27(\text{Ca}) + 0.44(\text{Na}) \\ & + 0.44(\text{Mg}) + 0.39(\text{K}) + 0.05(\text{alkalinity}) - 0.10(\text{stage}).\end{aligned} \tag{3-5}$$

These values thus represent the relative influence each loading has on the water sample for a given PC. While all surface- and groundwater sites were included in the PCA, only sites that reflect the greatest variation in water chemistry and most closely define the end-member compositions (i.e., those sites shown on Figure 3-4) are plotted in Figure 3-5B.

The advantage of plotting PC scores in this fashion over using Piper diagrams is that the variation in samples can be observed at a higher resolution, thereby revealing additional information and relationships previously unrecognized (e.g., Melloul and Collin 1992; Laaksoharju et al. 1999; Olofsson et al. 2006). For example, the strong positive loading of K^+ on both PC 1 and 2 suggests multiple sources of K^+, such as dissolution of K-bearing minerals,

application of fertilizers to the land surface, and seawater. This information is masked in the Piper diagram because Na^+ and K^+ are grouped together during ion balancing. Although samples from Wells 2, 4, and 7 lie along the mixing trend between the Ca-HCO_3 and Ca-Mg-SO_4-type end members in the Piper diagram (Figure 3-4), their projection in PC space allows observations of additional relationships and disparities (Figure 3-5B). For example, water from Wells 4 and 7 have slightly negative PC 1 scores with minimal variability, but show greater variability on PC 2. Conversely, water from Well 2 is highly variable on both PC 1 and PC 2 scores with the strongest positive PC 1 scores of any water sampled. In addition to the groundwater samples, surface-water samples from the River Sink and River Rise show some variance on PC 1, which are scattered and overlap each other on the negative side, but separate into two distinct groups on the positive side. Most of the variance in these samples occurs on the positive side of PC 2, which relates directly with stage and inversely with loadings of pH, alkalinity and Ca^{2+}.

Discussion

Temporal variations in spring discharge and chemistry have often been used to understand groundwater flow paths and sources of recharge in both telogenetic and eogenetic aquifers because springs are commonly assumed to reflect processes that occur over large scales and may be the only point of access to the groundwater (e.g., Shuster and White 1971; Dreiss 1989; Katz 2004; Vesper and White 2004; Toth and Katz 2006). Recent studies, however, suggest monitoring the spatial and temporal variations in groundwater may elucidate additional aquifer parameters unrecognized by only monitoring karst springs (Scanlon 1989; Martin and Dean 2001; Toran et al. 2007). In the following section, I use representative end-member water types to describe the sources of water to the sink-rise system, followed by a mass-balance calculation to estimate the relative contribution each source provides to spring discharge at the River Rise. Comparison of these results to physical conditions, including river stage, precipitation, and ET,

provides insight to the complex nature of the aquifer that could be overlooked if aquifer characteristics were determined only by monitoring the spring. This analysis illustrates the importance of coupling groundwater monitoring, physical conditions, and spring discharge and chemistry when interpreting the physical and chemical characteristics of karst aquifers.

End-member Chemistry and Sources of Water

Allogenic recharge

When PC loadings and scores are considered together, the source of water entering the River Sink has a statistical association with stage (Figure 3-5). Positive loadings of stage, K^+, Na^+, and Cl^- and negative loading of pH, Ca^{2+}, and alkalinity on PC 2 suggest allogenic recharge at the River Sink delivers increasing concentrations of K^+, Na^+, and Cl^-, but dilutes pH, Ca^{2+}, and alkalinity as stage increases (Figure 3-5A). These relationships indicate that water entering the River Sink during high flow is evolved rain water flowing overland or in the shallow subsurface during storm events with minimal groundwater contribution (cf. Sklash and Farvolden 1979). The evolved rain water accounts for the Na-Cl-type end member (③ in Figure 3-4), which has an average Na^+/Cl^- ratio of 0.81 ± 0.19 (1 σ), close to the 0.86 ratio of seawater.

Seawater could be an important contribution to major element chemistry with positive loading on PC 2 (Na^+, Cl^-, and K^+), although other factors such as introduction of contaminants and reactions with siliciclastic minerals in the confining Hawthorn Group also could be important. Seawater would be the primary source of Na^+ and Cl^- to the region as sea spray becomes entrained in precipitation when tropical storms and summertime convective thunderstorms move inland from the coast. Some of the water has Na^+/Cl^- ratios in excess of seawater values, which may reflect excess Na^+ due to leaching of soil particulates in the atmosphere (Junge and Werby 1958) or due to cation exchange in the siliciclastic Hawthorn Group (Rose 1989). Cation exchange could also remove Na^+ from the water, which would

explain the Na^+/Cl^- ratios that are below seawater value. Potassium is unlikely to be derived only from sea spray since the average K^+/Cl^- ratio of 0.08 ± 0.02 (1 σ) exceeds by a factor of 4 the 0.02 ratio of seawater. Although K^+ could result from dissolution of K-bearing minerals in the Hawthorn Group (Edwards et al. 1998), these minerals occur in trace amounts that would unlikely provide the observed concentrations. The elevated concentration of K^+ in allogenic water, as reflected by its strong positive loading on PC 2 (Figure 3-5A), probably results from leaching of artificial fertilizers used for agriculture (Katz et al. 2001; Chelette et al. 2003).

The negative loadings of pH, Ca^{2+}, and alkalinity on PC 2 reflect dilute rainwater entering the River Sink during high flow. In these conditions, pH values are lower than what would be expected for water buffered by dissolution of carbonate minerals, and mineral sources of Ca^{2+} and alkalinity (e.g., HCO_3^-) are scarce in upper sections of the Hawthorn Group (Scott 1988). Although middle portions of the Hawthorn Group contain limestone and dolostone units (Groszos et al. 1992), the negative loadings of Ca^{2+} and alkalinity and no loading of Mg^{2+} on PC 2 (Figure 3-5A) suggest allogenic recharge has not interacted with these carbonate minerals. Sulfate also shows no statistical association with stage on PC 2 (Figure 3-5A), suggesting this water has not dissolved mineral sources of S, such as gypsum, anhydrite, or pyrite, which exist in minor amounts throughout the Hawthorn Group (Lazareva and Pichler 2007).

During times of little precipitation, river stage drops as lesser amounts of runoff from the confined area contribute to river flow, and water at the River Sink trends towards an intermediate composition between the two groundwater end members (① and ② in Figure 3-4). This mixing between the three end members is observed in the PCA where River Sink scores on PC 2 show a strong positive association with stage during high flow, but become negative during low flow as loadings of pH, Ca^{2+}, and alkalinity exert a stronger influence on the composition of allogenic

water (Figure 3-5). These relationships suggest that, during low flow conditions, water at the River Sink is a mixture of allogenic runoff and groundwater from the UFA, which has a different composition than water entering the River Sink during high flow. Consequently, water entering the UFA through swallets may be time-dependent mixtures of water that originates from the surface or the surrounding aquifer depending on conditions such as river stage, precipitation, and ET.

Groundwater

The differences in chemical compositions between water from Wells 2 and 4 reflect two distinct sources. Well 4 has Ca-HCO_3-type water similar to most shallow groundwater of the UFA and results from rain water equilibrating with the Ocala Limestone (Sprinkle 1989). Although Well 4 is located only about 100 m from the conduit, its variation on PC 2 scores shows no statistical association with stage (Figure 3-5B). Most of the variation of Well 4 on PC 2 scores likely results from subtle changes in pH, Ca^{2+}, and alkalinity, whose loadings exert the greatest influence on the Ca-HCO_3-type water (Figure 3-5B). Water at Well 4 is likely to originate from diffuse recharge as indicated by the small variations in solute/Cl^- ratios (Figure 3-6A). The magnitude of diffuse recharge has been shown to exceed allogenic recharge at the River Sink depending on conditions including ET, soil saturation, and precipitation (Ritorto 2007).

The Ca-Mg-SO_4-type water from Well 2 results from processes other than, or in addition to, simple limestone dissolution. Although all wells are screened at similar depths below the land surface, water collected from Well 2 is the most mineralized in the region with the highest major element concentrations and SpC. Well 2 also has the highest T of all water collected (Table 3-1). Consequently, the positive loadings of K^+, Cl^-, Na^+, Mg^{2+}, and SO_4^{2-} on PC 1, coupled with the strong positive PC 1 scores of Well 2, suggest this water source delivers most of these ions to the

sink-rise system (Figure 3-5). Water with similar SO_4^{2-} concentrations (in excess of 400 mg/l, i.e. about 4.2 mmol/kg H_2O) was previously observed from a municipal well in High Springs, FL (less than 5 km away from Well 2) that was open to the UFA from about 105 to 150 mbgs (Hunn and Slack 1983). The nearby presence of deep, mineralized water could reflect a source of water that would give Well 2 its unique chemical composition. While the source of mineralized water deep within the Floridan aquifer system has not been determined (e.g., Phelps 2001), the increased salt contents cannot result from only mixing with seawater. Comparing ratios of dissolved components to Cl^- concentrations to their seawater values suggests the mineralized water at Well 2 has concentrations of Mg^{2+} and SO_4^{2-} that exceed values expected from seawater fractions by a factor of 11 and 49 times, respectively, and the average Na^+/Cl^- ratio of 0.96 ± 0.06 (1 σ) (Table 3-1) at Well 2 is about 10% higher than the seawater value. Nonetheless, elevated concentrations of K^+ at Well 2, as reflected by its strong positive loading on PC 1 (Figure 3-5A), suggests dilute seawater deep within the aquifer may account for some of the mineralized water since this is the likely source of K^+ in the UFA (Sprinkle 1989).

Other than seawater as a source of salts at Well 2, water-rock reactions could provide its elevated ion concentrations. Elevated concentrations could result from water reacting with minerals in leaky portions of the Hawthorn Group, which then moves along deep flow paths due to regional head gradients (Lawrence and Upchurch 1982). An alternate explanation for the elevated concentrations could result from evaporite dissolution and dedolomitization occurring deep within the aquifer (e.g., Plummer 1977; Hanshaw and Back 1979; Jones et al. 1993). In the lower portions of the UFA, evaporite minerals and dolomite are known to occur (Miller 1986) (Figure 3-1). Dissolution of gypsum or anhydrite releases Ca^{2+} and SO_4^{2-}, which initiates calcite

precipitation and subsequently promotes additional dissolution of gypsum or anhydrite and dolomite if present (Plummer and Back 1980).

Although near-surface reactions in the Hawthorn Group could elevate ion concentrations in the UFA, dissolution of evaporite minerals and dolomite in deeper portions of the aquifer are likely responsible for the observed concentrations at Well 2. These processes would elevate concentrations of SO_4^{2-}, Mg^{2+}, and Ca^{2+}, but would not increase the concentration of K^+ (Figure 3-6B). Dissolution of Ca-bearing minerals, however, would not explain the linearity between Na^+ and Cl^- or the value of Na^+/Cl^- molar ratio of 0.96 ± 0.06 (1 σ), which is similar to the Na/Cl molar ratio of halite and suggest halite dissolution although no halite has been reported in the Floridan Aquifer system (Miller 1986).

Influences of Vertical Flow on Shallow Water Chemistry

Most work on groundwater flow at the study site and other karst systems has focused on horizontal flow through conduits and surrounding aquifer following rapid recharge through swallets and discharge from springs (Martin and Dean 2001; Screaton et al. 2004; Martin et al. 2006; Ritorto et al. in press). Few studies have considered vertical flow through karst aquifers or the geographic distributions and controls of where vertical flow could occur (e.g., Sprouse 2004). The chemical variations at Well 2, where measured temperatures are significantly higher than surrounding wells, indicate that upward flow is important in the region, which I estimate below using Equations 3-2 and 3-4 (Figure 3-7). For T_Z, I use a measured T of 26 °C at Well 2, which represents the highest T observed at Well 2 and occurred following a one-year drought (S-15 and S-16, Figure 3-3). The drought may have increased hydraulic head differences between the deep and shallow portions of the aquifer as drought conditions have greater effect on the shallower portions of the aquifer. In addition to head differences, the drop in river stage during the drought

minimizes flow through conduits, thereby reducing horizontal flow which may also alter the T at the well (e.g., Lu and Ge 1996).

Considering this conceptualization of vertical flow at Well 2, I estimate z and L to be 23 and 423 m, respectively during this time (Figure 3-7). Although there is no water-table well near Well 2, I estimate T_O to be about 21 °C based on the average groundwater T (e.g., Wells 4 and 7, Table 3-1) and average air T for the area (Hunn and Slack 1983). I estimate a temperature of 28.6 °C for T_L at the base of the UFA, assuming an average geothermal gradient of about 1.8×10^{-2} °C/m across the region (Reel and Griffin 1971; Smith and Lord 1997). Solution to Equation 3-2 using these T values suggests β at Well 2 is about -19.6. Using a heat capacity of 4184 J/kg °C, density of 1000 kg/m^3 for water, and thermal conductivity of limestone of 3 W/m °C (Deming 2002), Equation 3-4 yields an upward Darcy velocity at Well 2 of about 1 m/yr.

Although I observe the temperature anomaly resulting from vertical flow only at Well 2, the deep-water source appears to have a significant impact on the regional shallow-water chemistry as shown by the chemical compositions at Wells 2 and 7, River Sink, and River Rise. During low flow conditions, water at the River Sink and River Rise appear to be intermediate mixtures of the groundwater end members (① and ② in Figure 3-4), although water from the River Sink lies closer to the Ca-HCO_3-type end member while the River Rise lies closer to the Ca-Mg-SO_4-type end member (Figure 3-4). This difference in water chemistry at low flow suggests the River Rise receives a greater contribution from the deep-water source than the River Sink.

Dilution of the deep-water source at Well 2 is shown by the variation in Well 2 scores on PC 1, which changes with SpC (Figure 3-5B). As dilute allogenic water reaches Well 2, the concentrations of K^+, Cl^-, Na^+, Mg^{2+}, and SO_4^{2-} decrease, resulting in PC 1 scores plotting

towards the graph's origin (Figure 3-5B). These changes suggest that Well 2 is more closely linked to surface water than the other wells, possibly through unmapped conduits (Figure 3-2). The deep-water source at Well 2 requires greater vertical permeability than the other wells. Higher permeability could result from vertical fractures that would provide a flow path for deep water, and if these fractures are linked to the conduit sourcing the River Rise, could explain the greater influence of deep water there than at the River Sink (Figure 3-4). The only other location with a signal from the deep-water source is Well 7 (Figure 3-4), but its location is about 1 km away from the closest known conduit (Figure 3-2). Although simulations of regional groundwater flow suggest water upwelling from deep flow paths exert little influence on first-magnitude springs draining the UFA (Bush and Johnston 1988), deep water at the sink-rise system suggests heterogeneous permeability can greatly alter groundwater flow fields and reflects the importance of multiple flow paths in karst aquifers (e.g., Knochemus and Robinson 1996).

Effects of Source Water and Flow Paths on Spring Discharge

Volumes of allogenic and diffuse recharge have been estimated for the River Rise (e.g., Martin and Dean 2001; Screaton et al. 2004; Ritorto et al. in press), but contributions from the deep source have not yet been included in water mass-balance estimates although the chemical composition of the Rive Rise water indicates the deep source contributes to its discharge. Estimating the volume of deep water sourcing the Rive Rise is difficult because of uncertainty in the chemical composition of the deep-water end member. While chemical compositions of end members represented by allogenic recharge and shallow sources can be measured directly at the River Sink and Well 4, respectively (e.g. Figure 3-4), the composition of the end member reflecting the deep-water source can not be directly sampled. Instead, water chemistry at Well 2 is a mixture of both deep and shallow water, and consequently mass-balance calculations can

only approximate the relative fractions of water sourcing the River Rise. While dissolution and precipitation reactions within the conduit may affect spring composition to some degree, I assume the mixing of the three representative end members largely accounts for most of the chemical variation at the River Rise (Figures 3-4 and 3-5B).

I use concentrations of Mg^{2+} and SO_4^{2-} to estimate the relative fractions of the three sources of water discharging from the River Rise. Concentrations of Mg^{2+} and SO_4^{2-} show strong linear correlations at the River Sink, River Rise, and Well 2 (Figure 3-8). The linear relationship suggests that concentrations are controlled by dilution, which is most likely to occur from mixing of allogenic recharge and the concentrated deep-water source as shown by the PCA (Figure 3-5). In contrast to the deep-water source at Well 2, concentrations of Mg^{2+} and SO_4^{2-} of diffuse recharge at Well 4 are low, remain relatively constant, and have nearly the same ratio through time (see Figures 3-6A and 3-8) suggesting this water is not affected by inputs of allogenic or deep water. Although Well 4 does exhibit a linear trend on PC 2 scores (Figure 3-5B), no systematic cause for the variation exists.

In order to observe how temporal variations in the magnitudes of sources affect spring discharge, water fractions were calculated using Mg^{2+} and SO_4^{2-} concentrations from each sample trip. Assuming contributions only from the three identified end members, water at the River Rise consists of volumetric fractions of each end member, X,

$$X_R = X_S + X_{W2} + X_{W4} \tag{3-6}$$

where the subscripts represent allogenic recharge at the River Sink (S), the deep source at Well 2 (W2), diffuse recharge at Well 4 (W4), and discharge at the River Rise (R), which equals 1. Individual equations were written for Mg^{2+} and SO_4^{2-} concentrations where:

$$X_R Mg_R = X_S Mg_S + X_{W2} Mg_{W2} + X_{W4} Mg_{W4} \tag{3-7}$$

$$X_R SO_{4R} = X_S SO_{4S} + X_{W2} SO_{4W2} + X_{W4} SO_{4W4} . \quad (3\text{-}8)$$

Rearranging Equation 3-6 for X_S and substituting into Equation 3-7 and solving for X_{W4} gives

$$X_{W4} = \frac{X_R (Mg_R - Mg_S) - X_{W2} (Mg_{W2} - Mg_S)}{Mg_{W4} - Mg_S} \quad (3\text{-}9)$$

and rearranging Equation 3-6 for X_{W4} and substituting into Equation 3-8 and solving for X_S gives

$$X_S = \frac{X_R (SO_{4R} - SO_{4W4}) - X_{W2} (SO_{4W2} - SO_{4W4})}{SO_{4S} - SO_{4W4}} . \quad (3\text{-}10)$$

Substituting Equations 3-9 and 3-10 into Equation 3-6 and solving for X_{W2} yields

$$X_{W2} = \frac{1 - \left(\frac{SO_{4R} - SO_{4W4}}{SO_{4S} - SO_{4W4}} \right) - \left(\frac{Mg_R - Mg_S}{Mg_{W4} - Mg_S} \right)}{1 - \left(\frac{SO_{4W2} - SO_{4W4}}{SO_{4S} - SO_{4W4}} \right) - \left(\frac{Mg_{W2} - Mg_S}{Mg_{W4} - Mg_S} \right)} . \quad (3\text{-}11)$$

Variables X_{W4} and X_S are found using back-substitution of solutions to Equation 3-11 into Equations 3-9 and 3-10, respectively. Equations 3-9, 3-10, and 3-11 provide the mixing fractions of source water contributing to discharge at the River Rise for all the sampling times except January 2003 (S-1, Figure 3-3) prior to the installation of Well 4 (Table 3-3).

Results of the mixing calculations show that flow through the sink-rise system is quite complex. Nonetheless, discharge at the Rive Rise correlates positively with allogenic recharge (River Sink), inversely with the deep-water source (Well 2), but lacks a correlation with diffuse recharge (Well 4) (Figure 3-9). These results agree with the PCA, which suggests that as allogenic recharge increases with stage the magnitude of the deep-water source decreases. This decrease in deep water may reflect elevated head in the conduit limiting upward flow. The lack of correlation between discharge and diffuse recharge as represented by the Well 4 fraction (Figure 3-9C) suggests that hydraulic head between the conduit and surrounding aquifer, and the related exchange of water between the conduit and matrix, do not change systematically with

river stage. During times when diffuse recharge exceeds allogenic recharge, hydraulic head in the surrounding aquifer could exceed conduit head as diffuse recharge elevates the water table and causes flow from the matrix to the conduit and ultimately to discharge from the River Rise (Martin and Dean 2001; Screaton et al. 2004; Martin et al. 2006; Ritorto et al. in press).

Certain sampling times provide information on how differences in hydraulic head between the conduit and surrounding aquifer may affect the chemical composition of water discharging from the River Rise. Prior to sampling on April 30, 2003 and January 17, 2006, river stage dropped rapidly, which would result in rapidly decreasing head in the conduit (indicated as △ in Figure 3-9). If head in the conduit dropped more quickly than head in the surrounding aquifer, pressure gradients would drive flow toward the conduit (Screaton et al. 2004; Martin et al. 2006), decreasing the fraction of allogenic water to the River Rise and simultaneously increasing the fractions of matrix water. Consequently, these two sample times show the elevated fraction of water from Well 4 (diffuse recharge) relative to the River Sink fractions (allogenic recharge) (Figure 3-9).

During times of low flow, the conduit acts as a low-resistance drain that allows water to converge on it (e.g., Freeze and Cherry 1979; Ford and Williams 2007). This process is observed during a drought from July 2006 to April 2007 (S-13 – S-16, Figure 3-3), when river stage constantly fell from about 10 to 9.7 masl, far below the average stage of 10.2 masl. During this time, discharge from the River Rise was close to an even mixture of allogenic water (River Sink) and groundwater (Wells 2 and 4) (see ○ in Figure 3-9). The fraction of deep water (Well 2) was at a maximum, averaging around 20% of the total discharge, suggesting that first-magnitude springs draining the UFA may receive significant contributions of flow from upward movement from deep flow paths (Katz, 2004). The fraction of diffuse water (Well 4) is more variable than

the fraction of deep water, ranging from about 20 to 40%. This variability likely reflects changes in head gradient between the conduit and surrounding aquifer due to differences in antecedent conditions such as prior precipitation and ET. Variations in these factors would alter the elevation of the water table so that different amounts of matrix water would flow to the conduit for similar river stages (Figure 3-3). Although matrix flow in unconfined eogenetic aquifers can provide significant amounts of spring discharge, its contribution through time at any one spring must be sensitive to processes affecting hydraulic head gradients between conduits and surrounding aquifer.

Conclusions

Spatial and temporal monitoring of surface- and groundwater chemistry along with observations of physical parameters including river stage, precipitation, and ET in the Santa Fe River Sink-Rise system of the eogenetic UFA provide insight on how multiple sources of water and several different flow paths may affect spring discharge in karst aquifers. Chemical monitoring and PCA suggest that mixing of two shallow sources (diffuse and allogenic recharge) and one upwelling deep-water source explains 91% of the chemical variation in the sink-rise system. The previously unrecognized deep-water source is the primary influence on major-element chemistry by providing most of Na^+, Mg^{2+}, K^+, Cl^-, and SO_4^{2-} to the system. Estimates of vertical flow, based on maximum observed temperatures, are on the order of 1 m/yr, and this flow appears to contribute up to nearly 20% of the discharge at the River Rise. The contribution from the deep source depends inversely on flow conditions. The presence of a deep source suggests that care must be taken in the evaluation of karst aquifers based on the chemical composition of spring water, which may not be restricted to shallow portions of the aquifer.

Water flowing through karst aquifers from allogenic inputs to springs should reflect an evolution of the recharged water by water-rock reactions along conduit flow paths. Comparison

of relative fractions of source water, however, suggest the deep-water source and local diffuse recharge cause significant changes in the chemical composition of discharge even in a system dominated by allogenic recharge and conduit flow. While variations in spring chemistry likely reflect water-rock reactions along conduit flow paths between sinks and springs, mixing of different sources may play a more dominate role in the temporal variability of spring chemistry. Consequently, any characterization of karst aquifers using spring-water chemistry requires understanding the variety of sources of waters and their chemical compositions.

Table 3-1. Summary of major ions, alkalinity, SpC, pH, and T of representative water samples.

Location	Cl			SO4			Ca			Na		
	range	x	CV	range	x	CV	range	x	CV	range	x	CV
River Sink	0.23 - 0.64	0.38	27	0.02 - 0.48	0.24	69	0.19 - 1.39	0.78	58	0.19 - 0.46	0.30	19
River Rise	0.32 - 0.64	0.47	17	0.02 - 1.15	0.63	61	0.20 - 2.02	1.24	55	0.24 - 0.52	0.39	23
Well 2	0.42 - 1.66	1.24	28	1.19 - 4.47	3.43	28	1.97 - 4.77	3.92	18	0.61 - 1.61	1.26	23
Well 4	0.22 - 0.28	0.25	6	0.02 - 0.05	0.04	18	2.07 - 2.36	2.21	3	0.18 - 0.22	0.20	6
Well 7	0.28 - 0.54	0.42	18	0.02 - 0.29	0.16	38	1.54 - 2.77	2.19	19	0.19 - 0.34	0.27	17

Table 3-1. Continued

Location	Mg			K			alkalinity			pH		
	range	x	CV	range	x	CV	range	x	CV	range	x	CV
River Sink	0.09 - 0.64	0.35	58	0.020 - 0.047	0.028	27	0.16 - 3.04	1.56	71	5.40 - 7.79	6.94	9
River Rise	0.09 - 0.72	0.44	54	0.024 - 0.041	0.027	15	0.16 - 3.16	1.90	58	4.70 - 7.37	6.90	9
Well 2	0.57 - 2.04	1.48	32	0.035 - 0.082	0.06	28	2.04 - 4.28	3.89	13	6.48 - 7.10	6.84	3
Well 4	0.05 - 0.09	0.06	16	0.005 - 0.010	0.009	14	2.80 - 4.30	4.03	9	6.48 - 7.19	6.87	3
Well 7	0.15 - 0.24	0.18	13	0.015 - 0.023	0.019	13	2.16 - 5.12	4.12	19	6.50 - 7.40	6.95	4

Table 3-1. Continued

Location	SpC			T		
	range	x	CV	range	x	CV
River Sink	73 - 412	256	48	10.0 - 27.7	19	27
River Rise	73 - 560	371	46	11.0 - 26.4	20	20
Well 2	488 - 1315	1058	20	22.0 - 26.3	25	4
Well 4	390 - 449	428	3	20.9 - 21.7	21	1
Well 7	306 -550	434	20	20.3 - 20.9	21	1

Range and mean (x) of concentrations in mmol/kg H_2O, coefficient of variation (CV) in percent, pH is unitless, SpC in µS/cm and T in °C.

Table 3-2. Variable loadings of PCA.

	Loadings		
Variables	PC 1	PC 2	PC 3
pH	0.08[a]	*-0.42*	*0.53*
Cl	*0.42*	0.15	0.00
SO_4	*0.44*	0.00	-0.07
Ca	0.27	*-0.46*	*-0.39*
Na	*0.44*	0.07	-0.02
Mg	*0.44*	0.02	0.07
K	*0.39*	*0.31*	0.09
Alkalinity	0.05	*-0.62*	*-0.36*
Stage	-0.10	*0.32*	*-0.65*
eigenvalues	4.87	2.13	1.16
% Variance	54	24	13
% Cumulative	54	78	91

[a]Loadings greater than |0.3| are in *italics*.

Table 3-3. Fraction of water discharging from the River Rise originating from the River Sink and two groundwater end members.

Sample Date	Sample Period	Rise Discharge (m^3/s)	River Sink (%)	Well 2 (%)	Well 4 (%)
3/2/03					
3/5/03	S-2	57.9	81[a]	0	19
3/19/03					
4/30/03	S-3	12.0	40	24	36
1/23/04	S-4	5.2	83	18	-1
3/8/04	S-5	9.6	74	5	21
5/5/04	S-6	6.1	57	20	23
1/19/05	S-7	18.0	87	19	-6
3/18/05	S-8	20.2	76	13	11
7/18/05	S-9	49.5	93	3%	3
10/27/05	S-10	15.7	76	11	13
1/17/06	S-11	30.4	65	4	31
4/12/06	S-12	10.3	74	20	6
7/13/06	S-13	7.5	55	16	29
10/10/06	S-14	5.2	46	20	34
01/17/07	S-15	3.9	67	17	17
04/10/07	S-16	3.6	42	21	37

[a]Percentages calculated based on solutions to Equations 3-9, 3-10, and 3-11.

Series		Hydrostratgraphic Unit	Lithostratgraphic Unit	Lithologic Description
Holocene		Surfical Aquifer System	Undifferentiated Pleistocene-Holocene Sediments	Fine-to-coarse grained, poorly-indurated quartz sands with minor amounts of clay
Pleistocene				
Pliocene			Miccosukee Formation Cypresshead Formation Nashua Formation	Interbedded clay, silt, sand, gravel siliciclastics with some fossiliferous carbonate sediments
Miocene		Confining Unit with lenses of the Intermediate Aquifer	Hawthorn Group	Interbedded siliciclastic-carboante sequences with occasional phosphate-rich units.
Oligocene		Upper Floridan Aquifer	Suwannee Limestone	Vuggy and muddy limestone
Eocene	Upper		Ocala Limestone	Fossiliferous limestone interbedded with vuggy, dolomitic limestone
	Middle		Avon Park Formation	Limestones and dolomites with interbedded evaporites in lower portion
			Oldsmar Formation	Gypsiferous limestone interbedded with gypsiferous dolomite
	Lower		Cedar Keys Formation	Dolomites and dolomitic limestones in upper portion and massive anhydrite beds in lower portion
Paleocene		Lower Confining Unit		

Figure 3-1. Lithostratigraphic and hydrostratigraphic units of the Santa Fe River Basin. Thickness of units not implied in the diagram. Modified from Miller (1986), Scott (1988), and Martin and Dean (2001).

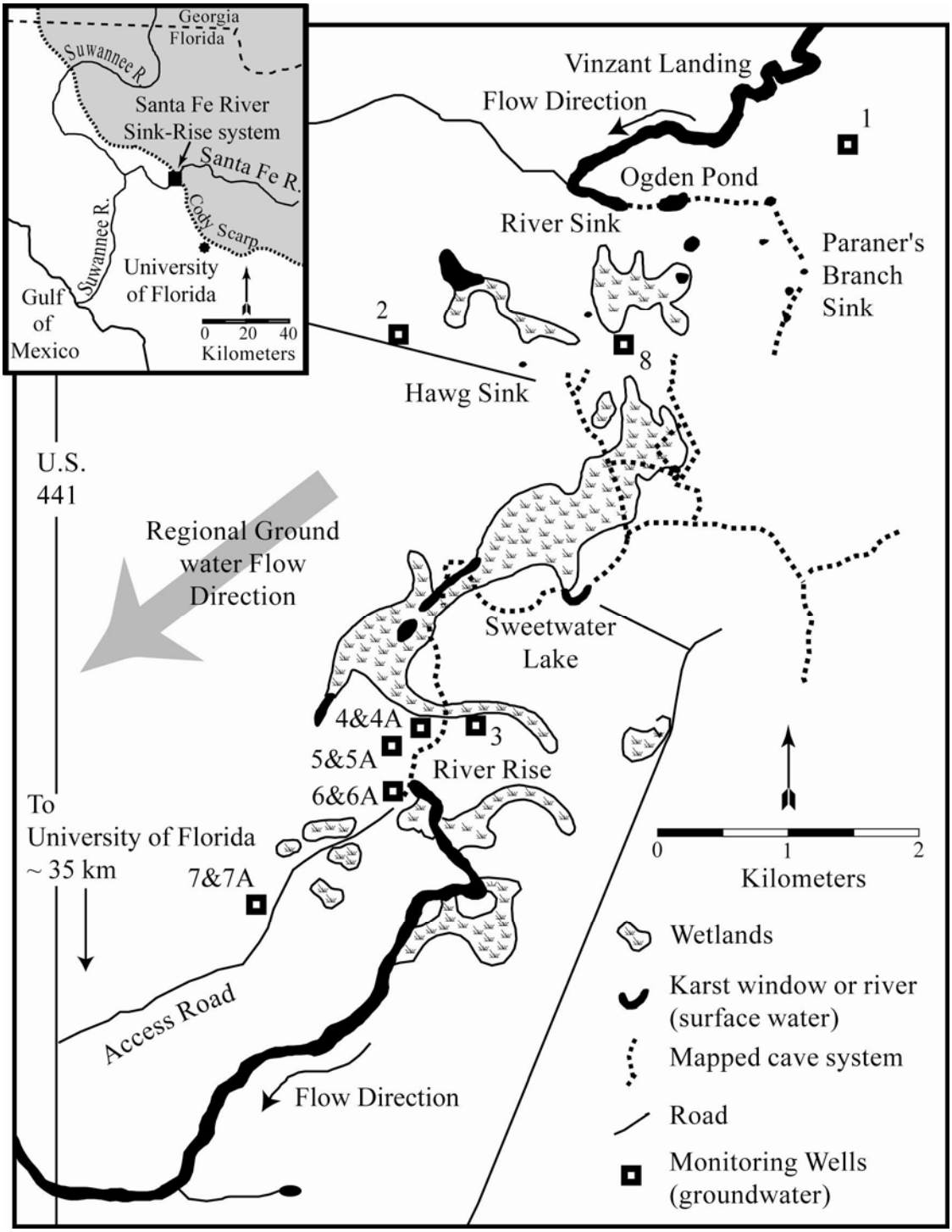

Figure 3-2. Site location of the Santa Fe Sink-Rise system showing locations of surface water and ground water sampling sites. Insert map shows location of Santa Fe Sink-Rise system in relation to north-central Florida. Dotted line represents erosional edge of the Hawthorn Group to the northeast (gray area) marking the confined portion of the Upper Floridan Aquifer, with the white area representing the unconfined portion of the UFA where the Hawthorn is absent.

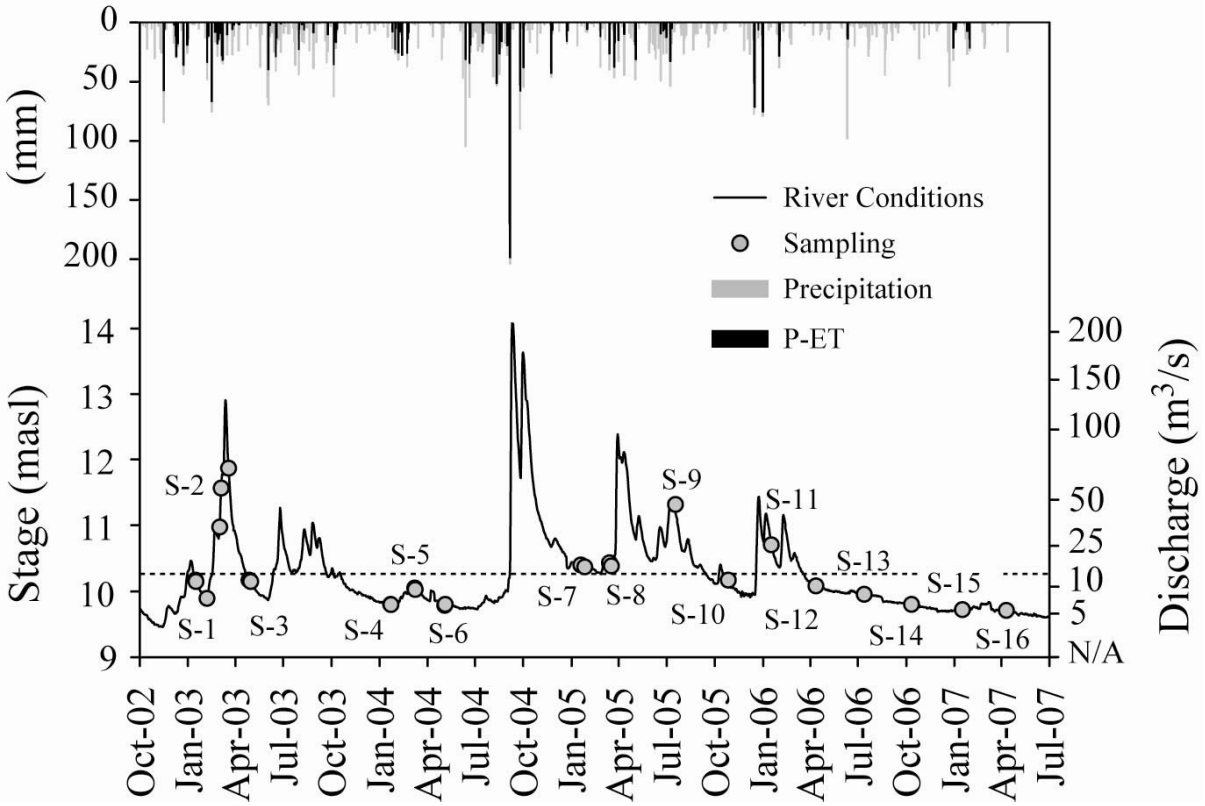

Figure 3-3. Stage and discharge of the Santa Fe River at the River Rise, and precipitation and potential recharge (precipitation minus evapotranspiration; P-ET) amounts estimated within O'Leno State Park. Gray dots represent times of sample collection. Dashed line represent average stage (10.2 masl) during study period.

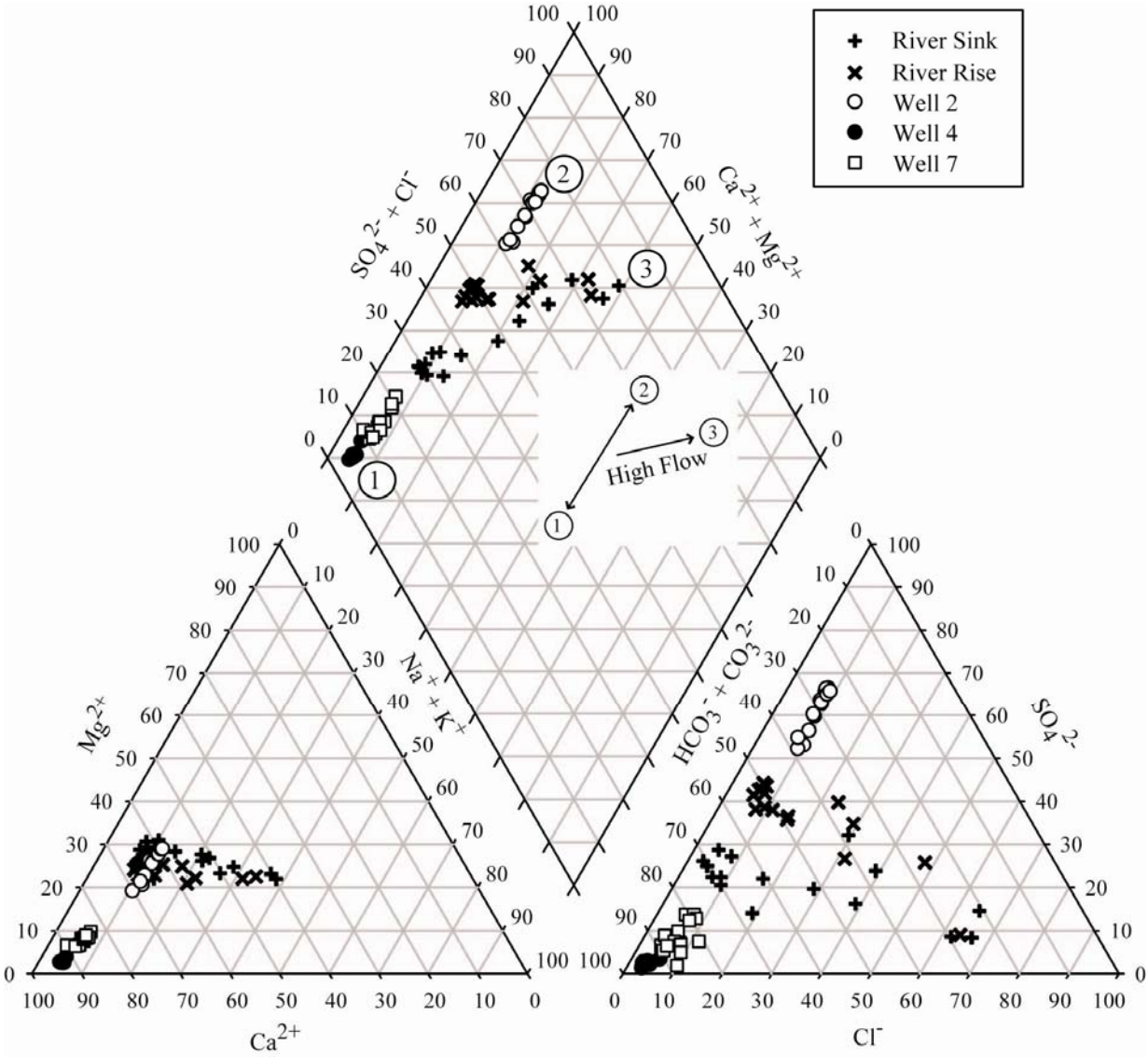

Figure 3-4. Piper diagram showing the hydrochemical facies of surface and groundwater in Santa Fe Sink-Rise system. Representative end members are 1) Ca-HCO_3 type water, 2) Ca-Mg-SO_4 type water, and 3) Na-Cl type water. Inset in diamond shows mixing trends between the three end members.

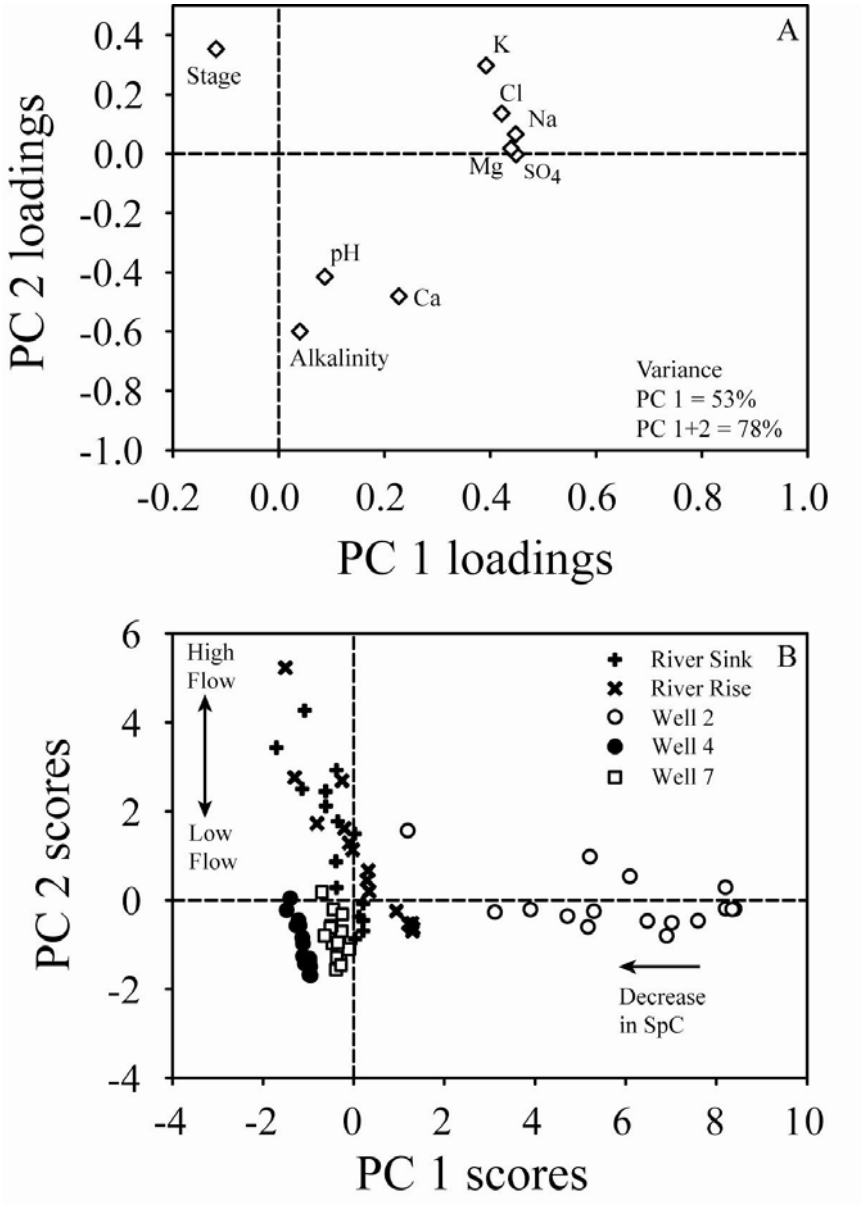

Figure 3-5. Principal component loading and scores for Santa Fe Sink-Rise water. A) Plot of PC loadings for major ions, alkalinity, pH, and river stage. B) Plot of PC scores for River Sink, River Rise, and Wells 2, 4, and 7.

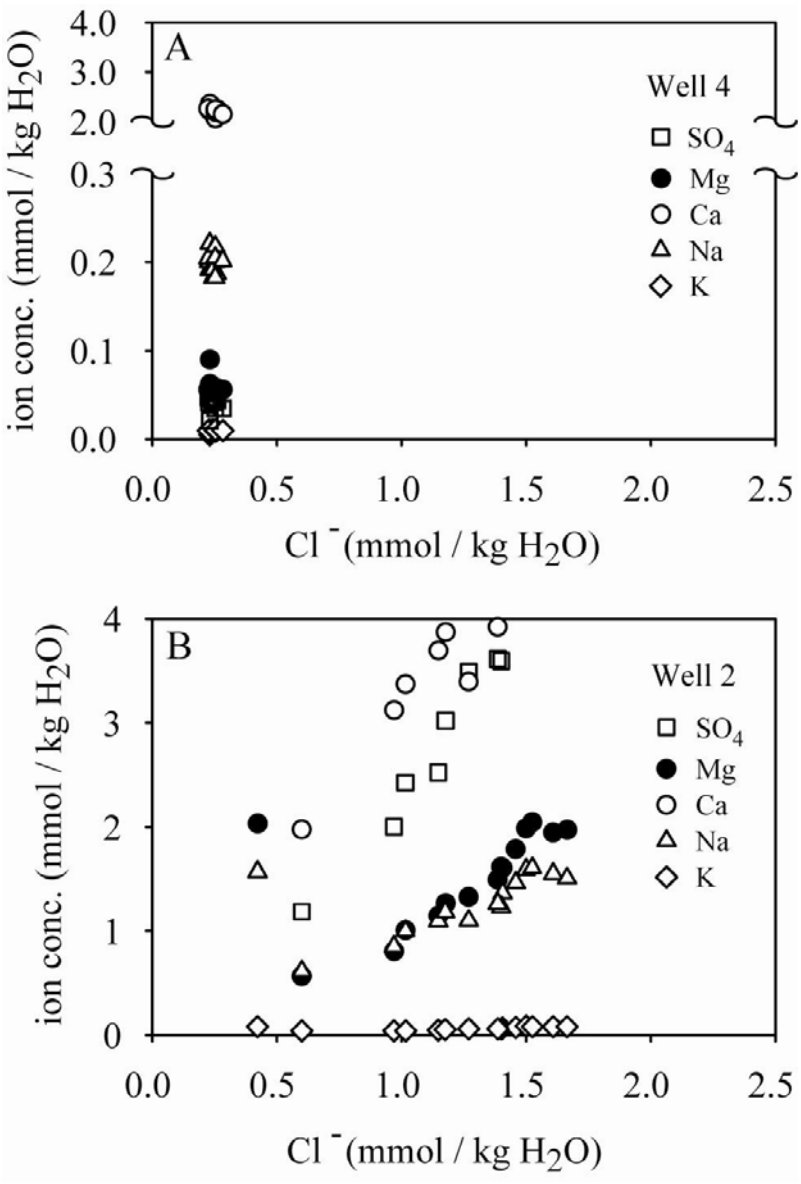

Figure 3-6. Plots of ion concentrations versus Cl^-. A) Water from Well 4. B) Water from Well 2.

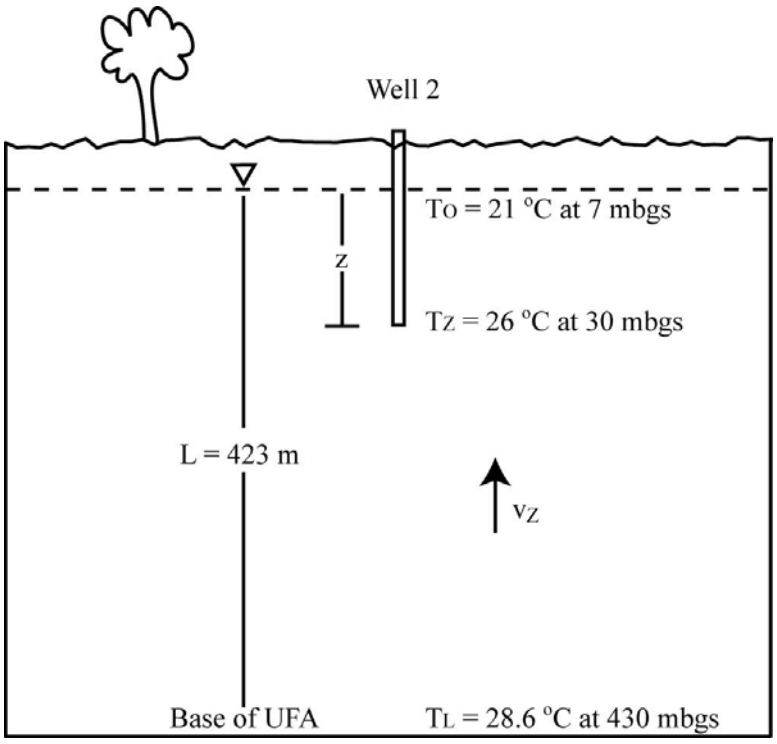

Figure 3-7. Diagrammatic sketch of boundary conditions for vertical steady-state flow and heat transfer at Well 2.

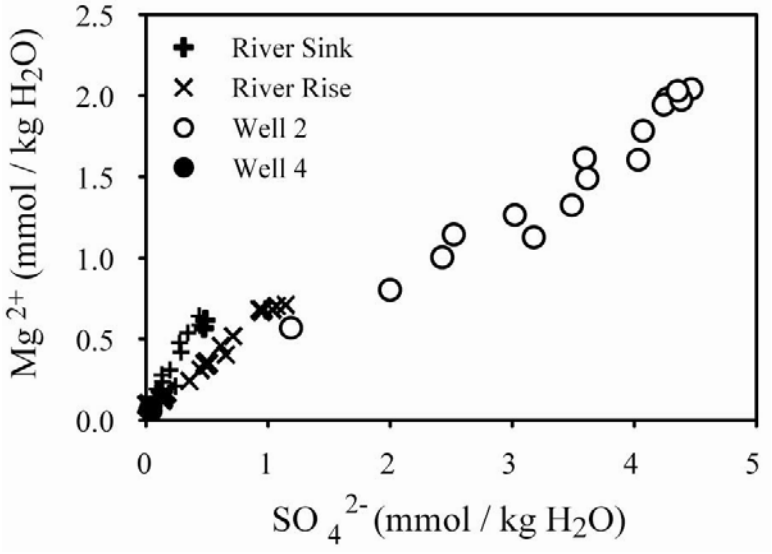

Figure 3-8. Plot of Mg^{2+} versus SO_4^{2-} concentrations showing the temporal, linear variation at the River Sink, River Rise, and Well 2. Well 4 shows little change near the origin of the graph.

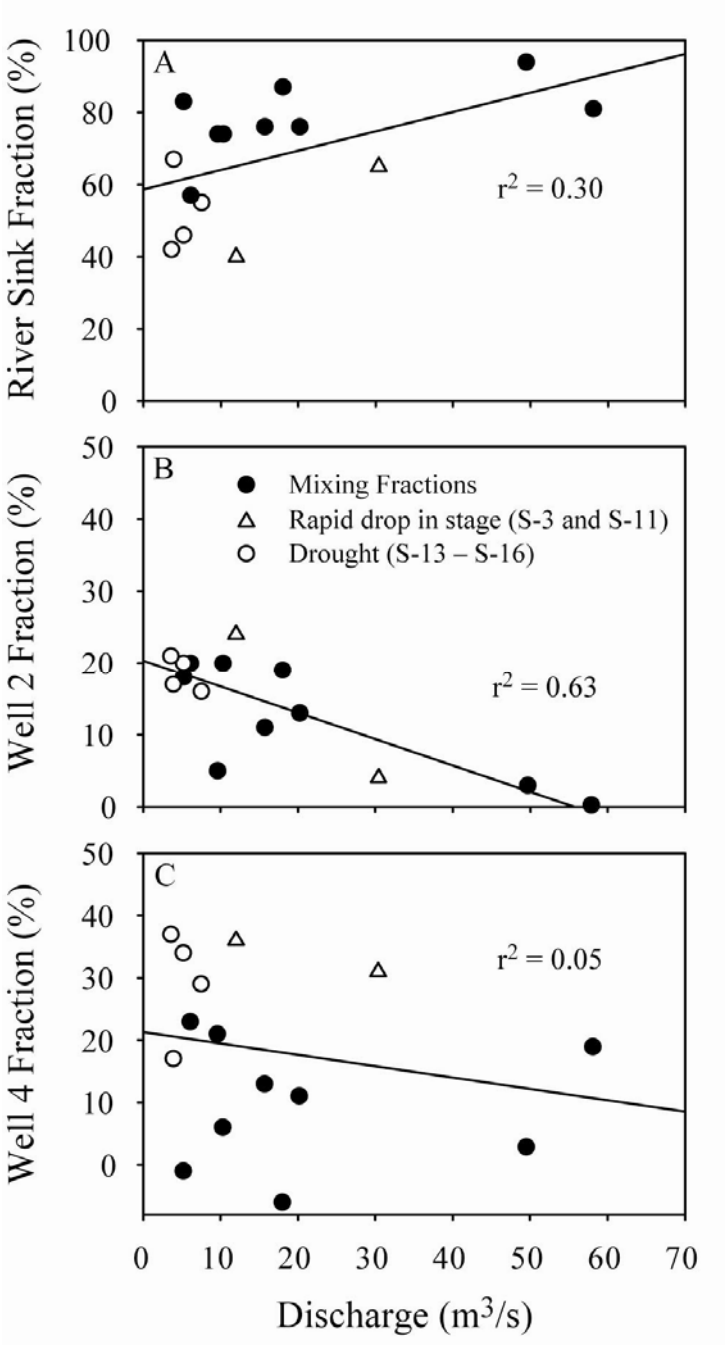

Figure 3-9. Plots of source contributions versus discharge at the River Rise. A) Percentage of River Sink source. B) Percentage of Well 2 source. C) Percentage of Well 4 source.

CHAPTER 4
CONDUIT ENLARGMENT IN AN EOGENETIC KARST AQUIFER

Introduction

Most models of karst aquifers are commonly based on studies of dense, recrystallized limestone (i.e., telogenetic karst, Vacher and Mylroie 2002). Within these aquifers, conduits are embedded in a network of joints, fractures, and fissures in a groundmass of otherwise low matrix porosity and permeability. Conduits develop along these initially narrow flow paths as a function of flow-path geometry, water chemistry, and flow rates (e.g., Ford and Ewers 1978; Palmer 1991). As conduits enlarge, they capture more of the flow, thereby enhancing dissolution and further enlarging the conduits until only a few routes carry the majority of flow (e.g., White 1988; Ford and Williams 2007). Low matrix permeability of telogenetic aquifers keep the flow focused within the developing conduit and cause enlargement through dissolution along the conduit wall. Flow and any dissolved $CaCO_3$ from the regional groundwater is considered negligible (e.g., Halihan and Wicks 1998).

The concepts of conduit flow in telogenetic karst aquifers allow dissolution rates to be estimated based on the magnitude of disequilibrium between the conduit water and carbonate minerals. Early calculations used kinetics of calcite dissolution to derive expressions for the retreat of conduit walls (Dreybrodt 1990; Palmer 1991). These kinetic expressions have been used to model the early development of conduits (e.g., Groves and Howard 1994; Kaufmann and Braun 1999; Gabrovšek and Dreybrodt 2001; Romanov et al. 2003a), morphologies of cave patterns (e.g., Palmer 1991; Howard and Groves 1995; Palmer 2001), leakage rates beneath dam sites (Romanov et al. 2003b), and to estimate the role of conduit growth on landscape evolution in a karst basin (Groves and Meiman 2005). Recent studies have suggested that dissolution rates may be expressed as a function of flow velocity through the conduit, whereby dissolved $CaCO_3$

at a spring reflects the amount of dissolution along the conduit flow path (Grasso and Jeannin 2002; Grasso et al. 2003). This understanding of how conduits develop appears to work for telogenetic limestone, especially where allogenic recharge to the conduit occurs through sinkholes and swallets (e.g., Palmer 2001), but may not fit for eogenetic karst aquifers, which have orders of magnitude greater matrix permeability than their telogenetic counterparts (Vacher and Mylroie 2002; Budd and Vacher 2004).

The limitations of telogenetic models of conduit development for explaining eogenetic karst conduits stems from high matrix permeability, which allows recharge to and discharge from aquifer storage. This exchange of water varies depending on hydraulic head between the conduit and surrounding aquifer, affecting both regional groundwater and spring chemistry (e.g., Katz et al. 1998; Crandall et al. 1999; Martin and Screaton 2001; Moore et al. submitted). For example, water that drains from the surrounding aquifer can constitute a substantial component of water flowing in the conduits that would be absent in telogenetic aquifers (e.g., Martin and Dean 2001; Florea and Vacher 2006). Conversely, water lost from the conduit to surrounding aquifer mostly occurs during high flow when water undersaturated with respect to calcite may drive dissolution within the aquifer matrix (Katz et al. 1998; Crandall et al. 1999; Screaton et al. 2004; Ritorto et al. in press). This interaction between the conduit and surrounding aquifer should affect how conduits enlarge in eogenetic karst, whereby dissolution occurs at the conduit wall as well as within the aquifer matrix. These observations suggest that new concepts may be necessary to describe conduit development in eogenetic karst.

The central question I address in this paper is how high matrix porosity and permeability of eogenetic karst aquifers affect the magnitude and distribution of conduit development and dissolution within the surrounding matrix porosity. I use groundwater chemistry, geochemical

reactions, and the physical and chemical variations of a first magnitude spring draining a portion of the Upper Floridan aquifer (UFA) to estimate magnitudes and locations of dissolution occurring within a 6-km long conduit network. Although recharge to the conduit occurs primarily by allogenic runoff, diffuse recharge through the rock matrix and deep-water upwelling also source the conduit (Ritorto et al. in press, Moore et al. submitted). I use compositions of water from each source and the mass transfer of calcite and CO_2 to estimate the extent of dissolution within conduit. These results suggest that concepts of conduit enlargement used in telogenetic karst may fail to properly explain conduit development in eogenetic karst. Although this study focuses on the eogenetic karst of north-central Florida, the results discussed here are relevant to other karst aquifers that retain high matrix porosity and permeability.

Background

Hydrologic and Geologic Conditions

The Santa Fe River is a tributary of the Suwannee River, with a watershed covering about 3600 km^2 in north-central Florida (Hunn and Slack 1983). In the watershed, the UFA is confined by the Hawthorn Group to the northeast, and is unconfined in the southwest due to erosion (Figure 3-2). The erosional edge of the Hawthorn Group, referred to as the Cody Scarp, forms the boundary between the confined and unconfined UFA (Puri and Vernon 1964). The Santa Fe River flows westward from Lake Santa Fe for about 40 km until it reaches the Cody Scarp, where it sinks into a 36-m deep sinkhole at the River Sink in O'Leno State Park (Figure 3-2). The river flows underground through a network of conduits until it reemerges about 6 km from the River Sink as a first magnitude spring, called the River Rise, marking the headwaters of the lower Santa Fe River (Martin and Dean 2001). The conduits rise to the surface intermittently between the Sink and Rise at several karst windows (Figure 3-2).

At the Santa Fe Sink-Rise system, the UFA is about 430 m thick, unconfined at the surface, and is covered by a thin veneer (about 4 m, depending on land-surface elevation) of unconsolidated sands and sediments (Miller 1986). No middle confining unit exists in this area and thus the UFA extends to the lower confining unit of the Cedar Key Formation (Miller 1986) (Figure 3-1). Potable water extracted from the aquifer is estimated to come from the upper 100 m of the Ocala Limestone, and the water becomes increasingly mineralized with depth into the aquifer (Hunn and Slack 1983; Miller 1986). In this area, the water table averages about 4 meters below ground surface (mbgs) (Ritorto et al. in press). Porosity and matrix permeability of the Ocala Limestone average about 30% and 10^{-13} m^2, respectively (Budd and Vacher 2004; Florea 2006). Exploration of the conduits upstream of the River Rise has resulted in over 15 km of surveyed passage, and represents one of the longest conduit systems in Florida (Poucher 2007). Average dimensions of the cross section of the conduits range from 18 to 24 m wide and 12 to 18 m high and they occur at an average depth of about 30 mbgs (Poucher 2007). Conduits have not been mapped to connect the River Sink to the River Rise, but high flow rates detected by natural and artificial tracers show the two locations must be linked by conduits (Hisert 1994; Martin and Dean 1999; Moore and Martin 2005).

Previous work has shown that water discharging from the River Rise varies between sources from the River Sink and from groundwater, defined here as water stored in the aquifer surrounding the conduits (e.g., Martin and Screaton 2001; Screaton et al. 2004; Martin et al. 2006). During high flow in the River Sink, discharge at the River Rise is mostly derived from water entering the conduit system at the River Sink. As river stage and input into the River Sink decrease, increasingly larger volumes of groundwater drain from the matrix into the conduit system to discharge at the River Rise (Martin and Screaton 2001).

River Conditions and Potential Recharge

River Rise stage data were recorded about 200 m downstream of the spring with an automatic pressure transducer with an accuracy of ±0.03 m (Moore et al. submitted). The relationship between stage and discharge at the River Rise was calculated based on the rating curve developed by Screaton et al. (2004), using data collected by the Suwannee River Water Management District (SRWMD). Potential recharge was estimated as precipitation minus evapotranspiration (P-ET) during the study period by Ritorto et al. (in press). Briefly, daily values of P-ET were calculated using daily precipitation data collected in O'Leno State Park with an automated rain gauge maintained by SRWMD (http://www.srwmd.state.fl.us/index.asp?NID=99), and the Penman-Monteith model for estimating daily ET, which estimates water loss to the atmosphere from a vegetative surface (Dingman 2002).

Over the study period from January 2003 to April 2007, the amount of recharge, estimated as P-ET, and river stage and discharge varied greatly, but not always in concert. Average annual P-ET was about 400 mm (Ritorto et al. in press), which resulted in an average river stage and discharge of 10.2 masl and 16 m^3/s, respectively (Figure 3-3). The maximum annual P-ET of about 990 mm occurred in 2004 when Hurricane Frances delivered a total of 400 mm, similar to the average annual P-ET, at the O'Leno State Park rain gauge over a 6-day period in September. This rainfall corresponds to the maximum stage and discharge of 14.1 masl and 200 m^3/s respectively, which occurred on September 10, 2004 (Figure 3-3). From April 2006 to April 2007 the area received a total of 83 mm of P-ET or less than a fifth of the average annual amount. This low rainfall resulted in the lowest stage and discharge during the study of 9.6 masl and 2.2 m^3/s, respectively. Sampling trips S-2, S-9, and S-11 occurred during high flow events when the river was above average stage. All other samples were collected during average or low flow.

Water Chemistry

Sixteen sampling trips were conducted from January 2003 to April 2007 to collect water from eight groundwater monitoring wells, one sinking stream (River Sink), one first magnitude spring (River Rise), and four intermediate karst windows (Figure 3-2) (Moore et al. submitted). Of the 14 sites sampled, two surface water sites (River Sink and River Rise) and three groundwater sites (Wells 2, 4, and 7) show the greatest variation in water chemistry (Moore et al. submitted). All of the other sites that were sampled during the study (data not reported here) have chemical compositions similar to one of these five sites, and thus these five sites are used to represent the continuum of water chemistry across the region (Figure 3-4). A statistical summary of the major chemistry is shown in Table 4-1.

The variation in water chemistry reflects three representative end-member water types identified by Moore et al. (submitted). These three end members include a Na-Cl-type water, Ca-HCO_3-type water, and Ca-Mg-SO_4-type water that result from three distinct sources and develop two mixing trends (Figure 3-4). One trend extends from the Ca-HCO_3-type water at Well 4 (① in Figure 3-4) to the Ca-Mg-SO_4-type water at Well 2 (② in Figure 3-4). The composition of Well 4 is similar to shallow groundwater of the UFA and reflects rain water equilibrating with the Ocala Limestone (Moore et al. submitted). Water found at Well 2 is the most mineralized in the region and likely reflects water upwelling from deep within the aquifer, where elevated temperatures reflect the geothermal gradient and elevated SO_4^{2-} and Mg^{2+} concentrations may reflect gypsum dissolution, calcite precipitation, and dedolomitization (Moore et al. submitted). Well 7 falls along the mixing trend between Wells 4 and 2, suggesting it may be influenced by both sources of water (Figure 3-4).

The third end member is characterized by elevated concentrations of Na^+ and Cl^-, and occurs at the River Sink at high flow (③ in Figure 3-4). This end member develops a second

mixing trend that is confined to water collected from surface-water sites and reflects evolved rain water flowing overland with little contact with carbonate rocks (Moore et al. submitted). When the river is below average stage (e.g., S-3, S-4, S-6, S-10, and S-12 through S-16: Figure 3-3), water from the River Sink and River Rise fall along the mixing line between Wells 4 and 2, reflecting little influence from the Na-Cl-type end member.

Chemical Analysis and Geochemical Modeling

Methods

The geochemical code, PHREEQC, Version 2.15.0, (Parkhurst and Appelo 1999), was used to determine the distribution of aqueous species, partial pressure of CO_2, ion-activity products (Q), and mineral saturation index (SI) for all water samples. The SI for a given mineral is found by

$$SI = \log\left(\frac{Q}{K}\right), \tag{4-1}$$

where K is the equilibrium constant for a given mineral. Samples within ±0.1 SI are assumed to be in equilibrium with respect to calcite and dolomite based on analytical errors in measurements of pH, alkalinity, and concentrations of Ca^{2+} (e.g., Langmuir 1997). Thermodynamic data for calculations were from the *phreeqc.dat* database. Ionic strength of water samples was < 0.1 molal and thus activity coefficients of aqueous species were calculated using an extended version of the Debye-Hückle equation (Truesdell and Jones 1974). Charge balance errors for most samples were less than ±5% except for samples whose concentrations were near instrument detection limits.

The inverse modeling code in PHREEQC was used to assess changes in major dissolved constituents between input at the River Sink and discharge at the River Rise as a means to estimate the extent of calcite dissolution along the conduit flow path. The mass-balance model

attempts to match the water composition at the River Rise based on mixing proportions of water with compositions of water found at the River Sink and Wells 2 and 4, and the phase transfer of calcite and CO_2 gas. In modeling mass transfer, I assume a quasi-steady state for each sample day and thus hydrodynamic dispersion and diffusion are assumed to be minor processes compared to the chemical evolution along the conduit flow path for that day (Wigley et al. 1978; Gandolfi et al. 2001). In this study, mass-balance calculations determined in PHREEQC are constrained by the concentration of Ca^{2+}, Mg^{2+}, Na^{+}, Cl^{-}, SO_4^{2-}, and alkalinity in the initial and final waters. Concentrations of K^{+} were not included in modeling because their low concentrations resulted in failed convergence of iterations in the mass-balance calculations. Prior to each simulation, each solution is charge balanced by adjusting the ion concentrations within predetermined uncertainty limits, which were set based on the charge imbalance for each water analysis. These limits allow the model to charge balance the initial and final solutions given the range of uncertainty within the analyzed water chemistry. If a solution can not be adjusted to charge balance using the given uncertainty limits, no models will be found.

Results

The UFA is mostly comprised of calcite with lesser amounts of dolomite and gypsum (Figure 3-1), and thus dissolution of the aquifer minerals can be described largely by reactions given in Table 4-2. Deviations from equilibrium of these reactions can be evaluated through calculations of SI and an activity-phase diagram that represents the major aquifer-bearing minerals in the basin (cf. Helgeson 1969) (Figure 4-1). In phase diagrams, boundaries between mineral phases are based on values of the equilibrium constants for the reactions; for example, the equilibrium between calcite and dolomite is derived from the expression for the equilibrium constant of Reaction 1 (Table 4-2), which in logarithmic form is

$$\log\left(\frac{a_{Ca^{2+}}}{a_{Mg^{2+}}}\right) = \log K, \quad (4\text{-}2)$$

where *a* represents ion activity and log K is 0.38 (Plummer and Busenberg 1982). All other phase boundaries in Figure 4-1 were calculated using the logarithmic form of the K expression for each reaction in Table 4-2.

Figure 4-1 depicts the relative stability of calcite, dolomite, and gypsum at 25 °C and 1 atm as a function of the activities of Ca^{2+}, Mg^{2+}, SO_4^{2-}, and CO_3^{2-} of the water collected during the study period. Although activities of Ca^{2+}, Mg^{2+}, and SO_4^{2-} are primarily controlled by mineral dissolution reactions, the activity of CO_3^{2-} is a function of pH and magnitude of the CO_2 dissolved in the water in the form of

$$H_2CO_3 = 2H^+ + CO_3^{2-}, \quad (4\text{-}3)$$

which can be represented by a K expression in logarithmic form

$$\log K_{H_2CO_3} = 2 \log a_{H^+} + \log a_{CO_3^{2-}} - \log a_{H_2CO_3}, \quad (4\text{-}4)$$

and has a log $K_{H_2CO_3}$ of -16.68 (Plummer and Busenberg 1982). Considering $a_{H_2CO_3}$ can be represented by $K_{CO_2} P_{CO_2}$ (Drever 1997), Equation 4-4 becomes

$$\log K_{H_2CO_3} = 2 \log a_{H^+} + \log a_{CO_3^{2-}} - \log K_{CO_2} - \log P_{CO_2}, \quad (4\text{-}5)$$

where log K_{CO_2} has a value of -1.47 at 25 °C (Plummer and Busenberg 1982). Rearranging Equation 4-5 for log $a_{CO_3^{2-}}$ and substituting values for log K_{CO_2} and log $K_{H_2CO_3}$ gives

$$\log a_{CO_3^{2-}} = \log P_{CO_2} + 2\,pH - 18.15. \quad (4\text{-}6)$$

Equation 4-6 shows how $a_{CO_3^{2-}}$ relates to the pH and P_{CO2} for each sample.

Samples from the five sites representing end-member water compositions fall into three groups on the phase diagram (Figure 4-1). Each group has $a_{Ca^{2+}}/a_{Mg^{2+}}$ ratios that vary little compared to their $a^2_{SO_4^{2-}}/a^2_{CO_3^{2-}}$ ratios, which suggests most variation in water chemistry results from changes in SO_4^{2-} concentration, P_{CO2}, and pH. The Ca-HCO_3-type water, as represented by samples from Well 4, plots in the calcite field with a constant $\log a_{Ca^{2+}}/a_{Mg^{2+}}$ ratio of about 1.58 (Figure 4-1). This ratio suggests the water reacts primarily with calcite and has little contact with dolomite. In contrast, the Ca-Mg-SO_4-type water from Well 2, as well as surface water from the River Sink and River Rise, plot on the phase boundary between calcite and dolomite, suggesting this water reacts with both minerals (Reaction 1 in Table 4-2). This water also plots closer to the phase boundaries of gypsum than water from the other wells, reflecting reactions with this mineral as well (e.g. Reactions 2 and 3, Table 4-2). Although some surface-water samples plot into the gypsum field, these samples were collected during high flow and thus are dilute with minor amounts of SO_4^{2-}, low pH and high P_{CO2} (Table 4-1). Water from Well 7 plots in the calcite field, intermediate between samples from Wells 4 and 2, but closer to the phase boundary between calcite and dolomite than Well 4. These relationships correspond to the mixing relationships shown in Figure 3-4, but reflect which minerals the water has reacted with.

While the phase diagram shows which minerals may have reacted with the water, the SI indicates whether the water can theoretically dissolve or precipitate a given mineral. Most of the water is undersaturated with respect to calcite, dolomite and gypsum (Figure 4-2). Some groundwater samples at all the wells are saturated with respect to calcite and some samples from Well 2 are saturated with respect to dolomite (Figures 4-2A and B). The SI of calcite and dolomite in the groundwater samples show a linear variation through time, although not systematically with river stage. Although all groundwater remains undersaturated with respect to

gypsum, a strong trend exists among the wells, with Well 2 water plotting closest to saturation (Figure 4-2C). The SI of surface-water sites decreases with river stage indicating that allogenic runoff becomes more dilute as stage increases (Figures 4-2D-F). Most surface water is undersaturated with respect to calcite, dolomite and gypsum, although some samples are at saturation with calcite and dolomite at low flow.

Discussion

Conduits in telogenetic karst result from dissolution along fractures, joints, and fissures depending on disequilibrium between the conduit water and wall rock (e.g., Palmer 1991; Grasso and Jeannin 2002). In eogenetic karst aquifers, however, high matrix permeability provides a significant component of flow (Budd and Vacher 2004; Florea and Vacher 2007), allowing multiple sources of water to converge on the conduits (e.g., Moore et al. submitted). Although fractures and partings have a strong influence on many conduits in eogenetic karst (Florea et al. 2007), the interaction of water with different chemistry and high matrix permeability should influence how these conduits enlarge over time. In the following sections, I use mass-balance modeling of groundwater and surface-water chemistry to evaluate how matrix permeability may influence the magnitude and distribution of conduit development in eogenetic karst aquifers.

Geochemical Evolution of Groundwater

Shallow groundwater in the sink-rise region, reflected in compositions of water from Well 4, is the product of CO_2-rich diffuse recharge dissolving Ocala Limestone to elevate concentrations of Ca^{2+} and HCO_3^- (e.g., Ritorto et al. in press; Moore et al. submitted). This CO_2 derives from root respiration and oxidation of organic matter in the soil and vadose zone (e.g., Atkinson 1977; Wood and Petraitis 1984; Ritorto et al. in press), which decreases pH and drives the water to undersaturation with respect to calcite and dolomite (Figures 4-2A and B). Although the Ocala Limestone has up to 2 mole % Mg and trace amounts of dolomite (Plummer 1977;

Miller 1986), insufficient amounts of the Mg is dissolved to cause the shallow groundwater to reach saturation with respect to dolomite (Figure 4-2B). The limited amount of Mg^{2+} in the shallow groundwater results in Well 4 water projecting well into the calcite field on the phase diagram (Figure 4-1).

Deep water in the region, as reflected in water at Well 2, is more mineralized than the shallow water. Although this mineralization could result from leaching of ions during recharge through leaky portions of the Hawthorn Group that flow along deep flow paths due to regional head gradients (Lawrence and Upchurch 1982; Wicks and Herman 1994; Katz et al. 2004), recent work suggests elevated concentrations reflect dissolution of calcium sulfate minerals and dedolomitization occurring deep within the aquifer (Moore et al. submitted). This observation is supported by the saturation indices with respect to calcite, dolomite and gypsum (Figures 4-2A-C) and the projection of Well 2 water on the phase boundary between calcite and dolomite and close to the phase boundary of gypsum (Figure 4-1), which suggests the deep water dissolved calcium sulfate minerals and may be at equilibrium with respect to both calcite and dolomite (cf. Plummer 1977; Hanshaw and Back 1979; Jones et al. 1993).

Surface water at the River Sink and River Rise is a mixture of allogenic recharge and groundwater, with proportions that vary with flow conditions (Moore et al. submitted) (Figure 3-4). Water budget calculations indicate that while input at the River Sink accounts for the largest amount of recharge to the sink-rise system, most of this water flows through the conduits and discharges at the River Rise without any loss to the surrounding aquifer (Ritorto et al. in press). Consequently, water from the River Sink and River Rise have similar chemistry and fall on the phase boundary between calcite and dolomite, but at various distances from the field for gypsum (Figure 4-1). The projection of surface water on the phase boundary between calcite and

dolomite reflects reaction with these minerals, although there is little dolomite in the stratigraphic section at the depths of the conduits as reflected in water compositions at Well 4 (Figure 4-1). Chemical compositions of River Sink and River Rise waters indicate some portion of their source was deeper within the stratigraphic section than where they were sampled, reflecting mixing with deep mineralized water as characterized by water compositions at Well 2 (cf. Jones et al. 1993).

Contributions of deep water to the sink-rise system correlate inversely with river stage and are greatest during droughts as surface water chemistry trends towards the Well 2 end member (Figures 3-4 and 4-1) (Moore et al. submitted). The projection of River Sink and River Rise water towards and into the gypsum field occurs only during high discharge conditions when runoff has dilute concentrations, low pH, and high P_{CO2} (Table 4-1 and Figure 4-1). This water is greatly undersaturated with respect to all minerals (Figures 4-2D-F). Consequently, although this water projects into the gypsum field (Figure 4-1), it most likely reflects decreasing $a_{CO_3^{2-}}$ from low pH and high P_{CO2} rather than an increase in the $a_{SO_4^{2-}}$ from reaction with calcium sulfate minerals. The only other location with a signal from the deep-water source is Well 7 (Figures 3-4 and 4-1), but its location is about 1 km away from the closest known conduit (Figure 3-2). The presence of mineralized water supports earlier observations that deep-water upwelling may be responsible for high SO_4^{2-} concentrations in shallow portions of the UFA throughout the region, although delivery of this water may be restricted to vertical flow paths such as fractures and faults (e.g., Hunn and Slack 1983; Moore et al. submitted).

Estimates of Conduit Dissolution in the Sink-Rise System

I estimate dissolution along the conduit flow path between the River Sink and River Rise using the inverse modeling code in PHREEQC. Results of the model are not unique, but do

provide insight to possible water-rock reactions that account for spring chemistry at the River Rise. In these simulations, the groundwater flow path is the conduit network and the final solution is the River Rise water, which is assumed to obtain its composition from mixing with the representative end member water types, i.e., River Sink and Wells 2 and 4 (Figure 3-4), and reactions with calcite and CO_2 gas. I allow the model to react only with stoichiometric calcite, since the conduits are confined to the Ocala Limestone, which contain only trace amounts of magnesium-bearing minerals (Miller 1986). Given that water from the River Rise is either at equilibrium or undersaturated with respect to calcite (Figure 4-2D), I assume calcite only dissolves, whereas CO_2 is allowed to be taken up or released from solution during the simulations.

Each simulation resulted in one inverse model that accounted for the chemical variation at the River Rise for all sampling times except January 2003 and March 2003 (S-1 and S-2, Figure 3-3). January 2003 was prior to the installation of Well 4 so data critical for the model were lacking for that sample time (Table 4-3). River stage was elevated during the March 2003 sampling, and thus the River Rise and River Sink are dilute and have similar compositions, reflecting minimal gain of groundwater by the conduits (Table 4-1). To estimate dissolution during this time, water at the River Rise was modeled by reacting calcite and CO_2 with River Sink water (SI_{CAL} = -4.2 and log P_{CO2} = -1.4) until achieving the SI of calcite and P_{CO2} determined in the River Rise water (SI_{CAL} = -4.8 and log P_{CO2} = -0.69). Modeling results show that most of the time water chemistry at the River Rise can be explained by mixing of representative end-member water types and mass transfer of calcite and CO_2, or in the case of March 2003, water from the River Sink alone reacting with calcite and CO_2. While dissolution along the conduit flow path only occurred five times, there was uptake and release of CO_2 during

each simulation suggesting that dissolution has a minor affect on the mass transfer of CO_2 (Table 4-3).

Uptake and release of CO_2 between the River Sink and River Rise may result from processes including mixing of different source waters, aerobic decay of organic carbon, and interaction with the atmosphere. Release of CO_2 could occur when the conduit water emerges to the surface at karst windows along the flow path (Figure 3-2). Uptake of CO_2 along the flow path reflects CO_2 being generated within the conduit and/or additional CO_2 entering the conduit from the surrounding aquifer. One source of CO_2 may result from aerobic decay of organic carbon that is flushed into the conduit. Dissolved organic carbon has been shown to exceed 30 mg/l at the River Sink during high flow (Zimmerman et al. 2006). In March 2003, CO_2 concentration is about 20 times more than occurred during the remaining 14 sample trips and the excess CO_2 may be derived from oxidation of organic carbon (Table 4-3). During this sampling time, hydraulic head in conduit exceeded hydraulic head in the surrounding aquifer (Martin et al. 2006) (S-3, Figure 3-3), restricting the amount of CO_2 that could enter the conduit from the matrix. The CO_2-charged water undersaturated with respect to calcite was lost from the conduit to the surrounding aquifer, and would have dissolved some of the aquifer matrix during its residence time there (Martin and Dean 2001; Screaton et al. 2004; Ritorto et al. in press). This loss of CO_2-rich water to the surrounding aquifer may also explain the strong linear variation in SI_{CAL} and SI_{DOL} at in the wells (Figures 4-2A and B), which would vary due to changes in pH and P_{CO2} of the groundwater (Eq. 4-6); however, no systematic cause for the variation exists (Moore et al. submitted). During average and low flow when hydraulic head gradients reverse, increases in CO_2 along the conduit flow path could result from a combination of aerobic decay and input of CO_2-rich water from the matrix (Table 4-1). The relative concentrations of these two sources

cannot be determined from these data, but could be assessed by measured changes in organic carbon concentrations and terminal electron acceptors (e.g., O_2, NO_3, and metal oxides) along the flow path.

Conduit wall retreat can be estimated during the five times dissolution was found (Table 4-3) assuming the conduit is about 6000 m long with an average cross-sectional area of about 386 m^2 (Screaton et al. 2004). These dimensions indicate a surface area of about 4 x 10^5 m^2. Using a measured value for discharge at the River Rise, a molar volume of calcite of 3.69 x 10^{-5} m^3 and 30% porosity for the Ocala Limestone, an estimated dissolution rate ranges from about 2 x 10^{-6} to 6 x 10^{-6} m/day (Table 4-4). Although the occasional sample trips make it difficult to estimate yearly averages, these daily values of dissolution agree well with estimates of maximum wall retreat in telogenetic conduits (3 x 10^{-6} to 3 x 10^{-7} m/day; Palmer 1991).

Implications of Conduit Enlargement in Eogenetic Karst Aquifers

The conduit network between the River Sink and River Rise represents a dynamic flow path that transmits water through the subsurface and increases Ca^{2+} concentrations at all sampling times (Figure 4-3). This increase in Ca^{2+} would be consistent with dissolution of the conduit wall rock in a telogenetic aquifer (Palmer 1991; Howard and Groves 1995; Grasso and Jeannin 2002), but most increases in Ca^{2+} concentrations at the River Rise can be explained by flow of allogenic and diffuse recharge to the conduit, coupled with upwelling of mineralized deep water based on a two component mixing model using only Mg^{2+} and SO_4^{2-} (Moore et al. submitted). Inverse modeling used here relies on concentrations of Mg^{2+} SO_4^{2-}, Ca^{2+}, Na^+, Cl^-, and alkalinity and thus may be more sensitive to estimates of mixing because of uncertainty limits set for each component (Table 4-3). Consequently, the increase in Ca^{2+} concentrations along the conduit flow path likely reflects dissolution within the surrounding aquifer with

subsequent flow to the conduit, rather than dissolution at the conduit wall (Screaton et al. 2004; Ritorto et al. in press).

Although water flowing from the River Sink to River Rise remains undersaturated with respect to calcite most of the time (Figure 4-2D), modeling results suggest dissolution is limited along the conduit flow path (Table 4-4). Rates of dissolution are controlled by the combination of a thin boundary layer of static water at the contact between wall rock and water, and reaction processes including the hydration of $CO_{2(aq)}$ (Kern 1960) and dissolution at the mineral surface by reaction with H^+ and $H_2CO_3^o$ (the 'PWP Equation'; Plummer et al. 1978). Thickness of the boundary layer depends on flow conditions through the conduit, but are generally on the order of a fraction of a millimeter (Dreybrodt and Gabrovšek 2002). This layer acts as a weak barrier between the undersaturated water and conduit wall rock, whereby reactants and dissolution products move through the layer by molecular diffusion (Liu and Dreybrodt 1997). However, as water from the matrix flows into the conduit, dissolution may be limited as reactants such as H^+, $H_2CO_3^o$, and $CO_{2(aq)}$ are restricted from contacting the conduit wall. These observations suggest that conduit enlargement in eogenetic karst may result from processes in addition to strict dissolution of the conduit wall.

Conduits may increase in size in eogenetic karst when allogenic recharge flows to the surrounding aquifer causing dissolution within the matrix porosity (Screaton et al. 2004; Ritorto et al. in press). Although the boundary layer also controls dissolution rates within these pore spaces, slower flow and longer residence time allows sufficient time for matrix water to reach saturation (e.g., Figure 4-2A). Water losses from the conduit typically occur during high flow when water has a SI_{CAL} of less than -3 SI (S-2, S-9, and S-11: Figure 3-3). Recent estimates of dissolution from allogenic water equilibrating with the matrix rock in the sink-rise system

suggested up to 500 m^3 of limestone could have dissolved over a 63 month period (Ritorto et al. in press). Averaging this amount over the surface area of the conduit wall (4×10^5 m^2), suggests a dissolution rate of about 2×10^{-4} m/yr or about 7×10^{-7} m/day. This value is about an order of magnitude lower than daily rates estimated along the conduit flow path (Table 4-4), but still within range of maximum wall retreat values determined for telogenetic karst (3×10^{-6} to 3×10^{-7} m/day; Palmer 1991). Although the loss of conduit water to the surrounding aquifer is episodic, this process suggests significant amounts of dissolution may occur adjacent to the conduit or high permeability zones where allogenic water can flow into the matrix (Ritorto et al. in press). Because of the high matrix porosity in eogenetic karst, dissolution by this process would result in a friable halo surrounding the conduit (Figure 4-4). Similar results were found from core samples collected from the walls of air-filled caves in west-central Florida, which show an order of magnitude increase in matrix permeability near the wall surface compared to matrix permeability within the wall interior (Florea 2006). This increase in matrix permeability would not be expected in telogenetic karst aquifers; instead, water lost to the surrounding aquifer in these settings will enlarge fracture flow paths within an otherwise impenetrable matrix (Ford and Williams 2007).

The development of a friable halo will largely depend on the movement of water between the conduit and surrounding aquifer, which varies due to differences in hydraulic conductivity (Martin et al. 2006) (Figure 4-4). Particle tracking simulations during the March 2003 flood (S-2, Figure 3-3) suggested the movement of water into the matrix ranges from about 0.4 to 8 m based on differences in hydraulic head between river stage at the River Sink and water levels in Wells 1 and 4 (Martin 2003) (Figure 3-2). Although these simulations assumed flow paths within a homogeneous and isotropic aquifer, preferential flow paths will allow water to move farther into

the matrix (Martin and Dean 2001) (K_2 in Figure 4-4). Following reversal of the hydraulic gradient between the wells and conduit, the simulated water was estimated to return to the conduit in about two weeks, indicating sufficient time for calcite dissolution in the matrix to drive the water to about 80 to 90% calcite saturation (Plummer et al. 1978; White 1988). This dissolution should also increase matrix permeability over time and allow more undersaturated water to flow into to the surrounding aquifer in a feed-back loop that would preferentially enlarge conduits along the flow path that already started. In addition, as matrix rock becomes less consolidated within the friable halo, physical erosion of the conduit wall rock should increase as suspended sediments and particles are transported through the conduit (e.g., Dogwiler and Wicks 2004). This development of a friable halo and removal of the wall rock by dissolution and/or sediment transport may explain the irregular solution pockets and spongework textures common to many Florida conduits that receive allogenic recharge (Kincaid 1999; am Ende 2000; Palmer 2007).

Conclusions

In the Santa Fe Sink-Rise area, water originates from three sources including allogenic water at the River Sink, diffuse recharge through the vadose zone that equilibrates with Ocala Limestone, and upwelling of water from deep in the aquifer, which is more mineralized than the shallow water following reactions with calcite, dolomite, and calcium sulfate minerals. Although allogenic recharge provides significant amounts of undersaturated water to the UFA, most of the recharge flows through the conduits discharging at the River Rise with little interaction with the surrounding aquifer. This limited interaction results in model estimates of dissolution occurring only during 5 of the 14 sampling times. When hydraulic head within the conduit exceeds hydraulic head in the surrounding aquifer, allogenic water undersaturated with respect to calcite is lost to the surrounding aquifer and dissolves matrix rock in the vicinity of the conduit. This

process generates a friable halo, suggesting conduit enlargement may result from both dissolution and physical erosion of less consolidated matrix rock. Extrapolating these results to eogenetic karst in general suggest that conduits develop in eogenetic karst aquifers by mixing of multiple water sources and flow into and out of the high matrix porosity.

Models describing conduit enlargement in telogenetic karst assume an impenetrable boundary at the conduit wall, whereby increases in Ca^{2+} concentration along the flow path reflect dissolution of the wall. In eogenetic karst, Ca^{2+} concentrations could increase in the conduit water from inputs of Ca-rich water from the matrix when hydraulic heads within the surrounding aquifer exceed hydraulic head in the conduit, a condition that is common in eogenetic karst. This flow of water from the matrix to the conduit would also limit dissolution of the conduit water by limiting contact of undersaturated water with the conduit wall. These processes may explain why dissolution within the conduit occurred only during 30% of the sampling times.

Although conduit wall retreat in the sink-rise system has daily rates comparable to those from telogenetic settings, this dissolution is not continuous. The long-term average dissolution of the conduit walls results from a combination of dissolution at the conduit wall, as well as within the matrix surrounding the conduit, which is a process not expected to occur in telogenetic karst aquifers with low matrix permeability. These results provide insight on the difficulty in applying concepts of conduit enlargement developed for telogenetic karst in eogenetic karst aquifers, and illustrate the influence of matrix permeability on groundwater flow and the conduit enlargement in eogenetic settings.

Table 4-1. Summary of major ions, alkalinity, SpC, pH, T, SI, and P_{CO2} of representative water samples.

Location	Cl			SO4			Ca			Na		
	range	x	CV	range	x	CV	range	x	CV	range	x	CV
River Sink	0.23 - 0.64	0.38	27	0.02[a] - 0.48	0.24	69	0.19 - 1.39	0.78	58	0.19 - 0.46	0.30	19
River Rise	0.32 - 0.64	0.47	17	0.02 - 1.15	0.63	61	0.20 - 2.02	1.24	55	0.24 - 0.52	0.39	23
Well 2	0.42 - 1.66	1.24	28	1.19 - 4.47	3.43	28	1.97 - 4.77	3.92	18	0.61 - 1.61	1.26	23
Well 4	0.22 - 0.28	0.25	6	0.02 - 0.05	0.04	18	2.07 - 2.36	2.21	3	0.18 - 0.22	0.20	6
Well 7	0.28 - 0.54	0.42	18	0.02 - 0.29	0.16	38	1.54 - 2.77	2.19	19	0.19 - 0.34	0.27	17

Table 4-1. Continued

Location	Mg			K			alkalinity			pH		
	range	x	CV	range	x	CV	range	x	CV	range	x	CV
River Sink	0.09 - 0.64	0.35	58	0.020 - 0.047	0.028	27	0.16 - 3.04	1.56	71	5.40 - 7.79	6.94	9
River Rise	0.09 - 0.72	0.44	54	0.024 - 0.041	0.027	15	0.16 - 3.16	1.90	58	4.70 - 7.37	6.90	9
Well 2	0.57 - 2.04	1.48	32	0.035 - 0.082	0.06	28	2.04 - 4.28	3.89	13	6.48 - 7.10	6.84	3
Well 4	0.05 - 0.09	0.06	16	0.005 - 0.010	0.009	14	2.80 - 4.30	4.03	9	6.48 - 7.19	6.87	3
Well 7	0.15 - 0.24	0.18	13	0.015 - 0.023	0.019	13	2.16 - 5.12	4.12	19	6.50 - 7.40	6.95	4

Table 4-1. Continued

Location	SpC			T			SI_{CAL}			SI_{DOL}		
	range	x	CV	range	x	CV	range	x	CV	range	x	CV
River Sink	73 - 412	256	48	10.0 - 27.7	19	27	-4.5 - 0.32	-1.40	n/a[b]	-9.0 - 0.4	-3.1	n/a
River Rise	73 - 560	371	46	11.0 - 26.4	20	20	-4.8 - 0.02	-1.10	n/a	-9.5 - -0.4	-2.5	-99
Well 2	488 - 1315	1058	20	22.0 - 26.3	25	4	-0.7 - 0.06	-0.19	n/a	-1.4 - -0.1	-0.7	63
Well 4	390 - 449	428	3	20.9 - 21.7	21	1	-0.7 - 0.04	-0.27	n/a	-1.5 - -1.4	-2	-22
Well 7	306 -550	434	20	20.3 - 20.9	21	1	-0.6 - 0.08	-0.23	n/a	-1.3 - -0.8	-1.5	-27

Table 4-1. Continued

Location	SI_{GYP}			log P_{CO2}		
	range	x	CV	range	x	CV
River Sink	-4 - -2.0	-2.7	-24	-2.7 - -1.4	-2.1	-14
River Rise	-4 - -1.6	-2.1	-32	-2.8 - -0.7	-2	-22
Well 2	-1.5 - -0.8	-0.9	-19	-2.0 - -1.1	-1.5	-15
Well 4	-3.1 - -2.8	-2.9	-3	-1.8 - -1.1	-1.5	-12
Well 7	-3.2 - -2.0	-2.3	-11	-2.1 - -1.0	-1.6	-22

Range and mean (x) of concentrations in mmol/kg H_2O, coefficient of variation (CV) defined as mean/standard deviation in percent, pH and SI values are unitless, SpC in µS/cm, T in °C, log P_{CO2} in atm, [a]minimum detectable value of SO_4^{2-}, [b]n/a is not applicable due to both positive and negative numbers.

Table 4-2. Chemical reactions involving UFA minerals.

	Chemical Reactions	log K
1	$2\ CaCO_3 + Mg^{2+} \leftrightarrow CaMg(CO_3)_2 + Ca^{2+}$	0.38
2	$2\ CaSO_4 \cdot 2\ H_2O + 2\ CO_3^{2-} \leftrightarrow 2\ CaCO_3 + 2\ SO_4^{2-} + 2\ H_2O$	7.99
3	$2\ CaSO_4 \cdot 2\ H_2O + Mg^{2+} + 2\ CO_3^{2-} \leftrightarrow CaMg(CO_3)_2 + Ca^{2+} + 2\ SO_4^{2-}\ 2\ H_2O$	8.37

Log K is the equilibrium constant for each reaction at 25 °C. Gibbs energy and enthalpy of formation for calcite from Plummer and Busenberg (1982), dolomite from Ball and Nordstrom (1991), and gypsum from Anderson and Crerar (1993).

Table 4-3. River Rise composition estimated by mixing of River Sink, Well 2, and Well 4 end-member compositions and mass transfer of calcite and CO_2.

Date	River Rise	pH	Alkalinity (mmolal)	Cl (mmolal)	SO4 (mmolal)	Ca (mmolal)	Na (mmolal)	Mg (mmolal)	Calcite (10^{-5} moles/l)	CO_2(g)	Uncertainty Limits River Sink (%)	Well 2 (%)	Well 4 (%)
3/5/03	Modeled composition[a]	4.70	0.165	0.358	0.021	0.193	0.274	0.099	0.3	716[b]	n/a[c]	n/a	n/a
	(%) difference	0	3	12	0	-5	10	4					
4/30/03	Modeled composition	6.80	2.240	0.539	0.622	1.397	0.422	0.404	--	29	7.5	7.5	7.5
	(%) difference	0	4	5	-5	-2	4	0					
1/23/04	Modeled composition	7.37	2.959	0.522	0.929	1.788	0.466	0.649	10	15	2.5	2.5	2.5
	(%) difference	0	5	3	-2	-5	5	-5					
3/8/04	Modeled composition	6.87	0.846	0.511	0.342	0.603	0.335	0.250	--	-2	2.5	2.5	2.5
	(%) difference	0	3	4	-4	0	4	3					
5/5/04	Modeled composition	7.36	3.022	0.516	1.035	1.833	0.509	0.717	--	6	2.5	2.5	2.5
	(%) difference	0	5	0	0	-4	-2	5					
1/19/05	Modeled composition	6.91	1.581	0.539	0.423	1.035	0.353	0.272	--	-27	5	2.5	15
	(%) difference	0	4	13	-6	11	4	-13					
3/18/05	Modeled composition	7.06	1.532	0.514	0.467	0.959	0.375	0.343	8.6	-27	6	2.5	2.5
	(%) difference	0	-7	0	-6	6	6	-2					
7/18/05	Modeled composition	6.59	0.533	0.374	0.145	0.357	0.219	0.133	--	-27	30	10	10
	(%) difference	0	3	7	10	-10	-10	0					

Table 4-3. Continued

Date	River Rise	pH	Alkalinity (mmolal)	Cl (mmolal)	SO4 (mmolal)	Ca (mmolal)	Na (mmolal)	Mg (mmolal)	Calcite (10^{-5} moles/l)	CO_2 (g)	Uncertainty Limits* River Sink (%)	Well 2 (%)	Well 4 (%)
10/27/05	Modeled composition	7.19	2.096	0.433	0.586	1.233	0.367	0.434	--	-47	6	6	6
1/17/06	Modeled composition	7.27	0.560	0.424	0.203	0.398	0.283	0.155	--	-33	5	5	5
	(%) difference	0	4	5	-5	-5	0	1					
4/12/06	Modeled composition	6.96	2.560	0.432	0.685	1.483	0.356	0.519	3.2	-11	2.5	2.5	15
	(%) difference	0	2	2	-4	-4	5	0					
7/13/06	Modeled composition	6.98	3.148	0.422	0.997	1.868	0.444	0.691	--	34	5	5	5
	(%) difference	0	5	0	4	-5	-1	5					
10/10/06	Modeled composition	7.15	3.259	0.502	1.024	1.925	0.483	0.739	--	-11	4.5	4.5	4.5
	(%) difference	0	5	-1	-5	-4	0	5					
1/17/07	Modeled composition	7.26	3.196	0.492	1.052	1.974	0.466	0.689	--	-37	4	4	6
	(%) difference	0	2	3	0	-2	0	-4					
4/10/07	Modeled composition	7.24	3.158	0.483	1.088	1.912	0.498	0.748	7.2	-8	7.5	7.5	7.5
	(%) difference	0	0	-5	-5	1	5	5					

[a]March 2003 composition was not determined by inverse modeling, but by reacting water from River Sink with calcite and CO_2 until achieving the SI of calcite and P_{CO2} determined in River Rise water. [b]negative sign denotes uptake and positive sign denotes release of CO_2. [c]n/a is not applicable for March 2003 due to different modeling approach.

Table 4-4. Inverse modeling of source water mixing and mass transfer of calcite and CO_2 along a conduit flow path.

Date	Rise Discharge (m^3/s)	Source Contribution			Calcite (10^{-6} m/day)	CO_2 (g) (moles/s)
		Well 2	Well 4	Sink		
3/5/03[a]	58.0	0.00	0.00	1.00	0.3[b]	415[c]
4/30/03	11.9	0.18[d]	0.07	0.74	--[e]	3
1/23/04	5.1	0.18	0.08	0.75	6	0.8
3/8/04	9.8	0.03	0.02	0.96	--	-0.2
5/5/04	6.1	0.17	0.04	0.78	--	0.4
1/19/05	18.0	0.17	0.14	0.69	--	-5
3/18/05	20.5	0.10	0.04	0.86	2	-5
7/18/05	49.5	0.04	0.04	0.92	--	-13
10/27/05	15.7	0.09	0.17	0.74	--	-7
1/17/06	30.4	0.02	0.01	0.97	--	-10
4/12/06	10.2	0.18	0.00	0.82	4	-1
7/13/06	7.4	0.14	0.10	0.76	--	3
10/10/06	5.1	0.16	0.11	0.73	--	-0.6
1/17/07	3.9	0.16	0.18	0.66	--	-1
4/10/07	3.7	0.15	0.07	0.78	3	-0.3

[a]Modeled by allowing River Sink water to achieve SI_{CAL} and P_{CO2} values determined at River Rise. [b]Dissolution rate calculated from flux of calcite at spring (Rise discharge times calcite concentration in moles/l (Table 4-3)), molar volume of calcite (3.69×10^{-5} m^3), 30% for Ocala Limestone, and surface area along the flow path of 4.2×10^5 m^2 (Screaton et al. 2004). [c]Positive signs indicates uptake of CO_2 and negative sign indicates release of CO_2. [d]Mixing fractions calculated by inverse modeling in PHREEQC. [e]-- indicates days when no dissolution occurred.

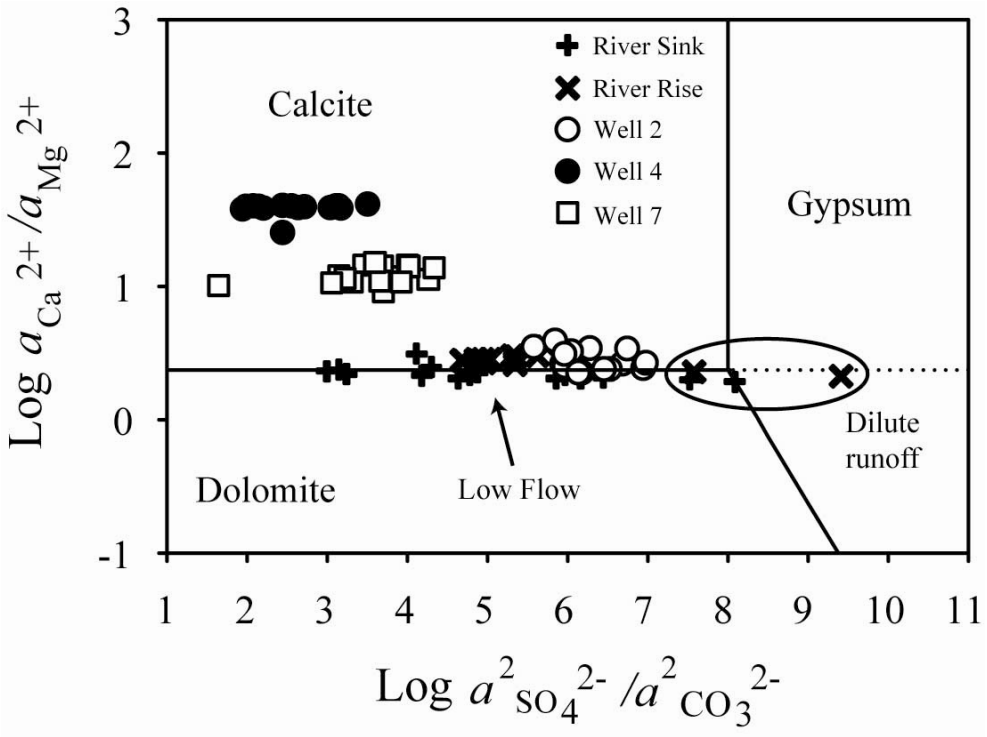

Figure 4-1. Phase diagram showing relations among sampled water and the aquifer-bearing minerals calcite, dolomite, gypsum. Lines on diagram represent calculated phase boundaries between minerals using reactions in Table 4-2. Solid lines represent equilibrium between mineral phases and dotted line represents metastable extension of calcite-dolomite phase boundary into the gypsum field. Oval indicates dilute surface samples collected during high flow, and arrow points to all other surface samples collected during average or low flow.

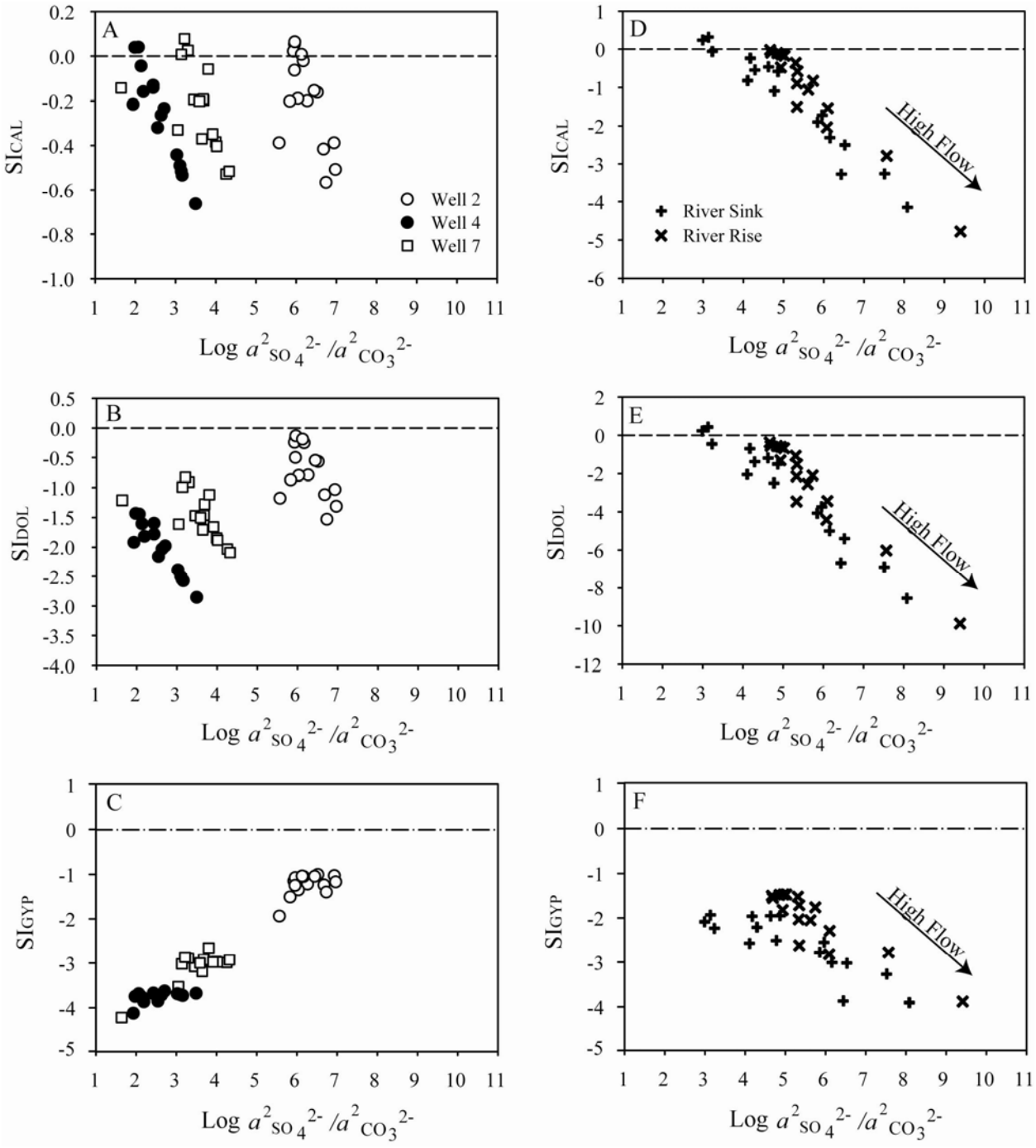

Figure 4-2. Saturation indices of calcite, dolomite, and gypsum versus Log $a^2_{SO_4^{2-}}/a^2_{CO_3^{2-}}$. A) SI_{CAL} at groundwater wells. B) SI_{DOL} at groundwater wells. C) SI_{GYP} at groundwater wells. D) SI_{CAL} at River Sink and River Rise. E) SI_{DOL} at River Sink and River Rise. F) SI_{GYP} at River Sink and River Rise. Dashed lines represents saturation (SI = 0).

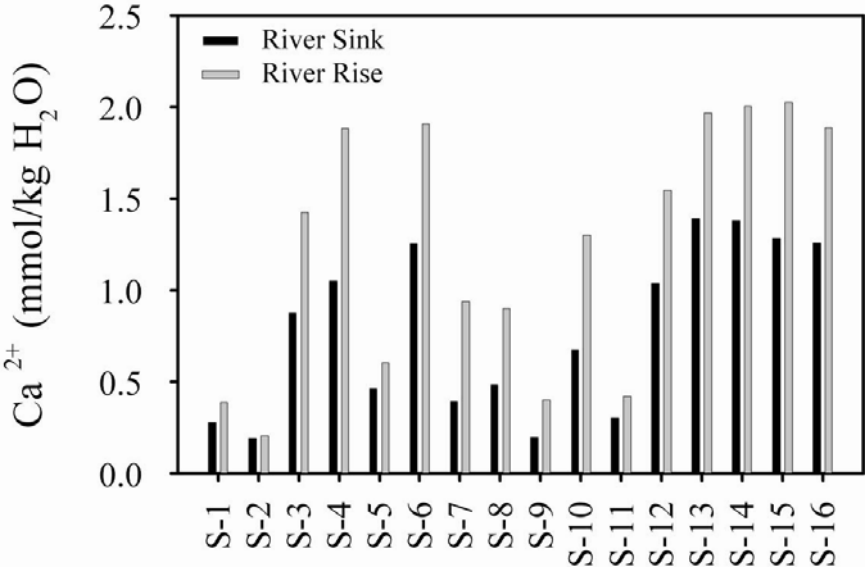

Figure 4-3. Bar graph showing Ca^{2+} concentrations at the River Sink (black bar) and River Rise (gray bar) for each sample trip highlighted on Figure 3-3.

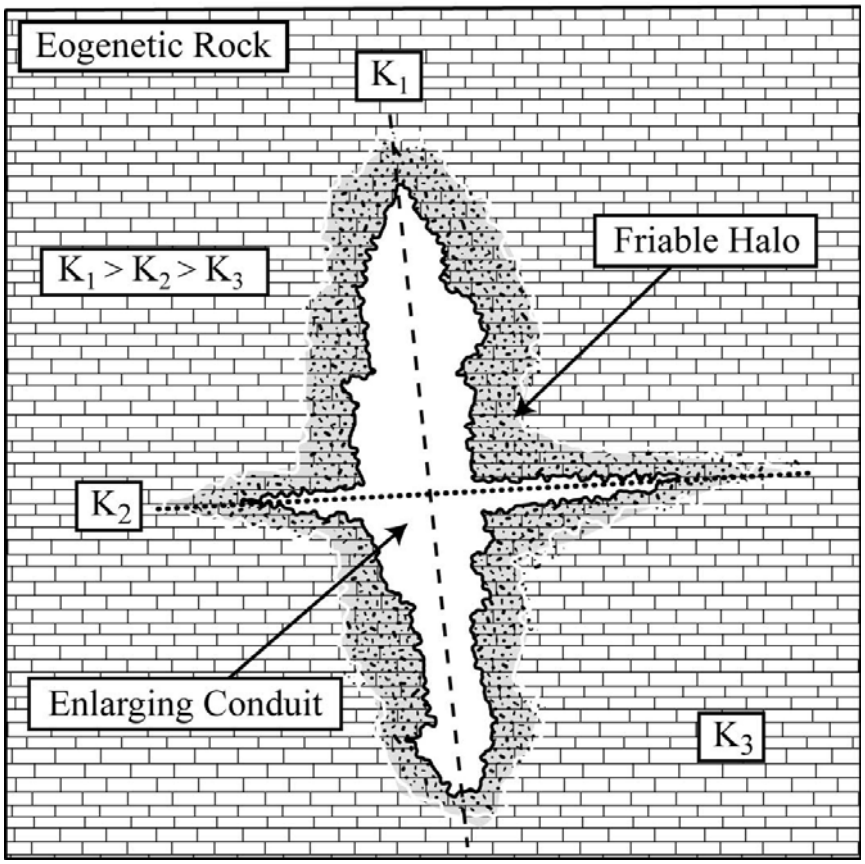

Figure 4-4. Conceptual sketch showing the cross-sectional area of a conduit in an eogenetic karst aquifer. Gray area represents the halo of dissolution in the matrix. Dashed line represents conduit developing along fracture with hydraulic conductivity (K_1), and dotted line represents secondary flow path with hydraulic conductivity (K_2) in a matrix of lower hydraulic conductivity (K_3).

CHAPTER 5
SUMMARY AND CONCLUSIONS

The evolution of porosity in carbonate rocks exerts a strong control on fluid flow and storage. Most previous studies on porosity evolution have focused on conduit development in telogenetic karst aquifers. Although conduits exist in eogenetic karst aquifers, high matrix porosity and permeability provide a major component of flow, and this flow can generate localized areas of large-scale secondary porosity where dissolution occurs. In this study, I evaluated how matrix flow affects the distribution and magnitude of secondary porosity development by coupling water chemistry and geochemical modeling with hydrodynamics from eogenetic karst aquifers of San Salvador Island, Bahamas and north-central Florida, USA.

On San Salvador Island, most dissolution occurs in low-salinity water from elevated concentrations of CO_2 rather than from the mixing of water with different chemical compositions as previously thought. Flow remains diffuse from recharge to discharge along the shoreline, and the generation of meter-scale secondary porosity within freshwater lenses stays focused along the water table, where flow velocities are greatest and increase to a maximum at the seaward edge of a lens. This dissolution coupled with flow dynamics near the water table at the lens edge are sufficient to produce flank margin caves and banana holes because reactions products are flushed from the zone of dissolution. Where local sources of CO_2 drive dissolution near the water table at the lens edge, flank margin caves may develop as reaction products are flushed to the ocean. Banana holes may form where local sources of CO_2 drive dissolution at the water table within the island's interior, but are smaller than flank margin caves because lower flow velocities away from the lens edge provide sufficient time for some reprecipitation. This hypothesis predicts that banana holes may be surrounded by more tightly cemented rock if reaction products are not move far beyond the developing void.

On the Florida platform, chemical and hydrologic observations of groundwater and spring discharge suggest that high matrix permeability provides a significant component of flow even in portions of an aquifer dominated by conduits. In the Santa Fe River Sink-Rise system, spring discharge, and thus water within the conduit, is composed of three chemically-distinct sources including allogenic recharge at a swallet, diffuse recharge through the vadose zone, and upwelling of mineralized water from deep within the aquifer. The relative amounts of these sources are controlled by variations in hydraulic head between the conduit and surrounding aquifer, which is a function of rainfall, evapotranspiration, and river stage. Dissolution along the conduit flow path is limited in eogenetic karst aquifers because the flow of Ca-rich water from the matrix to the conduit, which occurs most of the time, limits conduit water undersaturated with respect to calcite from contacting the conduit wall. Instead, most dissolution occurs when hydraulic head in the conduit exceeds hydraulic head in the surrounding aquifer during high-flow events and water undersaturated with respect to calcite enters the aquifer matrix in the vicinity of the conduit. This process predicts the generation of a friable halo of less consolidated matrix rock around the conduit, whereby enlargement results from both dissolution within the matrix as well as along the conduit wall. This conceptualization is distinct from that used for conduit enlargement in telogenetic karst aquifers.

Results of this dissertation show how matrix porosity and permeability allow meter-scale pores to develop in eogenetic karst aquifers. Isolated voids may form along water-table horizons lacking discrete inputs or outputs within a diffuse flow field, and conduits may enlarge, in part, from dissolution of the matrix rock surrounding a conduit. This work provides new concepts for better understanding how secondary porosity evolves in eogenetic karst aquifers, which is vital for long-term exploitation of natural resources including freshwater and hydrocarbons. One

important finding was that voids developing on small carbonate islands only require recharge catchments slightly larger than the size of the void itself, suggesting that catchment size may not limit cave development. In addition, the generation of these voids do not require mixing of freshwater and seawater, but only inputs of CO_2, which does not restrict porosity development only to areas where mixing occurs. Although this work addresses the enlargement of conduits that develop in sink-rise systems receiving allogenic recharge, many conduits draining eogenetic karst aquifers lack discrete inputs. An important question, that remains unanswered, is how do conduits that receive only calcite saturated diffuse flow from the aquifer matrix form. Part of the answer may lie in processes similar to those observed on small carbonate islands, whereby dissolution and flow at the water table generate isolated voids that later become submerged and breached at the surface.

APPENDIX

FIELD DATA AND CHEMICAL ANALYSIS OF WATER SAMPLES FROM SAN SALVADOR ISLAND, BAHAMAS

Table A-1. Water chemistry from San Salvador Island, Bahamas.

Location	Samples	pH	Temp. (ºC)	Sal. (psu)	Na^{+} (mM)	K^{+} (mM)	Mg^{2+} (mM)	Ca^{2+} (mM)	Sr^{2+} (mM)	Cl^{-} (mM)	SO_4^{2-} (mM)	Alk. (mM)
Majors Cave	MC0-05	7.68	23.8	27.8	358	7.33	41.9	8.82	0.095	424	21.5	2.40
Majors Cave	MC1-05	7.68	23.7	27.8	362	7.39	42.2	8.86	0.095	423	21.4	2.42
Majors Cave	MC2-05	7.67	23.7	27.8	362	7.38	42.4	9.04	0.095	425	21.5	2.44
Majors Cave	MC3-05	7.67	23.7	27.8	367	7.57	42.6	8.79	0.094	425	21.5	2.50
Majors Cave	MC4-05	7.59	23.8	28.0	370	7.74	43.1	9.23	0.097	429	21.8	2.48
Majors Cave	MC5-05	7.55	23.9	28.3	379	7.59	44.7	9.45	0.096	436	22.1	2.56
Majors Cave	MC6-05	7.68	23.5	27.8	362	7.42	42.3	8.97	0.094	426	21.6	2.37
Bat Nook	BN0-05	7.63	23.3	25.3	328	6.68	38.4	8.21	0.088	385	19.3	2.43
Bat Nook	BN1-05	7.55	23.8	27.1	363	7.30	42.0	8.48	0.096	413	20.8	2.46
Bat Nook	BN2-05	7.59	23.8	27.5	363	7.25	42.2	8.59	0.097	422	21.3	2.40
Watling's B.H.	WB-05	8.51	30.6	27.8	369	7.39	43.2	9.26	0.098	422	21.3	2.22
Ink Well	IW-05	7.70	24.2	5.2	66.5	1.29	7.1	3.32	0.039	77.8	3.71	2.85
Crescent Top Cave	CT-05	7.44	26.5	35.5	483	19.10	51.8	9.80	0.111	545	28.3	2.09
Crescent Pond	CP-05	8.44	28.4	37.8	492	10.30	57.6	11.20	0.115	581	30.4	2.08
Over Bridge Well 1	OBW1-05	7.87	26.1	0.3	3.1	0.00	1.8	1.56	0.049	2.9	0.31	4.02
Over Bridge Well 2	OBW2-05	7.87	27.8	0.5	4.4	0.00	2.4	1.66	0.048	4.3	0.4	5.05
North Point Well	NP-05	7.60	26.1	1.9	18.8	0.19	2.2	4.89	0.256	30.2	0.2	1.80
Six Pack Pond	SPP-05	8.37	25.3	51.7	679	13.70	78.3	15.30	0.194	781	38.7	2.52
Majors Cave	MC0-06	8.00	24.3	1.8	23	0.71	2.2	1.17	0.012	23.1	0.9	3.03
Majors Cave	MC1-06	7.84	24.2	7.6	93.2	2.32	9.5	2.77	0.028	104	4.8	2.71
Majors Cave	MC2-06	7.78	24.1	20.3	243	4.94	27.6	6.21	0.067	269	12.6	2.78
Majors Cave	MC3-06	7.76	24.1	27.8	330	6.99	38.6	8.19	0.089	390	19.8	2.82
Majors Cave	MC4-06	7.78	24.1	30.0	348	7.09	40.8	8.52	0.093	421	21.5	2.80
Majors Cave	MC5-06	7.72	24.1	31.0	356	7.48	41.3	8.48	0.094	424	21.6	2.81
Majors Cave	MC6-06	7.59	24.1	31.1	357	7.54	41.7	8.60	0.096	414	20.9	2.88
Bat Nook	BN0-06	7.64	24.1	27.4	324	6.79	37.8	7.96	0.088	366	18.3	2.94

Table A-1. Continued

Location	Samples	pH	Temp. (ºC)	Sal. (psu)	Na^{+} (mM)	K^{+} (mM)	Mg^{2+} (mM)	Ca^{2+} (mM)	Sr^{2+} (mM)	Cl^{-} (mM)	SO_4^{2-} (mM)	Alk. (mM)
Bat Nook	BN1-06	7.65	24.1	29.2	337	7.26	39.5	8.11	0.092	387	19.3	2.93
Bat Nook	BN2-06	7.61	24.1	30.3	355	7.46	41.1	8.39	0.091	403	20.2	2.81
Bat Nook	BN3-06	7.57	24.2	31.1	362	7.50	41.9	8.62	0.092	412	20.7	2.88
Bat Nook	BN4-06	7.54	24.2	31.5	368	7.77	42.7	8.71	0.096	416	20.9	2.86
Crescent Top Cave	CT-06	7.55	26.6	40.1	456	9.87	53.8	10.30	0.107	542	28.4	2.57
Field Station Wells	GRC1-06	7.40	27.3	0.5	4.6	0.15	2.1	1.98	0.148	7.4	0.4	4.84
Field Station Wells	GRC2-06	7.27	26.7	0.6	5.8	0.16	2.4	2.03	0.155	9.2	0.5	4.79
Museum Well	MW-06	7.37	27.3	0.9	10.6	0.26	1.6	1.76	0.161	15.8	0.6	4.37
North Victoria Well	NVH-06	7.48	26.5	10.0	113	1.97	13.0	3.85	0.066	128	6.4	3.47
Ink Well B.H.	IW0-07	6.58	24.2	3.0	36.4	0.91	3.8	1.72	0.021	39.2	2.1	2.87
Ink Well B.H.	IW1-07	6.89	23.4	0.5	6.5	0.34	1.1	1.21	0.005	9.2	0.5	3.01
Ink Well B.H.	IW2-07	6.72	23.9	2.7	32.3	0.82	3.4	1.61	0.017	33.6	1.9	2.69
Ink Well B.H.	IW3-07	7.19	24.3	12.2	145	2.98	15.8	2.58	0.044	156	8.5	3.88
Ink Well B.H.	IW4-07	6.74	24.5	17.5	205	4.38	23.5	5.22	0.058	225	11.6	3.88
Ink Well B.H.	IW5-07	7.27	24.6	8.1	107	2.39	11.7	3.46	0.037	123	6.0	3.61
Ink Well B.H.	IW6-07	7.32	24.1	1.4	18.1	0.51	2.0	1.25	0.014	19.2	1.3	2.52
Ink Well B.H.	IW7-07	7.47	23.9	0.5	6.5	0.34	1.0	1.22	0.013	9.2	0.5	3.17
Ink Well B.H.	IW8-07	7.50	24.6	0.5	6.5	0.35	1.1	1.22	0.013	9.2	0.5	3.12
Ink Well B.H.	IW9-07	7.42	23.8	0.5	6.5	0.33	1.0	1.17	0.013	9.3	0.5	3.15
Ink Well B.H.	IW10-07	7.22	24.6	3.4	52.7	1.28	5.7	2.34	0.025	59.2	2.9	3.22
Ink Well B.H.	IW11-07	7.13	24.8	14.4	170	3.66	19.4	4.48	0.050	183	9.6	3.97
Line Hole Well	LH1-07	7.29	27.1	0.3	3.9	0.07	0.4	2.32	0.027	6.2	0.2	4.56
Line Hole Well	LH2-07	7.53	27.1	0.3	4.2	0.09	0.5	1.84	0.019	5.7	0.3	3.95
Line Hole Well	LH3-07	7.27	27.1	0.2	2.8	0.05	0.3	2.30	0.079	3.9	0.2	4.52
Line Hole Well	LH4-07	6.94	27.1	0.8	7.9	0.09	0.6	4.19	0.079	13.6	0.4	7.41
Line Hole Well	LH5-07	7.04	26.8	0.5	4.36	0.04	0.4	3.44	0.039	7.11	0.2	6.15
Line Hole Well	LH6-07	6.95	26.2	2.0	20.8	0.31	1.9	4.28	0.088	22.7	1.0	6.96
Line Hole Well	LH7-07	7.04	26.2	1.3	14.5	0.17	1.2	3.87	0.065	15.3	0.8	6.14

Table A-1. Continued

Location	Samples	pH	Temp. (ºC)	Sal. (psu)	Na^+ (mM)	K^+ (mM)	Mg^{2+} (mM)	Ca^{2+} (mM)	Sr^{2+} (mM)	Cl^- (mM)	SO_4^{2-} (mM)	Alk. (mM)
Line Hole Well	LH8-07	7.06	26.4	0.90	9.6	0.13	0.8	3.00	0.055	15.4	0.5	6.25
Line Hole Well	LH9-07	6.98	26.3	0.90	7.5	0.09	0.7	4.11	0.117	15.6	0.3	6.58
Line Hole Well	LH10-07	7.17	26.4	0.80	6.9	0.20	0.7	3.56	0.029	14.8	0.2	6.58
Line Hole Well	LHA-07	7.05	26.9	0.40	2.7	0.03	0.3	3.54	0.098	3.9	0.2	7.38
Line Hole Well	LHB-07	7.22	26.6	2.40	25.2	0.49	2.9	3.70	0.052	27.2	1.3	7.12
Museum Well	MW-07	7.36	26.6	3.50	38.5	0.81	4.0	3.17	0.278	44.0	1.2	5.34
North Point Well	NP-0	7.79	26.0	0.70	11.9	0.46	0.6	0.90	0.046	8.6	1.2	6.60
Short Stop Well	SS-07	7.99	25.5	0.50	5.1	0.18	1.4	1.66	0.076	6.7	0.5	4.44
Watling's B.H.	WB-07	8.47	23.7	24	281	5.91	32.6	6.27	0.075	305	16.5	3.11

Table A-1. Continued

Location	Samples	DIC (mM HCO_3^-)	log PCO_2 (bars)	SI_{CAL} (log Q/K)	SI_{ARG} (log Q/K)	Charge Bal. (mM HCO_3^-)
Majors Cave	MC0-05	—[a]	-2.80	0.16	0.02	-0.3
Majors Cave	MC1-05	—	-2.80	0.17	0.02	0.3
Majors Cave	MC2-05	—	-2.79	0.17	0.02	0.2
Majors Cave	MC3-05	—	-2.78	0.17	0.02	0.8
Majors Cave	MC4-05	—	-2.70	0.11	-0.04	0.8
Majors Cave	MC5-05	—	-2.64	0.09	-0.06	1.4
Majors Cave	MC6-05	—	-2.81	0.16	0.01	-1.1
Bat Nook	BN0-05	—	-2.74	0.11	-0.04	0.3
Bat Nook	BN1-05	—	-2.66	0.03	-0.11	1.6
Bat Nook	BN2-05	—	-2.71	0.06	-0.08	0.6
Watling's B.H.	WB-05	—	-3.73	0.96	0.82	1.6
Ink Well	IW-05	—	-2.59	0.22	0.08	0.4
Crescent Top Cave	CT-05	—	-2.69	-0.05	-0.19	1.9
Crescent Pond	CP-05	—	-3.73	0.90	0.72	-0.4
Over Bridge Well 1	OBW1-05	—	-2.51	0.44	0.30	10.7
Over Bridge Well 2	OBW2-05	—	-2.42	0.66	0.51	10.8
North Point Well	NP-05	—	-2.63	0.29	0.15	1.1
Six Pack Pond	SPP-05	—	-3.63	0.90	0.76	1.2
Majors Cave	MC0-06	2.31	-2.82	0.27	0.13	4.3
Majors Cave	MC1-06	2.67	-2.78	0.19	0.05	1.6
Majors Cave	MC2-06	2.87	-2.79	0.28	0.13	3.1
Majors Cave	MC3-06	2.88	-2.80	0.30	0.16	-0.3
Majors Cave	MC4-06	2.83	-2.83	0.32	0.18	-1.6
Majors Cave	MC5-06	2.84	-2.77	0.26	0.11	-0.9
Majors Cave	MC6-06	—	-2.63	0.15	0.01	0.7
Bat Nook	BN0-06	3.09	-2.66	0.20	0.06	2.1
Bat Nook	BN1-06	—	-2.67	0.21	0.06	1.3

Table A-1. Continued

Location	Samples	DIC (mM HCO_3^-)	log PCO_2 (bars)	SI_{CAL} (log Q/K)	SI_{ARG} (log Q/K)	Charge Bal. (mM HCO_3^-)
Bat Nook	BN2-06	—	-2.66	0.15	0.01	1.8
Bat Nook	BN3-06	—	-2.60	0.13	-0.01	1.7
Bat Nook	BN4-06	3.83	-2.58	0.10	-0.04	2.1
Crescent Top Cave	CT-06	2.62	-2.65	0.12	-0.03	-0.6
Field Station Wells	GRC1-06	5.30	-1.96	0.26	0.11	-0.4
Field Station Wells	GRC2-06	5.06	-1.84	0.11	-0.03	-0.8
Museum Well	MW-06	4.33	-1.98	0.10	-0.05	-10.3
North Victoria Well	NVH-06	4.34	-2.30	0.09	-0.06	1.4
Ink Well B.H.	IW0-07	2.78	-1.60	-1.23	-1.37	3.3
Ink Well B.H.	IW1-07	2.90	-1.78	-0.81	-0.96	-4.7
Ink Well B.H.	IW2-07	2.66	-1.72	-1.08	-1.23	4.8
Ink Well B.H.	IW3-07	3.82	-2.03	-0.44	-0.58	2.4
Ink Well B.H.	IW4-07	3.95	-1.64	-0.70	-0.84	3.1
Ink Well B.H.	IW5-07	3.68	-2.10	-0.46	-0.33	0.4
Ink Well B.H.	IW6-07	2.48	-2.24	-0.46	-0.60	2.3
Ink Well B.H.	IW7-07	2.92	-2.29	-0.15	-0.30	-6.6
Ink Well B.H.	IW8-07	—	-2.66	0.15	0.01	1.8
Ink Well B.H.	IW9-07	—	-2.60	0.13	-0.01	1.7
Ink Well B.H.	IW10-07	3.83	-2.58	0.10	-0.04	2.1
Ink Well B.H.	IW11-07	2.62	-2.65	0.12	-0.03	-0.6
Line Hole Well	LH1-07	5.30	-1.96	0.26	0.11	-0.4
Line Hole Well	LH2-07	5.06	-1.84	0.11	-0.03	-0.8
Line Hole Well	LH3-07	4.33	-1.98	0.10	-0.05	-10.3
Line Hole Well	LH4-07	4.34	-2.30	0.09	-0.06	1.5
Line Hole Well	LH5-07	2.78	-1.60	-1.23	-1.37	3.3
Line Hole Well	LH6-07	2.90	-1.78	-0.81	-0.96	-4.7
Line Hole Well	LH7-07	2.66	-1.72	-1.08	-1.23	4.8

Table A-1. Continued

Location	Samples	DIC (mM HCO_3^-)	log PCO_2 (bars)	SI_{CAL} (log Q/K)	SI_{ARG} (log Q/K)	Charge Bal. (mM HCO_3^-)
Line Hole Well	LH8-07	6.37	-1.57	0.10	-0.04	-11.8
Line Hole Well	LH9-07	7.99	-1.41	0.24	0.10	-14.8
Line Hole Well	LH10-07	—	-1.61	0.37	0.22	-16.9
Line Hole Well	LHA-07	7.76	-1.46	0.31	0.17	-2.7
Line Hole Well	LHB-07	7.13	-1.69	0.33	0.18	3.4
Museum Well	MW-07	—	-1.93	0.27	0.13	1.9
North Point Well	NP-0	5.96	-2.28	0.34	0.19	-4.6
Short Stop Well	SS-07	3.76	-2.68	0.64	0.49	0.2
Watling's B.H.	WB-07	2.68	-3.54	0.90	0.75	3.6

[a]Sample not collected for analysis

LIST OF REFERENCES

AM ENDE, B., 2000, Wakulla 2 - building the first fully 3-D cave map: National Speleological Society News, v. 58, p. 131-140.

ANDERSON, G.M., and CRERAR, D.A., 1993, Thermodynamics in Geochemistry: New York, Oxford University Press, 588 p.

ANTHONY, S.S., PETERSON, F.L., MACKENZIE, F.T., and HAMLIN, S.N., 1989, Geohydrology of the Laura fresh-water lens, Majuro Atoll: a hydrogeochemical approach: Geological Society of America Bulletin, v. 101, p. 1066-1075.

ATKINSON, T.C., 1977, Carbon dioxide in the atmosphere of the unsaturated zone: An important control of groundwater hardness in limestones: Journal of Hydrology, v. 35, p. 111-123.

BACETA, J.I., PUJALTE, V., WRIGHT, V.P., and LAPOINTE, P., 2008, Eogenetic karstification and palaeohydrology of a Danian land-attached carbonate shelf (North Spain), *in* Sasowsky, I.D., Freazel, C.T., Mylroie, J.E., Palmer, A.N., and Palmer, M.V., eds., Karst from Recent to Reservoirs, Karst Waters Institute Special Publication 14, p. 21-22.

BACK, W., and HANSHAW, B.B., 1970, Comparison of chemical hydrogeology of the carbonate peninsulas of Florida and Yucatan: Journal of Hydrology, v. 10, p. 330-368.

BACK, W., HANSHAW, B.B., HERMAN, J.S., and VAN DRIEL, J.N., 1986, Differential dissolution of a Pleistocene reef in the ground-water mixing zone of coastal Yucatan, Mexico: Geology, v. 14, p. 137-140.

BALL, J.W., and NORDSTROM, D.K., 1991, User's Manual for WATEQ4F, with Revised Thermodynamic Data Base and Test Cases for Calculating Speciation of Major, Trace, and Redox Elements in Natural Waters: Open-File Report 91-183, United States Geological Survey, 192 p.

BEAR, J., and TODD, D.K., 1960, The transition zone between fresh and salt waters in coastal aquifers: Water Resources Centre Contribution, v. 29: Berkeley, Hydraulic Laboratory, University of California, 156 p.

BECK, B.F., 1986, Ground water monitoring considerations in karst on young limestones, In: Symposium on Environmental Problems in Karst Terranes and Their Solutions (October, 1986): Bowling Green, Kentucky, National Water Well Association, p. 229-248.

BEDDOWS, P.A., 2004, Groundwater hydrology of a coastal conduit carbonate aquifer: Caribbean coast of the Yucatan Peninsula [unpublished Ph.D. Diss.]: University of Bristol, 303 p.

BÖGLI, A., 1980, Karst hydrology and physical speleology: New York, Springer-Verlag, 284 p.

BOTTRELL, S.H., CAREW, J.L., and MYLROIE, J., 1993, Inorganic and bacteriogenic origins for sulfate crusts in flank margin caves, San Salvador Island, Bahamas, *in* White, B., ed., Proceedings of the Sixth Symposium on the Geology of the Bahamas: San Salvador, Bahamas, Bahamian Field Station, p. 17-21.

BOTTRELL, S.H., SMART, P.L., WHITAKER, F., and RAISWELL, R., 1991, Geochemistry and isotope systematics of sulphur in the mixing zone of Bahamian blue holes: Applied Geochemistry, v. 6, p. 97-103.

BREDEHOEFT, J.D., and PAPADOPULOS, I.S., 1965, Rates of Vertical Groundwater Movement Estimated from the Earth's Thermal Profile: Water Resources Research, v. 1, p. 325-328.

BUDD, D.A., 1988, Aragonite-to-calcite transformation during fresh-water diagenesis of carbonates: Insights from pore-water chemistry: Geological Society of America Bulletin, v. 100, p. 1260-1270.

BUDD, D.A., and VACHER, H.L., 1991, Predicting the thickness of fresh-water lenses in carbonate paleo-islands: Journal of Sedimentary Petrology, v. 61, p. 43-53.

BUDD, D.A., and VACHER, H.L., 2004, Matrix permeability of the confined Floridan Aquifer, Florida, USA: Hydrogeology Journal, v. 12, p. 531-549.

BUSH, P.W., and JOHNSTON, R.H., 1988, Ground-waer hydraulics, regional flow, and ground-water development of the Floridan Aquifer system in Florida and in parts of Georgia, South Carolina and Alabama: Professional Paper 1403-C, U.S. Geological Survey, 80 p.

CANT, R.V., and WEECH, P.S., 1986, A review of the factors affecting the development of Ghyben-Hertzberg lenses in the Bahamas: Journal of Hydrology, v. 84, p. 333-343.

CAREW, J.L., and MYLROIE, J.E., 1995a, Quaternary tectonic stability of the Bahamian Archipelago; evidence from fossil coral reefs and flank margin caves: Quaternary Science Reviews, v. 14, p. 145-153.

CAREW, J.L., and MYLROIE, J.E., 1995b, Depositional model and stratigraphy for the Quaternary geology of the Bahama Islands, *in* Curran, H.A., and White, B., eds., Terrestrial and Shallow Marine Geology of the Bahamas and Bermuda: Geological Society of America, Special Paper 300, p. 5-32.

CAREW, J.L., and MYLROIE, J.E., 1997, Geology of the Bahamas, *in* Vacher, H.L., and Quinn, T.M., eds., Geology and Hydrogeology of Carbonate Islands, Developments in Sedimentology 54: Amsterdam, Elsevier, p. 91-139.

CHELETTE, A.R., PRATT, T.R., and KATZ, B.G., 2003, Nitrate loading as an indicator of nonpoint source pollution in the lower St Marks-Wakulla Rivers watershed: Northwest Florida Water Management District, Water Resources Special Report 02-1, 138 p.

CHEN, J.H., CURRAN, H.A., WHITE, B., and WASSERBURG, G.J., 1991, Precise chronology of the last interglacial period: ^{234}U- ^{230}Th data from fossil coral reefs in the Bahamas: Geological Society of America Bulletin, v. 103, p. 82-97.

CHEN, K., JIAO, J.J., HUANG, J., and HUANG, R., 2007, Multivariate statistical evaluation of trace elements in groundwater in a coastal area in Shenzhen, China: Environmental Pollution, v. 147, p. 771-780.

CHOQUETTE, P.W., and PRAY, L.C., 1970, Geologic nomenclature and classification of porosity in sedimentary carbonates: American Association of Petroleum Geologists Bulletin, v. 54, p. 207-244.

CRAIG, D.H., 1988, Caves and Other Features of Permian Karst in San Andres Dolomite, Yates Field Reservoir, West Texas, *in* James, N.P., and Choquette, P.W., eds., Paleokarst: New York, Springer-Verlag, p. 342-363.

CRANDALL, C.A., KATZ, B.G., and HIRTEN, J.J., 1999, Hydrochemical evidence for mixing of river water and groundwater during high-flow conditions, lower Suwannee River basin, Florida, USA: Hydrogeology Journal, v. 7, p. 454-467.

CRUMP, M.A., and GAMBLE, D.W., 2006, Hydroclimatic Analysis of a Carbonate Island Pond Through the Development of a Hydrologic Landscape Unit Model: Physical Geography, v. 27, p. 554-570.

DAVIS, R.L., and JOHNSON, J., C.R., 1989, Karst hydrology of San Salvador, *in* Mylroie, J.E., ed., Proceedings on the 4th Symposium on the Geology of the Bahamas: San Salvador, Bahamas, Bahamian Field Station, p. 118-135.

DEMING, D., 2002, Introduction to Hydrogeology: New York, McGraw-Hill, 468 p.

DINGMAN, S.L., 2002, Physical Hydrology: Upper Saddle River, Prentice-Hall, 646 p.

DOGWILER, T., and WICKS, C.M., 2004, Sediment entrainment and transport in fluviokarst systems: Journal of Hydrology, v. 295, p. 163-172.

DREISS, S.J., 1989, Regional scale transport in a karst aquifer, 1. Component separation of spring flow hydrographs: Water Resources Research, v. 25, p. 117-125.

DREVER, J.I., 1997, The Geochemistry of Natural Waters: Englewood Cliffs, Prentice-Hall, 437 p.

DREYBRODT, W., 1990, The role of dissolution kinetics in the development of karst aquifers in limestone: Journal of Geology, v. 98, p. 639-655.

DREYBRODT, W., and GABROVSEK, F., 2002, Basic processes and mechanisms governing the evolution of karst, *in* Gabrovsek, F., ed., Evolution of Karst: From Prekarst to Cessation: Postojna-Ljubljana, Zalozba ZRC, p. 115-154.

EDWARDS, L.E., WEEDMAN, S.D., SIMMONS, K.R., SCOTT, T.M., BREWSTER-WINGARD, G.L., ISHMAN, S.E., and CARLIN, N.M., 1998, Lithostratigraphy, Petrography, Biostratigraphy, and Strontium-Isotope Stratigraphy of the Surfical Aquifer System of Western Collier County, Florida: Open-File Report 98-205, United States Geological Survey, 79 p.

EPA, 1983, Methods for the chemical analysis of water and wastes: Cincinnati, United States Environmental Protection Agency, 552 p.

FLOREA, L.J., 2006, The Karst of West-Central Florida [unpublished Ph.D. diss.]: University of South Florida, 564 p.

FLOREA, L.J., and VACHER, H.L., 2006, Springflow hydrographs: Eogenetic vs. telogenetic karst: Ground Water, v. 44, p. 352-361.

FLOREA, L.J., and VACHER, H.L., 2007, Eogenetic karst hydrology: Insights from the 2004 hurricanes, peninsular Florida: Ground Water, v. 45, p. 439-446.

FLOREA, L.J., MYLROIE, J.E., and PRICE, A., 2004, Sedimentation and porosity enhancement in a breached flank margin cave: Carbonates and Evaporites, v. 19, p. 75-85.

FLOREA, L.J., VACHER, H.L., DONAHUE, B., and NAAR, D., 2007, Quaternary cave levels in peninsular Florida: Quaternary Science Reviews, v. 26, p. 1344-1361.

FORD, D.C., and EWERS, R.O., 1978, The development of limestone cave systems in the dimensions of length and depth: Canadian Journal of Earth Science, v. 15, p. 1783-1798.

FORD, D.C., and WILLIAMS, P.W., 2007, Karst Hydrogeology and Geomorphology: Chichester, Wiley, 562 p.

FOURNIER, M., MASSEI, N., BAKALOWICZ, M., DUSSART-BAPTISTA, L., RODET, J., and DUPONT, J.P., 2007, Using turbidity dynamics and geochemical variability as a tool for understanding the behavior and vulnerability of a karst aquifer: Hydrogeology Journal, v. 15, p. 689-704.

FREEZE, R.A., and CHERRY, J.A., 1979, Groundwater: Englewood Cliffs, Prentice-Hall, 290 p.

GABROVŠEK, F., and DREYBRODT, W., 2001, A model of the early evolution of karst aquifers in limestone in the dimensions of length and depth: Journal of Hydrology, v. 240, p. 206-224.

GABROVŠEK, F., ROMANOV, D., and DREYBRODT, W., 2004, Early karstification in a dual-fracture aquifer; the role of exchange flow between prominent fractures and a dense net of fissures: Journal of Hydrology, v. 299, p. 45-66.

GANDOLFI, C., FACCHI, A., and WHELAN, M.J., 2001, On the Relative Role of Hydrodynamic Dispersion for River Water Quality: Water Resources Research, v. 37, p. 2365-2375.

GRASSO, D.A., and JEANNIN, P.-Y., 2002, A global experimental system approach of karst springs hydrographs and chemographs: Ground Water, v. 40, p. 608-617.

GRASSO, D.A., JEANNIN, P.Y., and ZWAHLEN, F., 2003, A deterministic approach to the coupled analysis of karst springs' hydrographs and chemographs: Journal of Hydrology, v. 271, p. 65-76.

GRIGGS, J.E., and PETERSON, F.L., 1993, Ground-water flow dynamics and development strategies at the atoll scale: Ground Water, v. 31, p. 209-220.

GROSZOS, M., CERYAK, R., ALLISON, D., COOPER, R., WEINBERG, M., MACESICH, M., ENRIGHT, M.M., and RUPERT, F., 1992, Carbonate units of the Intermediate Aquifer system in the Suwannee River Water Management District, Florida: Open-file report 54, Florida Geological Survey, 22 p.

GROVES, C., and MEIMAN, J., 2005, Weathering, geomorphic work, and karst landscape evolution in the Cave City groundwater basin, Mammoth Cave, Kentucky: Geomorphology, v. 67, p. 115-126.

GROVES, C.G., and HOWARD, A.D., 1994, Early development of karst systems 1. Preferential flow path enlargement under laminar flow: Water Resources Research, v. 30, p. 2837-2846.

HALIHAN, T., and WICKS, C., 1998, Modeling of storm response in conduit flow aquifers with reservoirs: Journal of Hydrology, v. 208, p. 82-91.

HALIHAN, T., SHARP, J.M., JR., and MACE, R.E., 2000, Flow in the San Antonio segment of the Edwards aquifer: Matrix, fractures, or conduits?, *in* Sasowski, I.D., and Wicks, C.M., eds., Groundwater Flow and Contaminant Transport in Carbonate Aquifers: Rotterdam, A.A. Balkema, p. 129-146.

HANSHAW, B.B., and BACK, W., 1979, Major geochemical processes in the evolution of carbonate-aquifer systems: Journal of Hydrology, v. 43, p. 287-312.

HARRIS, J.G., MYLROIE, J.E., and CAREW, J.L., 1995, Banana holes: unique karst features of the Bahamas: Carbonates and Evaporites, v. 10, p. 215-224.

HATTIN, D.E., and WARREN, V.L., 1989, Stratigraphic analysis of a fossil Neogoniolithon-capped patch reef and associated facies, San Salvador, Bahamas: Coral Reefs, v. 8, p. 19-30.

HELGESON, H.C., 1969, Thermodynamics of hydrothermal systems at elevated temperatures and pressures: American Journal of Science, v. 267, p. 729-804.

HESS, J.W., and WHITE, W.B., 1988, Storm response of the karstic carbonate aquifer of south central Kentucky: Journal of Hydrology, v. 99, p. 235-252.

HISERT, R.A., 1994, A multiple tracer approach to determine the ground and surface water relationships in the western Santa Fe River, Columbia County, Florida [unpublished Ph.D. diss.]: University of Florida, 211 p.

HOWARD, A.D., and GROVES, C.G., 1995, Early development of karst systems 2. Turbulent flow: Water Resources Research, v. 31, p. 19-26.

HUGHES, J.D., VACHER, H.L., and SANFORD, W.E., 2007, Three-dimensional flow in the Florida platform: Theoretical analysis of Kohout convection at its type locality: Geology, v. 35, p. 663-666.

HUNN, J.D., and SLACK, L.J., 1983, Water resources of the Santa Fe River Basin, Florida: Water-Resources Investigations Report 83-4075, United States Geological Survey, 105 p.

HUNTOON, P.W., 1995, Is it appropriate to apply porous media groundwater circulation models to karstic aquifers?, *in* El-Kadi, A.I., ed., Groundwater Models for Resource Analysis and Management: Boca Raton, Lewis Publishers, p. 339-358.

JAEGGI, D., 2006, Multiscalar porosity structure of a Miocene reefal carbonate complex [unpublished PhD. diss.]: Swiss Federal Institute of Technology (ETH), 196 p.

JOHNSON, J.W., OELKERS, E.H., and HELGESON, H.C., 1992, SUPCRT92; a software package for calculating the standard molal thermodynamic properties of minerals, gases, aqueous species, and reactions from 1 to 5000 bar and 0 to 1000 degrees C: Computers and Geosciences, v. 18, p. 899-947.

JOLLIFFE, I.T., 2002, Principle component analysis: New York, Springer, 487 p.

JONES, I.C., VACHER, H.L., and BUDD, D.A., 1993, Transport of calcium, magnesium and SO_4 in the Floridan aquifer, west-central Florida: implications to cementation rates: Journal of Hydrology, v. 143, p. 455-480.

JUNGE, C.E., and WERBY, R.T., 1958, The concentration of chloride, sodium, potassium, calcium, and sulfate in rain water of over the United States: Journal of the Atmospheric Sciences, v. 15, p. 417-425.

KATZ, B.G., 2004, Sources of nitrate contamination and age of water in large karstic springs of Florida: Environmental Geology, v. 46, p. 689-706.

KATZ, B.G., BÖHLKE, J.K., and HORNSBY, H.D., 2001, Timescales for nitrate contamination of spring waters, northern Florida, USA: Chemical Geology, v. 179, p. 167-186.

KATZ, B.G., CHELETTE, A.R., and PRATT, T.R., 2004, Use of chemical and isotopic tracers to assess sources of nitrate and age of ground water, Woodville Karst Plain, USA: Journal of Hydrology, v. 289, p. 36-61.

KATZ, B.G., CATCHES, J.S., BULLEN, T.D., and MICHEL, R.L., 1998, Changes in the isotopic and chemical composition of ground water resulting from a recharge pulse from a sinking stream: Journal of Hydrology, v. 211, p. 178-207.

KAUFMANN, G., and BRAUN, J., 1999, Karst aquifer evolution in fractured rocks: Water Resources Research, v. 35, p. 3223-3238.

KAUTZ, R., STYS, B., and KAWULA, R., 2007, Florida Vegetation 2003 and Land Use Change Between 1985-89 and 2003: Florida Scientist, v. 70, p. 12-23.

KERN, D.M., 1960, The hydration of carbon dioxide: Journal of Chemical Education, v. 37, p. 14-23.

KINCAID, T., 1999, Morphologic and Fractal Characterization of Saturated Karstic Caves [unpublished Ph.D. diss.]: University of Wyoming, 174 p.

KNOCHEMUS, L.A., and ROBINSON, J.L., 1996, Descriptions of anisotropy and heterogeneity and their effect on ground-water flow and areas of contribution to public supply wells in a karst carbonate aquifer system: Water-Supply Paper 2475, United States Geological Survey, 47 p.

KOHOUT, F.A., HENRY, H.R., and BANKS, J.E., 1977, Hydrogeology related to geothermal conditions of the Floridan Plateau, *in* Smith, K.L, and Griffin, G.M., The geothermal nature of the Floridan Plateau: Florida Department of Natural Resources, Bureau of Geology Special Publication 21, 1-41 p.

LAAKSOHARJU, M., TULLBORG, E.-L., WIKBERG, P., WALLIN, B., and SMELLIE, J., 1999, Hydrogeochemical conditions and evolution at the Äspö HRL, Sweden: Applied Geochemistry, v. 14, p. 835-859.

LABOURDETTE, R., and MYLROIE, J.E., 2008, Flank margin caves: Preservation probability and burial outcomes, *in* Sasowsky, I.D., Feazel, C.T., Mylroie, J.E., Palmer, A.N., and Palmer, M.V., eds., Karst from Recent to Reservoirs, Karst Waters Institute Special Publication 14, p. 107-114.

LABOURDETTE, R., LASCU, I., MYLROIE, J.E., and ROTH, M.J., 2007, Process-like modeling of flank margin caves: From genesis to burial evolution: Journal of Sedimentary Research, v. 77, p. 965-979.

LANGMUIR, D., 1997, Aqueous Environmental Geochemistry: Upper Saddle River, Prentice-Hall, 600 p.

LASCU, I., 2005, Speleogenesis of large flank margin caves of the Bahamas [unpublished M.S. thesis]: Mississippi State University, 218 p.

LAWRENCE, F.W., and UPCHURCH, S.B., 1982, Identification of recharge areas using geochemical factor analysis: Ground Water, v. 20, p. 680-687.

LAZAREVA, O., and PICHLER, T., 2007, Naturally occurring arsenic in the Miocene Hawthorn Group, southwestern Florida: Potential implication for phosphate mining: Applied Geochemistry, v. 22, p. 953-973.

LIU, Z., and DREYBRODT, W., 1997, Dissolution kinetics of calcium carbonate minerals in H_2O-CO_2 solutions in turbulent flow; the role of the diffusion boundary layer and the slow reaction $H_2O + CO_2 = H^+ + HCO_3^-$: Geochimica et Cosmochimica Acta, v. 61, p. 2879-2889.

LOPER, D.E., WERNER, C.L., CHICKEN, E., DAVIES, G., and KINCAID, T., 2005, Coastal Carbonate Aquifer Sensitivity to Tides: Eos, Transactions, American Geophysical Union, v. 86, doi:10.1029/2005EO390001.

LU, N., and GE, S., 1996, Effect of horizontal heat and fluid flow on the vertical temperature distribution in a semi-confining layer: Water Resources Research, v. 32, p. 1449-1453.

LUCIA, F.J., 1995, Rock-fabric petrophysical classification of carbonate pore space for reservoir characterization: American Association of Peteroleum Geologists Bulletin, v. 79, p. 1275-1300.

MARTIN, J.M., 2003, Quantification of the matrix hydraulic conductivity in the Santa Fe River Sink/Rise system with implications on the exchange of water between the matrix and conduits [unpublished MS thesis]: University of Florida, 64 p.

MARTIN, J.B., and DEAN, R.W., 1999, Temperature as a natural tracer of short residence times for ground water in karst aquifers, *in* Palmer, A.N., Palmer, M.V., and Sasowsky, I.D., eds., Karst Modeling: Karst Waters Institute Special Publication 5, p. 236-242.

MARTIN, J.B., and GORDON, S.L., 2000, Surface and ground water mixing, flow paths, and temporal variations in chemical compositions of karst springs, *in* Sasowsky, I.D., and Wicks, C., eds., Groundwater Flow and Contaminant Transport in Carbonate Aquifers: Rotterdam, A.A. Balkema, p. 65-92.

MARTIN, J.B., and DEAN, R.W., 2001, Exchange of water between conduits and matrix in the Floridan Aquifer: Chemical Geology, v. 179, p. 145-165.

MARTIN, J.B., and SCREATON, E.J., 2001, Exchange of Matrix and Conduit Water with Examples from the Floridan Aquifer, *in* Kuniansky, E.L., ed., United States Geological Survey Karst Interest Group: St. Petersburg, Florida, United States Geological Survey, p. 38-44.

MARTIN, J.B., and MOORE, P.J., 2008, Sr concentrations and isotope ratios as tracers of ground-water circulation in carbonate platforms: Examples from San Salvador Island and Long Island, Bahamas: Chemical Geology, v. 249, p. 52-65.

MARTIN, J.M., SCREATON, E.J., and MARTIN, J.B., 2006, Monitoring well responses to karst conduit head fluctuations: Implications for fluid exchange and matrix transmissivity in the Floridan aquifer, *in* Wicks, C.M., and Harmon, R.S., eds., Perspectives on Karst Geomorphology, Hydrology, and Geochemistry: A Tribute Volume to Derek C. Ford and William B. White: Geological Society of America, Special Publication 404, p. 209-217.

MATSUDA, H., TSUJI, Y., HONDA, N., and SAOTOME, J.-I., 1995, Early diagenesis of Pleistocene carbonates from a hydrogeochemical point of view, Irabu Island, Ryukyu Islands: porosity changes related to early carbonate diagenesis, *in* Budd, D.A., Harries, P.M., and Saller, A., eds., Unconformities and Porosity in Carbonate Strata: American Association of Petroleum Geologists Memoir, v. 63, p. 35-54.

MCCLAIN, M.E., SWART, P.K., and VACHER, H.L., 1992, The hydrogeochemistry of early meteoric diagenesis in a Holocene deposit of biogenic carbonates: Journal of Sedimentary Research, v. 62, p. 1008-1022.

MCCONNELL, J., and HACKE, C.M., 1993, Hydrogeology, water quality, and water resources development potential of the Upper Floridan aquifer in the Valdosta area, south-central Georgia: Water-Resources Investigations Report 93-4044, United States Geological Survey, 44 p.

MELLOUL, A., and COLLIN, M., 1992, The 'principal components' statistical method as a complementary approach to geochemical methods in water quality factor identification; application to the Coastal Plain aquifer of Israel: Journal of Hydrology, v. 140, p. 49-73.

MILLER, J.A., 1986, Hydrogeologic framework of the Floridan aquifer system in Florida and parts of Georgia, Alabama, and South Carolina: Professional Paper 1403-B, United States Geological Survey, 91 p.

MOORE, C.H., 2001, Carbonate reservoirs porosity evolution and diagenesis in a sequence stratigraphic framework, Developments in sedimentology 55: Amsterdam, Elsevier, 444 p.

MOORE, P.J., and MARTIN, J.B., 2005, Exchange of water between conduit and matrix porosity in eogenetic karst? Evidence from a quantitative dye trace: Geological Society of America Abstracts with Programs, v. 37, p. 435.

MOORE, P.J., and MARTIN, J.B., 2008, Water chemistry on San Salvador Island, Bahamas, *in* Parks, L., and Freile, D., eds., Proceedings of the 13th Symposium on the Geology of the Bahamas and Other Carbonate Regions: San Salvador, Bahamas, Gerace Research Centre, p. 1-10.

MOORE, P.J., MARTIN, J.B., and GAMBLE, D.W., 2006, Carbonate Water Mixing in a Flank Margin Cave, *in* Davis, R.L., and D.W., G., eds., Proceedings of the 12th Symposium on the Geology of the Bahamas and Other Carbonate Regions: San Salvador, Bahamas, Gerace Research Center, p. 123-129.

MOORE, P.J., MARTIN, J.B., and SCREATON, E.J., submitted, Geochemical and statistical evidence of recharge, mixing, and controls on spring discharge in an eogenetic karst aquifer: Journal of Hydrology.

MORSE, J.W., and MACKENZIE, F.T., 1990, Geochemistry of sedimentary carbonates, Developments in Sedimentology 48: Amsterdam, Elsevier, 707 p.

MULLINS, H.T., and LYNTS, G.W., 1977, Origin of the northwestern Bahama Platform; review and reinterpretation: Geological Society of America Bulletin, v. 88, p. 1447-1461.

MYLROIE, J.E., and CAREW, J.L., 1990, The flank margin model for dissolution cave development in carbonate platforms: Earth Surface Processes and Landforms, v. 15, p. 413-424.

MYLROIE, J.E., and CAREW, J.L., 1995, Karst development on carbonate islands, *in* Budd, D.A., Harris, P.M., and Saller, A., eds., Unconformities and Porosity in Carbonate Strata: American Association of Petroleum Geologists Memoir, v. 63, p. 55-76.

MYLROIE, J.E., and VACHER, H.L., 1999, A conceptual view of carbonate island karst, *in* Palmer, A.N., Palmer, M.V., and Sasowsky, I.D., eds., Karst Modelling: Karst Waters Institute Special Publication 5, p. 48-57.

MYLROIE, J.E., CAREW, J.L., and VACHER, H.L., 1995, Karst development in the Bahamas and Bermuda, *in* Curran, H.A., and White, W.B., eds., Terrestrial and Shallow Marine Geology of the Bahamas and Bermuda: Geological Society of America, Special Paper 300, p. 251-267.

NG, K.-C., and JONES, B., 1995, Hydrogeochemistry of Grand Cayman, British West Indies; implications for carbonate diagenetic studies: Journal of Hydrology, v. 164, p. 193-216.

OLOFSSON, B., JERNBERG, H., and ROSENQVIST, A., 2006, Tracing leachates at waste sites using geophysical and geochemical modelling: Environmental Geology, v. 49, p. 720-732.

PALMER, A.N., 1991, Origin and morphology of limestone caves: Geological Society of America Bulletin, v. 103, p. 1-21.

PALMER, A.N., 2001, Dynamics of cave development by allogenic water: Acta Carsologica, v. 30, p. 14-32.

PALMER, A.N., 2007, Cave Geology: Dayton, Cave Books, 454 p.

PALMER, A.N., PALMER, M.V., and SASOWSKY, I.D. (Editors), 1999, Karst Modeling: Charles Town, Karst Waters Institute, 265 p.

PARKHURST, D.L., and APPELO, C.A.J., 1999, User's guide to PHREEQC (Version 2): Water-Resources Investigations Report 99-4259, United States Geological Survey, 326 p.

PETERSON, F.L., 1997, Hydrogeology of the Marshall Islands, *in* Vacher, H.L., and Quinn, T.M., eds., Geology and Hydrogeology of Carbonate Islands, Developments in Sedimentology 54: Amsterdam, Elsevier, p. 611-636.

PHELPS, G.G., 2001, Geochemistry and Origins of Mineralized Waters in the Floridan Aquifer System, Northeastern Florida: Water-Resources Investigations Report 01-4112, United States Geological Society, 70 p.

PLUMMER, L.N., 1975, Mixing of sea water with calcium carbonate ground water, *in* Whitten, E.H.T., ed., Quantitative Studies in the Geological Sciences: Geological Society of America Memoir, v. 142, p. 219-238.

PLUMMER, L.N., 1977, Defining reactions and mass transfer in part of the Floridan Aquifer: Water Resources Research, v. 13, p. 801-812.

PLUMMER, L.N., and BACK, W., 1980, The mass balance approach; application to interpreting the chemical evolution of hydrologic systems: American Journal of Science, v. 280, p. 130-142.

PLUMMER, L.N., and BUSENBERG, E., 1982, The solubilities of calcite, aragonite and vaterite in CO_2-H_2O solutions between 0 and 90°C, and an evaluation of the aqueous model for the system $CaCO_3$-CO_2-H_2O: Geochimica et Cosomochimica Acta, v. 46, p. 1011-1040.

PLUMMER, L.N., WIGLEY, T.M.L., and PARKHURST, D.L., 1978, The kinetics of calcite dissolution in CO_2-water systems at 5° to 60° C and 0.0 to 1.0 ATM CO_2: American Journal of Science, v. 278, p. 179-216.

PLUMMER, L.N., VACHER, H.L., MACKENZIE, F.T., BRICKER, O.P., and LAND, L.S., 1976, Hydrogeochemistry of Bermuda; a case history of ground-water diagenesis of biocalcarenites: Geological Society of America Bulletin, v. 87, p. 1301-1316.

PLUMMER, L.N., BUSENBERG, E., MCCONNELL, J.B., DRENKARD, S., SCHLOSSER, P., and MICHEL, R.L., 1998, Flow of river water into a Karstic limestone aquifer. 1. Tracing the young fraction in groundwater mixtures in the Upper Floridan Aquifer near Valdosta, Georgia: Applied Geochemistry, v. 13, p. 995-1015.

POUCHER, M., 2007, O'Leno/Old Bellamy cave exploration, http://cavesurvey.com/ob_cave.htm, accessed on: February 20, 2009.

PURI, H.S., and VERNON, R.O., 1964, Summary of the Geology of Florida and a Guidebook to the Classic Exposures: Special Publication 5, Florida Geological Survey, 312 p.

QUINLAN, J.F., DAVIES, G.J., JONES, S.W., and HUNTOON, P.W., 1996, The applicability of numerical models to adequately characterize ground-water flow in karstic and other triple-porosity aquifers, *in* Ritchey, J.D., and Rumbaugh, J.O., eds., Subsurface fluid-flow (ground-water and vadose zone) modeling: West Conshohocken, American Society for Testing and Materials, Special Technical Paper 1288, p. 114-133.

RAEISI, E., and MYLROIE, J.E., 1995, Hydrodynamic behavior of caves formed in the fresh-water lens of carbonate islands: Carbonates and Evaporites, v. 10, p. 207-214.

REEL, D.A., and GRIFFIN, G.M., 1971, Potentially petroliferous trends in Florida as defined by geothermal gradients: Transactions - Gulf Coast Association of Geological Societies, v. 21, p. 31-36.

REZAEI, M., SANZ, E., RAEISI, E., AYORA, C., VAZQUEZ-SUNE, E., and CARRERA, J., 2005, Reactive transport modeling of calcite dissolution in the fresh-salt water mixing zone: Journal of Hydrology, v. 311, p. 282-298.

RITORTO, M., 2007, Impacts of diffuse recharge on transmissivity and water budget calculations in the unconfined karst aquifer of the Santa Fe River basin [unpublished Ms. thesis]: University of Florida, 145 p.

RITORTO, M., SCREATON, E.J., MARTIN, J.B., and MOORE, P.J., in press, Magnitudes and chemical effects of diffuse and focused recharge in an eogenetic karst aquifer: An example from the unconfined Floridan aquifer: Hydrogeology Journal.

ROMANOV, D., and DREYBRODT, W., 2006, Evolution of porosity in the saltwater-freshwater mixing zone of coastal carbonate aquifers: An alternative modelling approach: Journal of Hydrology, v. 329, p. 661-673.

ROMANOV, D., GABROVŠEK, F., and DREYBRODT, W., 2003a, The impact of hydrochemical boundary conditions on the evolution of limestone karst aquifers: Journal of Hydrology, v. 276, p. 240-253.

ROMANOV, D., GABROVŠEK, F., and DREYBRODT, W., 2003b, Dam sites in soluble rocks: a model of increasing leakage by dissolutional widening of fractures beneath a dam: Engineering Geology, v. 70, p. 17-35.

ROSE, S., 1989, The heavy-metal adsorption characteristics of Hawthorne Formation (Florida, U.S.A.) sediments: Chemical Geology, v. 74, p. 365-370.

RUNNELLS, D.D., 1969, Diagenesis, chemical sediments, and the mixing of natural waters: Journal of Sedimentary Research, v. 39, p. 1188-1201.

SCANLON, B.R., and THRAILKILL, J., 1987, Chemical Similarities among Physically Distinct Spring Types in a Karst Terrain: Journal of Hydrology, v. 89, p. 259-279.

SCANLON, B.R., 1989, Physical Controls on Hydrochemical Variability in the Inner Bluegrass Karst Region of Central Kentucky: Ground Water, v. 27, p. 639-646.

SCHLUMBERGER MARKET ANALYSIS, 2007, http://www.slb.com/content/services/ solutions/ reservoir/carbonates.asp, accessed on February 20, 2009.

SCHWABE, S.J., CAREW, J.L., and HERBERT, R.A., 2008, Making caves in The Bahamas: Different recipes, same ingredients, *in* Park, L.E., and Freile, D., eds., Proceedings of the 13th Symposium on the Geology of the Bahamas and Other Carbonate Regions: San Salvador, Bahamas, Gerace Research Centre, p. 153-168.

SCOTT, T.M., 1988, The lithostratigraphy of the Hawthorn Group (Miocene of Florida), Florida Geological Survey Bulletin 59, 147 p.

SCREATON, E., MARTIN, J.B., GINN, B., and SMITH, L., 2004, Conduit properties and karstification in the Santa Fe River Sink-Rise System of the Floridan Aquifer: Ground Water, v. 42, p. 338-346.

SEALEY, N.E., 1994, Bahamian landscapes; an introduction to the physical geography of the Bahamas: Nassau, Media Publishing, 128 p.

SHUSTER, E.T., and WHITE, W.B., 1971, Seasonal fluctuations in the chemistry of limestone springs: A possible means for characterizing carbonate aquifers: Journal of Hydrology, v. 14, p. 93-128.

SKLASH, M.G., and FARVOLDEN, R.N., 1979, The role of groundwater in storm runoff: Journal of Hydrology, v. 43, p. 45-65.

SMART, P.L., and HOBBS, S.L., 1986, Characterisation of carbonate aquifers: a conceptual base, In: Symposium on the Environmental Problems in Karst Terranes and their Solutions (October, 1986): Bowling Green, Kentucky, National Water Well Association, p. 1-14.

SMART, P.L., DAWANS, J.M., and WHITAKER, F., 1988, Carbonate dissolution in a modern mixing zone: Nature, v. 335, p. 811-813.

SMART, P.L., BEDDOWS, P.A., COKE, J., DOERR, S., SMITH, S., and WHITAKER, F.F., 2006, Cave development on the Caribbean coast of the Yucatan Peninsula, Quintana Roo, Mexico, *in* Harmon, R.S., and Wicks, C.M., eds., Perspectives on Karst Geomorphology, Hydrology, and Geochemistry - A Tribute Volume to Derek C. Ford and William B. White: Geological Society of America, Special Paper 404, p. 105-128.

SMITH, D.L., and FULLER, W.R., 1977, Terrestrial heat flow values in Florida and the effects of the aquifer system, *in* Smith, K.L., and Griffen, G.M., eds., The Geothermal Nature of the Floridan Plateau: Florida Department of Natural Resources, Bureau of Geology Special Publication 21, p. 91-130.

SMITH, D.L., and LORD, K.M., 1997, Tectonic evolution and geophysics of the Florida basement, *in* Randazzo, A.F., and Jones, D.S., eds., The geology of Florida: Gainesville, University Press of Florida, p. 13-26.

SPRINKLE, C.L., 1989, Geochemistry of the Floirdan Aquifer System in Florida and in Parts of Georgia, South Carolina, and Alabama: Professional Paper 1403-I, United States Geological Survey, 105 p.

SPROUSE, B.E., 2004, Chemical and isotopic evidence for exchange of water between conduit and matrix in a karst aquifer: An example from the Santa Fe River Sink/Rise system [unpublished M. Sc. thesis]: University of Florida, 84 p.

STETZENBACH, K.J., FARNHAM, I.M., HODGE, V.F., and JOHANNESSON, K.H., 1999, Using multivariate statistical analysis of groundwater major cation and trace element concentrations to evaluate groundwater flow in a regional aquifer: Hydrological Processes, v. 13, p. 2655-2673.

STETZENBACH, K.J., HODGE, V.F., GUO, C., FARNHAM, I.M., and JOHANNESSON, K.H., 2001, Geochemical and statistical evidence of deep carbonate groundwater within overlying volcanic rock aquifers/aquitards of southern Nevada, USA: Journal of Hydrology, v. 243, p. 254-271.

STOESSELL, R.K., WARD, W.C., FORD, B.H., and SCHUFFERT, J.D., 1989, Water chemistry and $CaCO_3$ dissolution in the saline part of an open-flow mixing zone, coastal Yucatan Peninsula, Mexico: Geological Society of America Bulletin, v. 101, p. 159-169.

TEETER, J.W., 1995, Holocene saline lake history, San Salvador Island, Bahamas, *in* Curran, H.A., and White, W.B., eds., Terrestrial and Shallow marine Geology of the Bahamas and Bermuda: Geological Society of America, Special Paper 300, p. 117-124.

TERNAN, J.L., 1972, Comments on the use of a calcium hardness variability index in the study of carbonate aquifers, with reference to the central Pennines, England: Journal of Hydrology, v. 129, p. 87-108.

THRAILKILL, J., 1968, Chemical and hydrologic factors in the excavation of limestone caves: Geological Society of America Bulletin, v. 79, p. 19-45.

TORAN, L., HERMAN, E.K., and WHITE, W.B., 2007, Comparison of flowpaths to a well and spring in a karst aquifer: Ground Water, v. 45, p. 281-287.

TOTH, D., and KATZ, B., 2006, Mixing of shallow and deep groundwater as indicated by the chemistry and age of karstic springs: Hydrogeology Journal, v. 14, p. 1060-1080.

TRUESDELL, A.H., and JONES, B.F., 1974, WATEQ, a computer program for calculating chemical equilibria of natural waters: Journal Research 2, United State Geological Survey, p. 233-248.

UNDERWOOD, M.R., PETERSON, F.L., and VOSS, C., 1992, Groundwater lens dynamics of atoll islands: Water Resources Research, v. 28, p. 2889-2902.

UPCHURCH, S.B., 1992, Quality of water in Florida's aquifer systems, Florida's Ground Water Quality Monitoring Program: Tallahassee, Florida Geological Survey Special Publication 34, p. 12-51.

VACHER, H.L., and MYLROIE, J.E., 2002, Eogenetic karst from the perspective of an equivalent porous medium: Carbonates and Evaporates, v. 17, p. 182-196.

VACHER, H.L., BENGTSSON, T.O., and PLUMMER, L.N., 1990, Hydrology of meteoric diagenesis; residence time of meteoric ground water in island fresh-water lenses with application to aragonite-calcite stabilization rate in Bermuda: Geological Society of America Bulletin, v. 102, p. 223-232.

VESPER, D.J., and WHITE, W.B., 2004, Storm pulse chemographs of saturation index and carbon dioxide pressure: implications for shifting recharge sources during storm events in the karst aquifer at Fort Campbell, Kentucky/Tennessee, USA: Hydrogeology Journal, v. 12, p. 135-143.

VOGEL, P.N., MYLROIE, J.E., and CAREW, J.L., 1990, Limestone petrology and cave morphology on San Salvador Island, Bahamas: Cave Science, v. 17, p. 19-30.

WHITAKER, F.F., and SMART, P.L., 1997a, Climatic control of hydraulic conductivity of Bahamian limestones: Ground Water, v. 35, p. 859-868.

WHITAKER, F.F., and SMART, P.L., 1997b, Hydrogeology and hydrology of the Bahamian archipelago, *in* Vacher, H.L., and Quinn, T.M., eds., Geology and Hydrogeology of Carbonate Islands, Developments in Sedimentology 54: Amsterdam, Elsevier, p. 183-216.

WHITAKER, F.F., and SMART, P.L., 1997c, Groundwater circulation and geochemistry of a karstified bank-marginal fracture system, South Andros Island, Bahamas: Journal of Hydrology, v. 197, p. 293-315.

WHITAKER, F.F., and SMART, P.L., 2007a, Geochemistry of meteoric diagenesis in carbonate islands of the northern Bahamas; 2, Geochemical modelling and budgeting of diagenesis: Hydrological Processes, v. 21, p. 967-982.

WHITAKER, F.F., and SMART, P.L., 2007b, Geochemistry of meteoric diagenesis in carbonate islands of the northern Bahamas; 1, Evidence from field studies: Hydrological Processes, v. 21, p. 949-966.

WHITE, W.B., 1977, Role of solution kinetics in the development of karst aquifers, *in* Tolson, J.S., and Doyle, F.L., eds., Karst Hydrology: Huntsville, UAH Press, p. 503-517.

WHITE, W.B., 1988, Geomorphology and Hydrology of Karst Terrains: New York, Oxford University Press, 464 p.

WHITE, W.B., 1999, Conceptual models for karstic aquifers, *in* Palmer, A.N., Palmer, M.V., and Sasowsky, I.D., eds., Karst Modeling: Karst Waters Institute Special Publication 5, p. 11-16.

WHITE, W.B., 2002, Ground water flow in karst: matrix flow and conduit flow with implications for the Floridan Aquifer, *in* Martin, J.B., Wicks, C.M., and Sasowski, I.D., eds., Hydrologeology and Biology of Post-Paleozoic Carbonate Aquifers: Charles Town, Karst Waters Institute Special Publication 7, p. 9-13.

WICKS, C.M., and HERMAN, J.S., 1994, The effect of a confining unit on the geochemical evolution of ground water in the Upper Floridan aquifer system: Journal of Hydrology, v. 153, p. 139-155.

WIGLEY, T.M.L., and PLUMMER, L.N., 1976, Mixing of carbonate waters: Geochimica et Cosomochimica Acta, v. 40, p. 989-995.

WIGLEY, T.M.L., PLUMMER, L.N., and PEARSON JR, F.J., 1978, Mass transfer and carbon isotope evolution in natural water systems: Geochimica et Cosmochemica Acta, v. 42, p. 1117-1139.

WOLD, S., ESBENSEN, K., and GELADI, P., 1987, Principal component analysis: Chemometrics and Intelligent Laboratory Systems, v. 2, p. 37-52.

WOLERY, T.J., 1992, EQ3NR, A computer program for geochemical aqueous speciation solubility calculations: Theoretical manual, user's guide, and related documentation (Version 7.0), Lawrence Livermore National Laboratory

WOOD, W.W., and PETRAITIS, M.J., 1984, Origin and Distribution of Carbon-Dioxide in the Unsaturated Zone of the Southern High-Plains of Texas: Water Resources Research, v. 20, p. 1193-1208.

WORTHINGTON, S.R.H., 1994, Flow velocities in unconfined carbonate aquifers: Cave and Karst Science, v. 21, p. 21-22.

WORTHINGTON, S.R.H., FORD, D.C., and CAVIES, G.J., 2000, Matrix, fracture and channel components of storage and flow in a Paleozoic limestone aquifer, *in* Sasowsky, I.D., and Wicks, C.M., eds., Groundwater Flow and contaminant Transport in Carbonate Aquifers: Rotterdam, A.A. Balkema, p. 113-128.

ZIMMERMAN, A.R., MOORE, P.J., and MARTIN, J.B., 2006, Dissolved organic matter-mineral-microbe interaction in a karst aquifer: The Santa Fe River Sink/Rise system, Floridan Aquifer, Florida: Eos Trans. AGU, v. 87, Fall Meeting Abstract B33A-1146.

BIOGRAPHICAL SKETCH

Paul Joseph Moore III (PJ) was born south of Interstate 10 in Pascagoula, Mississippi on a crisp November morning in 1975. After receiving his diploma from Pumpkin Patch Kindergarten in Moss Point, Mississippi, he continued his education at Escatawpa Elementary School in Escatawpa, Mississippi, where he completed years one through six. Following an incendiary year in 1988, PJ transferred from Magnolia Junior High School in Moss Point, Mississippi to Vancleave Middle School in Vancleave, Mississippi to complete year seven. He graduated from Vancleave High School in May 1994. Following graduation, PJ worked as a marine electrician at Ingalls Shipbuilding (now Northup Grumman) in Pascagoula, MS for about four years before continuing his education at Mississippi State University in 1998. He graduated from Mississippi State University with a Bachelor of Science in geology in May 2002. After an unexpected one-year hiatus, PJ matriculated into the doctoral program in the Department of Geological Sciences at the University of Florida under the tutelage of Dr. Jonathan B. Martin. He received his Ph.D. in May 2009 and soon after stated, "…what a long, strange trip it's been."